INJURY RISK TO THE UPPER EXTREMITY RESULTING FROM BEHIND SHIELD BLUNT TRAUMA

INJURY RISK TO THE UPPER EXTREMITY RESULTING FROM BEHIND SHIELD BLUNT TRAUMA

By JULIA DE LANGE, B.Eng., M.A.Sc.

A Thesis Submitted to the School of Graduate Studies in Partial Fulfilment of the Requirements for the Degree Doctor of Philosophy

McMaster University DOCTOR OF PHILOSOPHY (2023) Hamilton, Ontario

(Biomedical Engineering)

TITLE:	Injury risk to the upper extremity resulting from behind shield blunt trauma
AUTHOR:	Julia de Lange, B.Eng., M.A.Sc., McMaster University
SUPERVISOR:	Cheryl E. Quenneville, B.Sc., M.E.Sc., Ph.D.
NUMBER OF PAGES:	xix, 174

Lay Abstract

Ballistic shields used by defence personnel are designed to stop incoming bullets by deflecting or absorbing them. In the process, the back-face of the shield undergoes a rapid deformation that can potentially cause an upper extremity injury to users, an injury mechanism termed behind shield blunt trauma. This work aimed to quantify the injury risk that this mechanism poses at four locations along the upper extremity: the hand, wrist, forearm, and elbow. This was conducted by modifying and employing a crash test dummy upper extremity and measuring loads applied to the upper extremity in a ballistic testing range. Assessment of whether these loads caused injury was conducted using cadaveric specimens and testing them to failure. An existing finite element human body model was also assessed for its applicability to predict injury in these high-rate loading scenarios. Results from this work will inform a protective standard to assess ballistic shields.

Abstract

Ballistic shields are supported by a user's arm, placing the upper extremity at close proximity to the back-face of the shield. Although ballistic shields must pass a protective standard that outlines projectile (bullet) penetration; there is no standard that stipulates the amount of acceptable deformation when ballistic shields stop or deflect projectiles. There are no injury criteria developed for the high-rate, short duration and focal loading that is typical of shield back-face deformation from these events.

In this research, an anthropomorphic test device (ATD) was modified to allow for additional instrumentation capable of measuring these loads. It was then used in a ballistic testing facility to quantify loading at the hand, wrist, forearm, and elbow. A lightweight projectile was created that matched the shape and stiffness of the deforming ballistic shield and impacts within 5% of the peak force measured in the ballistic testing facility were applied with it to post-mortem human subjects (PMHS) until failure. Eight 50th percentile male PMHS pairs were segmented at the mid-humerus and impacted to failure to determine the fracture threshold of the hand, wrist, forearm, and elbow, confirmed by x-ray imaging. The peak force required to generate fracture varied significantly among anatomical location, indicating boundary conditions influence failure threshold. Further, these injury criteria were substantially different than previously reported criteria for other loading events (*e.g.*, automotive), highlighting the importance of developing injury criteria specific for the intended application.

An existing finite element human body model designed for automotive impacts was also assessed for its applicability to predict injury in these high-rate loading scenarios, and performed well for peak force, but not for the force-time curve shape. This is the first study of its kind to

assess injury risk resulting from shield behind armour blunt trauma, and results from this work will inform a protective standard to assess ballistic shields.

Acknowledgements

Thank you to my supervisory committee for their feedback and direction with bringing this project to completion. Cheryl, I am extremely grateful to have had a supervisor as encouraging and positive as you. Your input throughout this project was invaluable, and it is challenging to put into words how grateful I am for all of the amazing opportunities and guidance (both personally and professionally) you've provided over the years. Thank you. A special thank you is also due to Dr. Wohl for the project and career mentorship, but also for always lending a laugh in the lab over the last 6 years. Thank you for being a good sport with the 50th Male jokes; I hope you're at ease knowing these jokes likely end with me.

Thank you to McMaster University, the Ontario Graduate Scholarship and the Liburdi Engineering PhD Scholarship for the scholarship funding. Thank you to the Defence Research and Development Canada technical team for your financial support and expertise in this field. The contributions of Jean-Sébastien Binette were especially valuable. Big thanks to the shop guys; John, Mark, Rob, Steve, and of course, Michael. I truly appreciate your patience with teaching me various aspects of mechanical design, and the laughs when things didn't go as planned.

Thank you to all the Injury Biomechanics lab members over the years who have helped make grad school more enjoyable: Aiden, Ali, Annie, Ariana, Ary, Carson, Cole, Fatemeh, Julian, and Taylor. A very heartfelt thank you to the lab members involved in the DRDC project: Liam and Noah, you both provided technical support that I have deeply appreciated and made the long lab days some of my favourite. This project wouldn't be what it is without you.

Thank you to my family for their support in this venture as well, and for always finding a way to celebrate the little things. Yes, I am finally done with school (for now). Lastly, to my amazing partner, Elliott. Thank you for your never-ending support, curiosity, and feedback, and for being my biggest champion. I can’t wait to spend my life with you.

Dedication

I would like to dedicate this work to my father. I trust he would be proud of this accomplishment.

Table of Contents

List of Figures

List of Tables

List of Abbreviations and Symbols

AIS	Abbreviated Injury Scale
ANOVA	Analysis of Variance
ATD	Anthropomorphic Test Device
BABT	Behind Armour Blunt Trauma
BFD	Back-face Deformation
BMD	Bone Mineral Density
BSBT	Behind Shield Blunt Trauma
CoV	Coefficient of Variation
CT	Computed Tomography
DAQ	Data Acquisition System
DIC	Digital Image Correlation
DRDC	Defence Research and Development Canada
F	Force
FEM	Finite Element Modelling
G	Acceleration due to Gravity (9.81 m/s^2)
GHBMC	Global Human Body Model Consortium
HU	Hounsfield Unit
Hz	Hertz
IARV	Injury Assessment Reference Value
IRC	Injury Risk Curve
J	Joule

kg	Kilogram
m	Meter
ms	Millisecond
n	Number of Observations
N	Newton
NATO	North Atlantic Treaty Organization
NI	National Instruments
NIJ	National Institute of Justice
Pa	Pascals
PMHS	Post-mortem human subjects
PMMA	Polymethyl-methacrylate
psi	Pounds per square inch
R^2	Coefficient of Determination
s	Second
SD	Standard Deviation
TAB	Trauma-attenuating backing
THUMS	Total Human Model for Safety
U.S.	United States of America
UHMWPE	Ultra-high molecular weight polyethylene
VRC	Valcartier Research Center
WorldSID	Worldwide Harmonized Side Impact Dummy

Declaration of Academic Achievement

The following is a declaration that I, Julia de Lange, acknowledge that the studies conducted in this thesis were a result of collaborative efforts. The contribution that each individual made are detailed below.

Chapter 1: Julia de Lange wrote the chapter, Cheryl Quenneville reviewed the chapter.

Chapter 2: Julia de Lange proposed the study design, modified the ATD, conducted data collection, data analysis and wrote the manuscript; Liam Burrows analyzed the high-speed video, assisted with data collection and reviewed the manuscript; Jean-Sébastien Binette contributed to the study design, assisted with data collection and reviewed the manuscript; Benoît Gauthier and Stephen Kelly assisted with ballistic testing; Cheryl Quenneville contributed to study design and reviewed the manuscript.

Chapter 3: Julia de Lange proposed the study design, conducted data collection and analysis, and wrote the manuscript; Liam Burrows contributed to the study design, assisted with data collection and reviewed the manuscript; Carly Kivinen, Vanessa Reis and Lyndsay Simmons conducted imaging of the specimens; Akshay Wadera graded the fractures from the x-ray images; Cheryl Quenneville contributed to the study design and reviewed the manuscript.

Chapter 4: Julia de Lange proposed the study design, conducted data collection and analysis, and wrote the manuscript; Liam Burrows contributed to the study design, assisted with data collection and reviewed the manuscript; Carly Kivinen, Vanessa Reis and Lyndsay Simmons conducted imaging of the specimens; Akshay Wadera graded the fractures from the x-ray images; Cheryl Quenneville contributed to the study design and reviewed the manuscript.

Chapter 5: Julia de Lange proposed the study design, conducted the data collection and analysis and wrote the chapter; Carson Brewer assisted with segmenting the THUMS upper extremity; Ary Shakib assisted with troubleshooting the THUMS model; Cheryl Quenneville contributed to the study design and reviewed the chapter.

Chapter 6: Julia de Lange wrote the chapter; Cheryl Quenneville reviewed the chapter.

Chapter 1 – Introduction

Overview: *Energy transferred to users resulting from back-face deformation as ballistic shields absorb energy may cause injuries to the upper extremity. Currently, there are no standards in place that limit the amount of back-face deformation permitted by ballistic shields, and there has been limited research into characterizing this event. This introductory chapter details the bony anatomy of the upper extremity, and common injuries to this region and their associated thresholds. It also discusses surrogates that can be used to assess upper extremity injury, and specific studies (experimental and computational) that pertain to the tolerance of the upper extremity. It concludes with the study rationale, objectives, hypotheses, and a thesis overview.*[1]

1.1 Preface

There is a push for light-weight materials in personal armour systems to increase mobility of the users to decrease fatigue, while also providing protection against most threats and keeping costs reasonable. A large problem associated with this trade-off is increased risk of injury from behind armour blunt trauma (BABT) mechanisms. Behind-armour blunt trauma refers to bodily injuries that may occur as a result of the rapid deformation caused by projectiles striking protective equipment [1]. Ballistic shields, used by defence personnel to protect against projectiles, gunfire,

[1] Due to the interdisciplinary nature of this work, a glossary of frequently used anatomical terms is included in Appendix A.

and explosions, fall into this category of protective equipment. They are supported by a user's arm and are an important factor in the first line of defence. The back-face deformation of ballistic shields may impact the user's upper extremity, which may cause an injury. It could also cause the user to drop the shield, which could pose a greater risk of injury. There are currently no known standards in place to limit the back face deformation of ballistic shields, only standards that pertain to projectile penetration [2].

1.2 The Upper Extremity

The upper extremity can generally be divided into four regions: the shoulder (or shoulder girdle), the arm (*i.e.*, the humerus), forearm (the ulna and radius), and the hand. The elbow joint is the joint connecting the humerus and the forearm, and the wrist is the joint connecting the hand and the forearm (Figure 1.1).

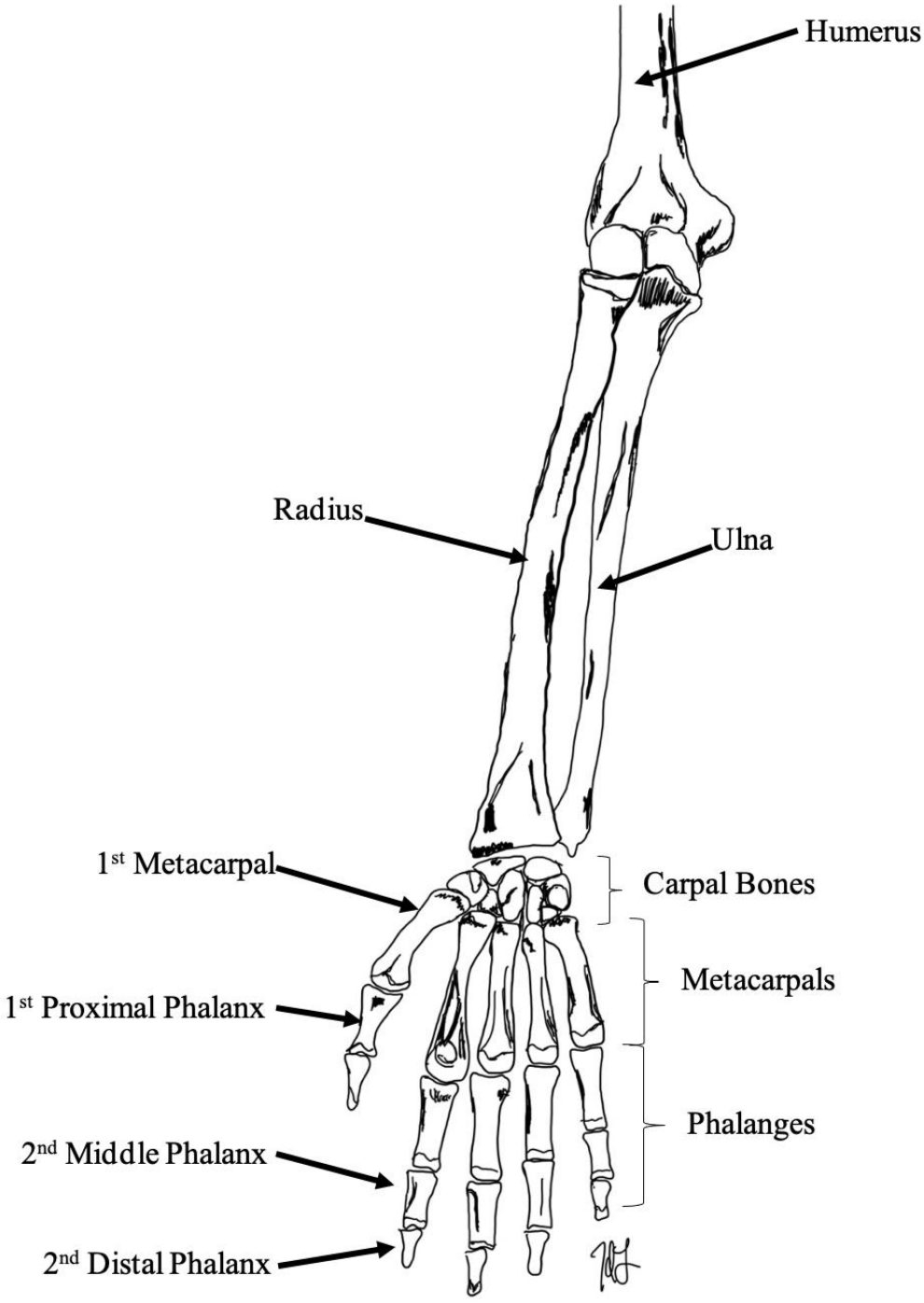

Figure 1.1: Bony anatomy of the upper extremity.
Posterior view of the entire upper extremity. The joint at which the humerus meets the radius and ulna is the elbow. The radius and ulna form the forearm. The joint at which the carpal bones meet the distal (*i.e.*, closer to the fingers) radius and ulna is the wrist.

1.2.1 Bony Anatomy

Three bones comprise the shoulder girdle: the clavicle, scapula and humerus. The humerus is located distal to the shoulder and is the longest and largest bone of the upper extremity, forming the arm. The elbow contains three joints: the ulnohumeral, radiohumeral, and proximal radioulnar. It connects the humerus to the forearm, which consists of the ulna and radius. The elbow allows flexion and extension of the forearm towards and away from the humerus, while also contributing to forearm pronation and supination rotations [3]. This joint is composed of two articulations, where the humerus connects to the radius and ulna, and is a modified hinge joint. There are two strong ligament complexes at the elbow joint, the medial collateral ligaments (MCL) on the ulna side, and the lateral collateral ligaments (LCL) on the radius side.

The ulna, the longer of the two forearm bones, is located on the medial aspect of the forearm while the radius is located on the lateral aspect of the forearm (Figure 1.2). The proximal end of the ulna has a posterior projection, the olecranon, forming the prominence of the elbow, and an anterior projection, the coronoid process [4]. These processes together form the trochlear notch, which articulates with the humerus. The radial notch of the ulna articulates with the head of the radius and is located lateral and inferior to the trochlear notch. The distal end of the ulna contains a styloid process on the posterior side. The radius and ulna articulate with one another at both the proximal and distal ends, called the radioulnar joints, and through a strong fibrotic band known as the syndesmosis in between the two end joints. Long bones are comprised of a central shaft, referred to as the diaphysis, and a segment at each end, the epiphysis. The shaft of the radius widens distally to form a styloid process on the lateral side of the forearm as well, proximal to the thumb. The distal end of the radius articulates with three bones of the wrist (the lunate, scaphoid and triquetrum) to form the radiocarpal (*i.e.*, wrist) joint. The diaphyses of long bones are

composed primarily of cortical bone, while the epiphysis is primarily cancellous bone, with a cortical casing (bone architecture is discussed further in Section 1.2.2, Bone Structure and Material Properties).

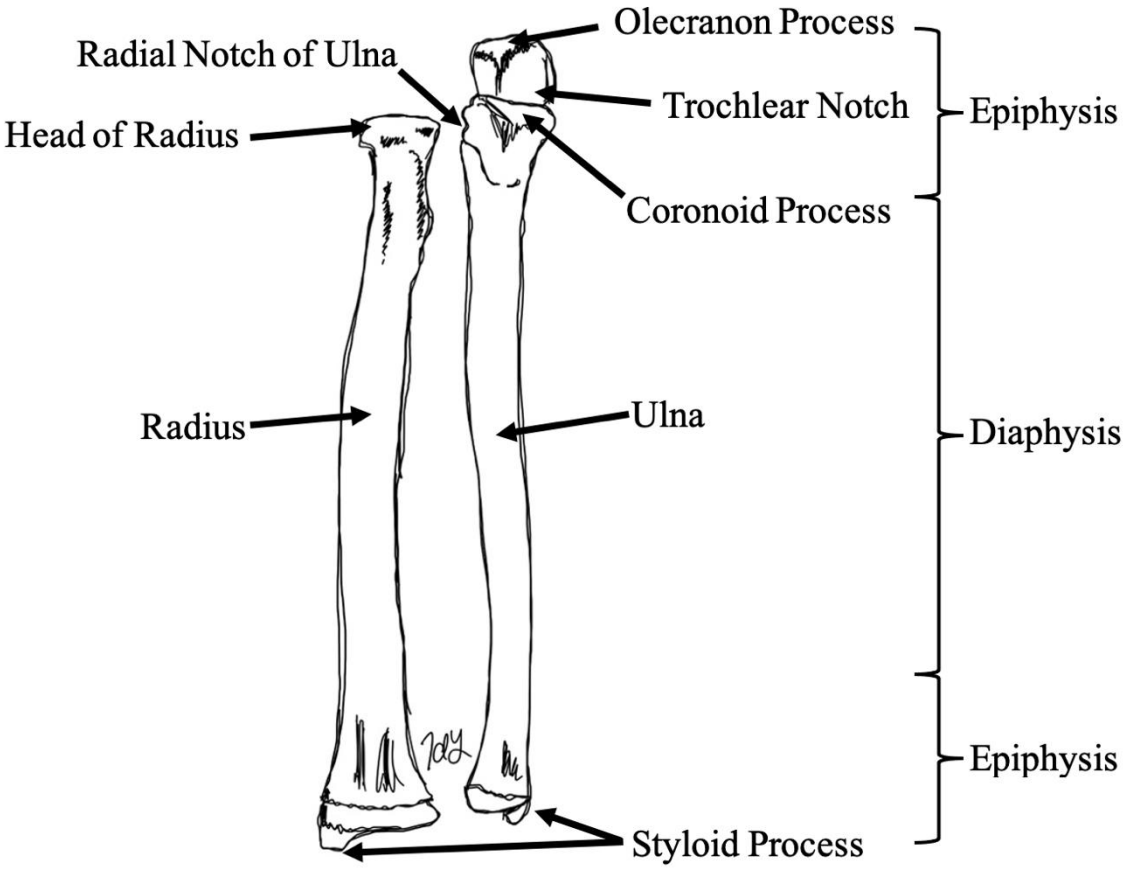

Figure 1.2: Long bones of the forearm - the radius and ulna.
The diaphysis is the central shaft of long bones, while the epiphyses refer to the ends of the long bones.

The pronation and supination of the forearm is also controlled by rotating the wrist, which connects the forearm to the hand. There are 27 bones in the hand and wrist, which can be divided into three distinct regions: the carpus (*i.e.*, the wrist), metacarpus, and digiti. The carpus consists

of eight small bones that connect the hand to the forearm. The carpal bones then articulate with the five metacarpal bones (the palm of the hand) forming the carpometacarpal joints. There are five metacarpal bones, numbered 1 to 5 and starting with the thumb running lateral to medial. The heads of the metacarpals are bony protrusions commonly referred to as the knuckles. These each in turn articulate with the phalanges to form the metacarpophalangeal joints. There are 14 phalangeal bones that form the digits. The digits are similarly numbered 1 to 5 beginning with the thumb. The thumb only has two phalanges (proximal and distal), while the other four digits have three phalanges (proximal, middle and distal).

1.2.2 Bone Structure and Material Properties

Bone tissue consists of cells embedded in an extracellular matrix. It is comprised of two different microstructures – cortical (or compact) and cancellous (or trabecular) bone (Figure 1.3). The distinction between these two types of bone types is largely attributed to porosity: cortical bone has low porosity (5-15% [5]) and composed of many microscopic cylindrical structures (osteons), that are densely aligned. Cancellous bone porosity ranges from 40 to 95% and has a lattice-like structure [5].

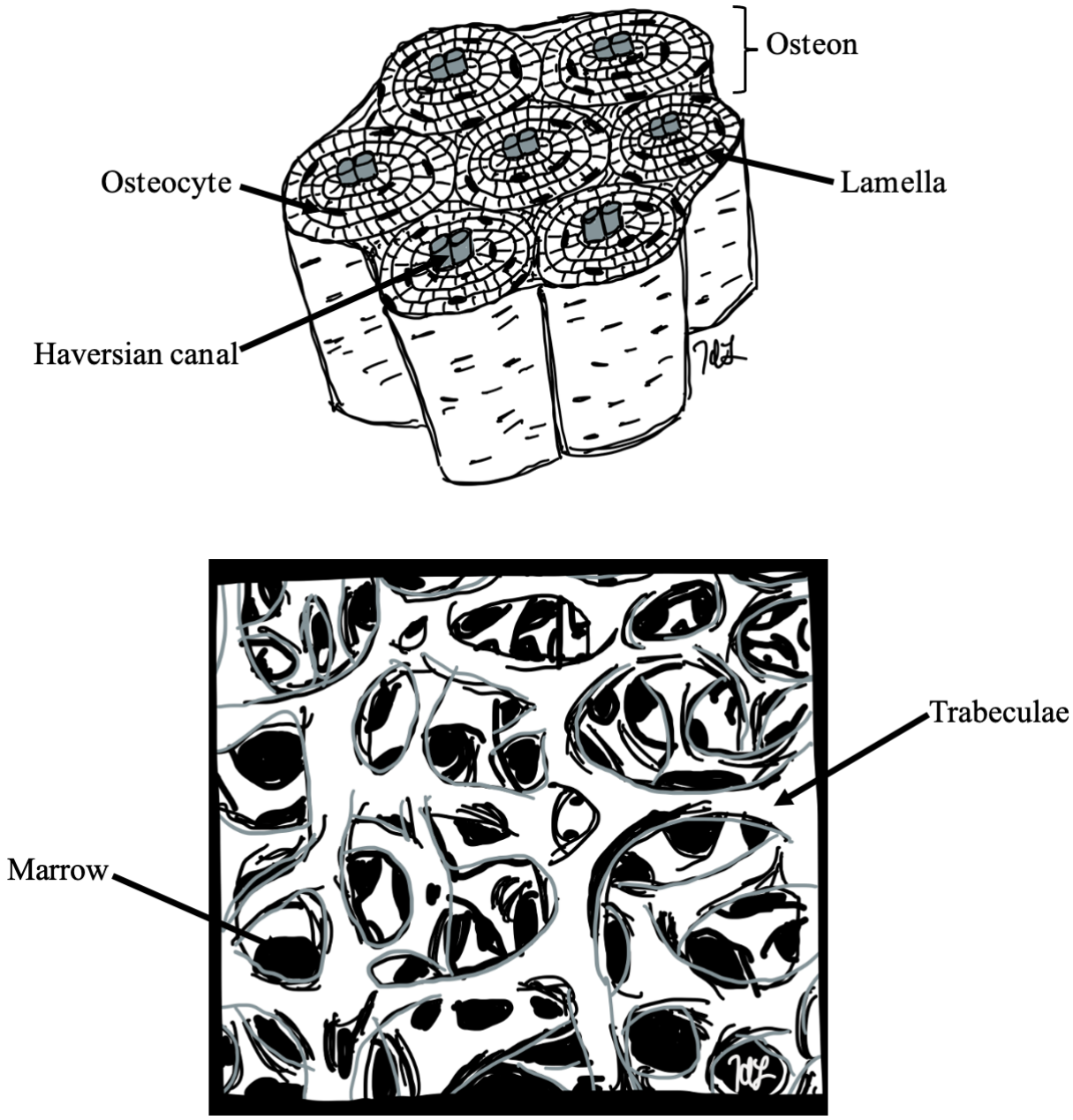

Figure 1.3: Microstructure of cortical (top) and trabecular (bottom) bone.
Cortical bone (top) is composed of cylindrical structures (osteons) containing concentric rings of bone (lamellae) surrounding a central canal, which houses the Haversian canal. They are aligned axially to support loading. Trabecular bone (bottom) consists of an open network of bone plates called trabeculae, and bone marrow can be found in the voids.

Cortical bone is the stronger and heavier type of bone, and its microarchitecture plays an important role in dictating its mechanical properties. The Haversian system (or osteons) are the histologic features of the microscopic components of compact bone that are responsible for maintaining the metabolism of bone cells and dictate how compact bone responds to an applied load [6]. The primary structures of Haversian systems are concentric rings of bone (lamellae) surrounding a central canal. Lamellae are made up of mineralized collagen threads and provide bone with its hardness. Within each lamella, there are cavities called lacunae, which contain mature bone cells (osteocytes) suspended in nutrient-rich fluid. Failure of bone is related to a number of factors, including the number and size of the osteons or Haversian systems contained within the bone [5].

Cancellous or trabecular bone does not have Haversian systems but consists of an open network of bone plates called trabeculae. It exists in a scaffold nature and the pores between trabeculae are filled with bone marrow. The trabecular network porosity varies according to anatomical location, biomechanical function, and age.

1.2.3 Bone Properties

Bone is viscoelastic, meaning that its response is dependent on the loading rate. Rapidly loaded bone has a greater modulus of elasticity, and greater ultimate tensile strength, resulting in more brittle fracture [7]. Bone is also anisotropic, meaning its material properties vary in different directions [6], and as such loading orientation of bone affects the structural response. Bodily injury occurs when a tissue is loaded beyond its failure tolerance. Bone is no exception, and when loaded above its mechanical injury threshold, can fail in a number of mechanisms. As bone properties are highly variable depending on the rate and loading direction of testing, the properties vary. The

cortical bone of the humerus has been reported to have a modulus of elasticity ranging from 17.1 – 20.0 GPa, while the ultimate stress was reported as 122.6 – 154.9 MPa. Similarly, the ultimate stress of the radius and ulna have been reported as approximately 149 – 177 MPa, and 148 – 178 MPa, respectively, while the elastic modulus for the radius and ulna ranged from 18.5 – 21.4 GPa and 18.4 – 21.2 GPa, respectively (*e.g.*, [5]). These properties were established through a variety of measurement techniques [8].

1.2.4 Bone Mineral Density

There are many age-related changes that affect the mechanical properties of bone, attributed to increased porosity, microdamage accumulation, and decreased quantity of non-collagenous proteins, among others [5]. Skeletal health is typically measured by quantifying Bone Mineral Density (BMD), conducted through imaging modalities that measure radiation passing through bone. It is common practice in both injury biomechanics and clinical practice to quantify BMD to assess fracture risk [9] as a reduction in BMD imposes as elevated risk of fracture.

Currently (as of 2023) the World Health Organization (WHO) uses Dual-energy X-Ray Absorptiometry (DXA) scans as their gold standard for classifying osteoporosis, which describes the general skeletal disorder of reduced BMD [10]. The measured BMD from DXA is then normalized to a reference population to calculate a T-score, representing the number of standard deviations below or above the average of the reference population (Table 1.1). However, recent investigations into the two-dimensional nature of DXA has been shown to introduce error [11, 12]. As such, quantitative Computed Tomography (qCT) is a good alternative as it provides a three-dimensional quantification of bone quality using volumetric BMD (vBMD) expressed in mg/cm^3. Further, qCT allows for distinguishing among cortical and trabecular bone for individual

assessment. The American College of Radiology has produced an equivalency of vBMD with T-score in order to assess whether osteoporosis is present.

Table 1.1: qCT and DXA equivalence for classifying BMD.
The relationship between volumetric BMD and diagnostic category which influences bone fracture risk.

Diagnostic Category	WHO T-Score Classification [10]	Equivalent BMD [13]
Normal	≥ -1	> 120 mg/cm^3
Osteopenia	< -1 and > -2.5	≤ 120 mg/cm^3 and ≥ 80 mg/cm^3
Osteoporosis	≤ -2.5	< 80 mg/cm^3

1.3 Measurement Techniques

In order to assess the injury potential as a result of BABT, the strains, accelerations and forces experienced by the user must be quantified. Injury causation from these quantified metrics can be proposed as injury thresholds. These are common metrics used in injury biomechanics to determine injury limits.

1.3.1 Strain Gauges

Strain gauges offer a non-invasive way to estimate internal bone loads by measuring strain on the surface of the bone. Strain gauges are metal-foil resistors that measure change in resistance in proportion to the applied strain. The external force applied to a ferritic material generates physical deformation and an electrical resistance change of the material. They are designed such that they are long loops of wire oriented in the direction they are intended to measure, and the change in shape (elongation and reduction in wire area) can be directly related to the strain of the specimen. The electrical resistance material measures strain proportional to resistance changes.

Normally, this variation in electrical resistance as a result of applied strain is very small, so strain gauges are configured in a Wheatstone bridge.

Strain gauges are only sensitive to changes in strain along the length of its wires and cannot be used to measure shear strain. To account for this, strain gauges can be stacked on top of one another to create a strain gauge rosette, which allows for quantifying two plane strains and one shear strain. This allows for calculating stresses and principal strains acting on the bone.

1.3.2 Force Sensors

Force sensors are transducers that convert a mechanical load (*e.g.*, tension, compression, pressure, *etc.*) into an electrical signal. Dynamically applied forces are frequently measured with ring-style sensors, in which piezoelectric materials used to measure dynamic compression are stiff and stable. These are suitable for measuring short duration events, such as typical in BABT events.

1.3.3 Accelerometers

Accelerometers are a type of sensor that measure the rate of change of velocity of a body relative to free fall (*i.e.*, relative to the Earths gravitational constant, approximately 9.81 m/s^2 or 1 ‘g’). In piezoelectric accelerometers, there is a piezoelectric crystal that is sandwiched between two electrodes, and a seismic mass is kept overtop of the crystal. The crystal is connected to the solid base through springs, and when a force is applied to the crystal, it develops voltage across its surface, which can be measured from the electrodes. Since the mass is constant, Newton’s second law can be used to determine the applied acceleration, relative to the force applied to the crystal. In injury biomechanics, acceleration is commonly reported in ‘g’s’.

1.4 Behind Armour Blunt Trauma

Behind armour blunt trauma (BABT) is the spectrum of injuries resulting from the impact of projectiles on personal armour. Although armour is designed to stop the penetration of the projectile through it, the energy dissipated into the armour by the slowed projectile may be transferred through the armour backing and body wall [1]. Behind-armour blunt trauma may occur behind flexible textile-based armours as well as from rigid (ceramic-based) armours.

Behind armour blunt trauma is becoming increasingly relevant in an effort to reduce the weight and thickness of armour [14]. This has been conducted in an effort to increase the mobility of military personnel but may pose a risk of not sufficiently dissipating the energy within the armour. Composite ballistic shields offer much lower areal density than traditional shield materials (*i.e.*, steel) and are corrosion-proof with no maintenance [15]. Although armours are designed to absorb energy, the rapid deformations of the armours may result in a greater proportion of this energy of the slowed projectile being propagated to the wearer in comparison to other materials that do not deform.

1.5 Ballistic Shields

1.5.1 General Protection Mechanics

The key protection parameters for ballistic shields are first, to resist complete penetration by a projectile, and second, limit behind shield blunt trauma. The general principles of minimizing the effects of energy transfer from a bullet to an individual are to either absorb or redistribute the incoming energy [16]. Impact energy is absorbed in shields by material plastically deforming, stretching, or compressing and work being conducted before it gains access to the body. This in

turn extends the time over which the energy is applied to the body, reducing the impulse and thereby injury potential. Secondly, redistributing this energy into a larger area reduces the pressure acting on the body, also decreasing injury potential. Lastly, extending the duration of the energy application also reduces the force experienced by the user.

The focus of the current study is large 'torso protector' shields (commonly 20 by 30 inches or 24 by 36 inches) rather than strictly upper extremity protection (Figure 1.4). As such, any back-face deformation close to the arm support may cause injury to the upper extremity due to its proximity to the shield. The user then becomes vulnerable to injury if this causes the user to drop the shield, exposing them to greater risk of bodily harm.

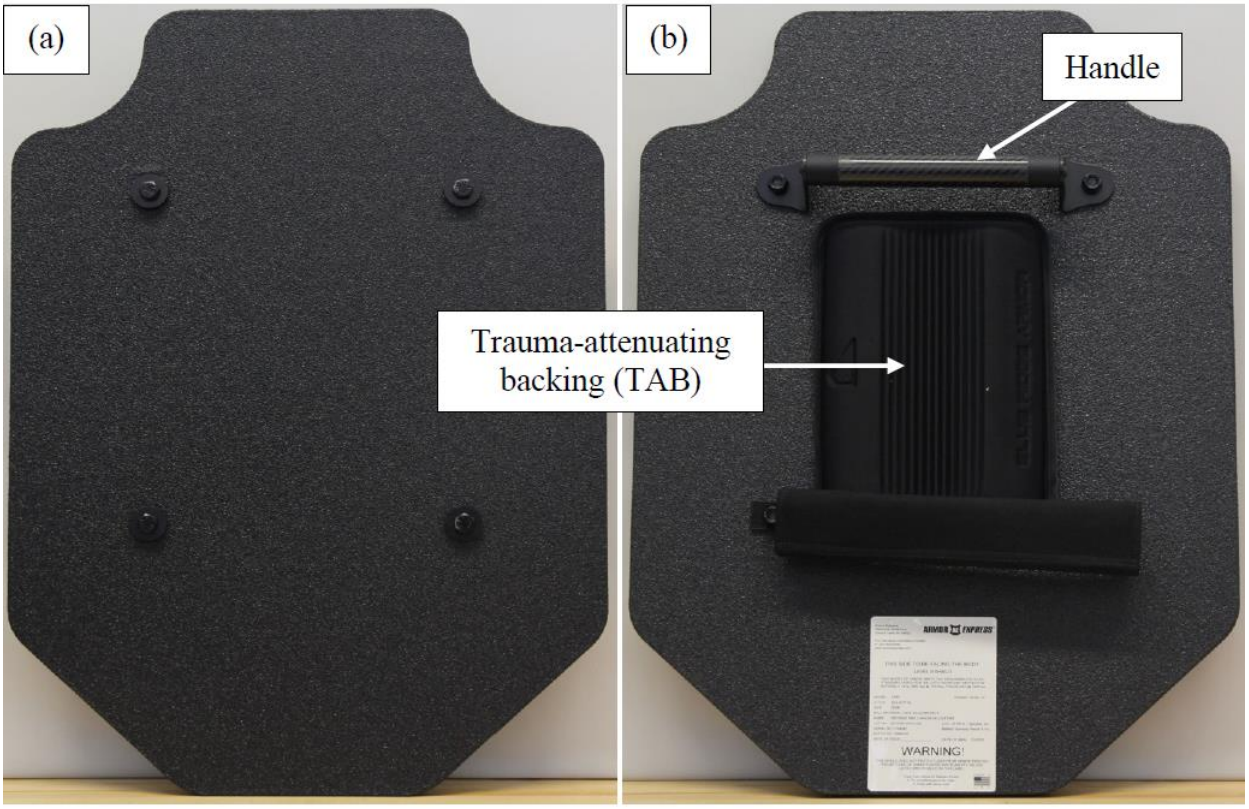

Figure 1.4: Composite ballistic shields.
This is (a) the front and (b) the back of a type of torso protector shield, which are the focus of this study. Shields this size weigh approximately 7.1 kg and are approximately 50.8 cm wide and 76.2 cm tall.

1.5.2 Shield Composition

The high velocity and calibre of bullets requires shields to be able to stop both the penetration of projectiles and disperse their large kinetic energy. As such, shields are designed using composite materials as traditional single-material designs (*e.g.*, wood, metal) are no longer desirable due to the increased weight. Currently, composite shields are composed of ductile materials placed between hard brittle layers. Layers of fabric such as polymer composites with aramid fibers (*e.g.*, Kevlar®), polyethylene fibres (*e.g.*, Dyneema®) or even metallic foams are used in composite shields, which sometimes contain shear thickening fluid to further dissipate energy during impacts [17]. These layers are then separated by brittle polymer films such as polyimide, metallic films, or ceramic films. The hard layers act to fracture the projectile, while the ductile materials deform to absorb impact energy. Kinetic energy of the projectile can be absorbed through the plastic deformation of the material, and once a projectile is shattered, the fragments disperse through the material allowing the remaining energy to be displaced over a greater impact area [18]. The degree of a shield's ballistic protection is affected by the capacity for dispersion of kinetic energy from the projectile, which is determined by many factors, including the thickness of the individual layers, properties of the materials that are used, and the geometry of the components within the layers [18].

Many armour manufacturers will also offer trauma attenuating backings, or TABs, aimed to limit injuries as a result of behind-armour blunt trauma. They vary in composition depending on the threat they are intended to defeat but are generally constructed of a thick layer of low-density polymer [16]. Although not yet evaluated for characterizing their effectiveness to ballistic shields, they have been shown to improve protection against behind armour blunt trauma for the

thorax [19]. A 91% decrease in transient peak pressure of the trunk was reported with the addition of a TAB [19].

1.5.3 Current Shield Standards

Most shield specifications offer testing standards for varying levels of protection to address the type of ammunition the shield must defeat. There are protection levels for handguns, rifles, and shotguns. Rifles typically travel faster (732 – 847 m/s) in comparison to handguns (approximately 440 m/s) and shot guns (approximately 430 m/s).

There are standards in place for shields in order to prevent against projectile penetration. This falls under NIJ Standard 0108.01, 'Ballistic Resistant Protective Materials' [2]. It specifies the testing setup and ballistic requirements based on the level of protection, and the number of test shots to be conducted without permitting projectile penetration and is currently in use for Canadian shields. The standard fails to indicate an allowable peak back-face deformation, or allowable load transmission to the user.

1.5.4 Current Body Armour Standards

As the back-face deformation (BFD) of ballistic protective material is generally unavoidable, there are various test standards in place to limit the allowable deformation. Most of these standards, which provide a static post-impact indentation limit, are taken as pass/fail criteria. The most widely referenced standard is developed by the National Institute of Justice (NIJ Standard-0101.06, 2008 revision), specifying both testing and performance standards for body armour [20]. There are five types (II-IV) of protection classifications, classified according to the type of ammunition a material must protect against, that specify an allowable back-face deformation (BFD) limit [21]. The test specifies performance requirements in which the static

indentation in a Roma Plastilina No. 1 (an oil-based modelling clay) plate measured post-test must be less than 44 mm [20]. This deformation limit is consistent among all protection classifications. The United Kingdom has a smaller limiting depth, where the back-face signature must not exceed 25 mm [21]. There are no such standards currently in place to limit ballistic shield deformation.

The National Institute of Justice standard was developed with respect to injury potential to the torso, and was validated on goats, the results of which were scaled to humans [22]. There are many limitations to this standard. This clay does not match the response of living soft tissue during impact and is almost entirely plastic. This standard does not address that impact is a dynamic event and injury is also dependent on the motion of the struck object (*e.g.*, the body). Further, it was developed using soft armour and only two relatively low-energy projectiles [23]. Roberts *et al*. have demonstrated that this does not adequately account for all bodies, *e.g.*, smaller females [24]. It was also developed using two relatively low-energy projectiles at an approximate velocity of 243 m/s [25]. It has been widely established that this 44 mm maximum BFD standard is poor [26] [27] [22] [24] [28], as it is unknown how exactly it correlates to injury. In an effort to correlate level of injury with a given depth of deformation in clay, Bir and colleagues re-created real-world cases identified from survivors' databases by matching the ammunition and stand-off distances of field instances. They found a 50% risk of severe injury was associated with 43.6 ± 27.3 mm of deformation in the clay block [27]. That means 50% of individuals would sustain a severe injury while meeting safety standards. In automotive standards, a 5% risk of injury occurring is the prescribed limit, as this is when injury is considered unlikely to occur [29]. The defence standards differ slightly, with a 10% risk of AIS 2+[2] injury accepted as a pass/fail criterion in some body

[2] The Abbreviated Injury Scale (AIS) AIS is a standardized system for classifying the type and severity of injuries. It ranks injuries on an ordinal scale of 1 (minor injury) to 6 (nonsurvivable/currently untreatable injury). This is further discussed in Section 1.6.1 Abbreviated Injury Scale (AIS).

regions [30]. Nonetheless, a 50% probability of sustaining a severe injury resulting from behind armour blunt trauma is higher than broadly accepted.

1.5.5 Stand-Off Distances in Shields on the Market

There are numerous manufacturers that produce composite ballistic shields used for police and defence personnel that conform to the National Institute of Justice standards. These include Armour Express (AE), Protech, Paraclete, TYR Tactical, RTS Tactical, and NP Aerospace, among others. Several stand-off distances are employed in the field, defined as the distance from the back of the shield to the front of the upper extremity. These range from 0 mm to 50 mm. In the 0 mm stand-off, the arm is directly in contact with a thick foam pad. There is usually no indication of the pad thickness, but it can range from approximately 20 to 50 mm. Varying stand-off distance is a potential design approach that may influence the amount of shield deformation the upper extremity experiences thus altering the severity of the impact.

1.6 Injury Criteria, Scales, and Injury Risk

Injury criteria are fundamental tools in assessing the severity of loading and the consequent risk of sustaining an injury. They are used when developing standards to assess protective equipment to determine an acceptable level of risk to which an individual may be exposed. Injury criteria correlate physical parameters, such as force or acceleration, with a probability of a certain body region being injured in a specific fashion.

1.6.1 Abbreviated Injury Scale (AIS)

Injury classification scales are typically based on medical diagnoses. The Abbreviated Injury Scale (AIS) is the most widely used and provides scores for each body region for six levels of increasing injury severity. It was developed in 1971 and is regularly revised and updated by the Association for the Advancement of Automotive Medicine (AAAM). It has been continuously improved since its conception and is currently on the AIS© 2015 revision. The basis for this scoring is threat to life rather than disability resulting from injury, where 6 is maximum injury (*i.e.*, currently untreatable, Table 1.2 [31]. The AIS is a single, time-independent value for each injury which does not consider a cumulative injury effect [32]. It is also the basis for the Injury Severity Score (ISS), which is a calculation of the multiply injured individual, and can include up to three contributing injuries. A statistical approach such as regression analysis is used to account for large variations in tolerance data. Injury severity, or the AIS score, is related to independent input variables such as acceleration, force, *etc.* In defence, the acceptable potential injury is generally AIS 2+ (*i.e.*, a moderate or greater injury) for pass/fail criterion [30]. The Maximum AIS (MAIS) represents the maximum injury severity of an occupant at an AIS level (*i.e.*, the highest single AIS for a person with one or more injuries) and is commonly used in the automotive safety environment [33].

Table 1.2: The AIS Classification
The AIS severity score is described with respect to the importance to the whole body, assuming the injury occurs to the otherwise healthy adult [32].

AIS Code	Injury
0	Non-injured
1	Minor
2	Moderate
3	Serious
4	Severe
5	Critical
6	Maximal
9	Unknown

1.6.2 Injury Risk Curves

These injury criteria are statistical probabilities that are used to predict the likelihood of injury occurring based on an applied load (force, moment, acceleration, *etc.*, Figure 1.5). Injury criteria are expressed as probability curves rather than absolute thresholds due to the wide variation in biologic factors that exist for a given population or loading scenario. Once they are developed, an acceptable level of injury risk can be selected, and a corresponding load (or another factor) limit can be specified. They are developed on cadaveric specimens and applied to mechanical surrogates (*e.g.*, Anthropomorphic Test Devices) to relate the risk of sustaining a specific injury to a measured value. The injury risk curves developed for the upper extremity will be discussed in more detail in Section 1.8, Injury Risk to the Upper Extremity.

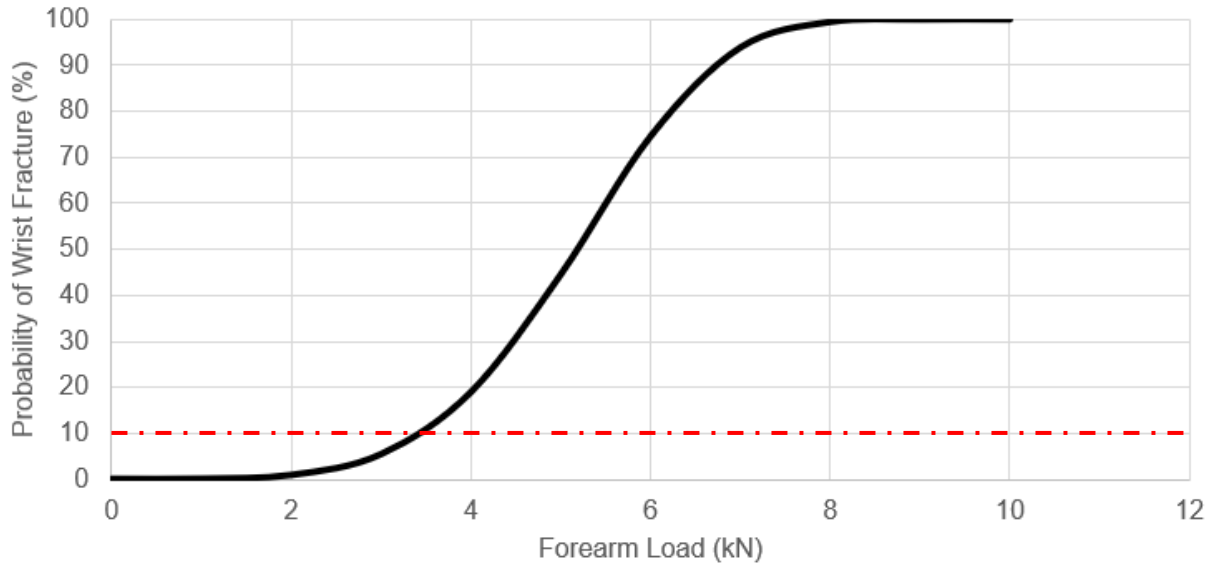

Figure 1.5: Example Injury Risk Curve
A demonstrative injury risk curve relates the probability of sustaining a specific injury to an applied load. This curve relates the probability of wrist fracture to forearm force (measured in kN). The 10% prescribed injury risk here would be approximately 3.5 kN. Note this is not based on existing experimental data and uses an exemplar dataset.

1.6.3 Injury Assessment Reference Values

An Injury Assessment Reference Value (IARV) is a threshold value that is defined such that below this value a specified significant injury is considered unlikely to occur for the scenario in question [34]. Depending on the type and severity of injury, the threshold can range from 5 to 50% risk of injury and is dependent on the type of ATD used (due to varying stiffness parameters). Note that if a measure falls below an IARV this does not ensure that significant injury will not occur, since IARVs are not specified for every type of injury to which one may be exposed [34]. The Insurance Institute for Highway Safety (IIHS) published IARV for significant injury-related parameters. The side impact crashworthiness evaluation is most relevant to behind shield blunt trauma loading mechanisms [35]. The only metric it considers in the upper extremity region is lateral shoulder deflection, which cannot exceed 60 mm.

1.7 Surrogates

As it is ethically irresponsible to conduct injurious testing on living human subjects, models must be used to represent the human response.

1.7.1 Animal Models

The use of instrumented animal models allows for the pathophysiological effects of the cardiovascular and respiratory systems during injuries. As you cannot ethically subject human volunteers to injurious testing, animals provide the only potential surrogate to study the pathophysiological response to impact injury and characterize the sequalae following an injury [36]. This is particularly relevant in behind armour blunt trauma studies, where there are significant physiological effects that can cause serious injury. The contusion response can have serious effects (*e.g.*, pulmonary contusions can be a critical AIS 5 injury). Animal models also allow for a younger donor population. Although valuable information is obtained from animal models, scaling these data and applying it to human injury risk must be conducted with caution.

1.7.2 Post-Mortem Human Subjects (PMHS)

Post-Mortem Human Subjects (PMHS) are used to establish injury limits, as it is ethically irresponsible to conduct these tests on live subjects. Human cadaveric testing currently provides the most realistic biological response to injury as they are exact geometrical and anatomical representations of human tissue. It is advantageous as it allows for the insertion of instrumentation to measure forces and moments and can undergo injury [37]. Furthermore, it allows for the investigation of specific population responses. Careful selection can allow for some control of surrogate properties like biological sex, age, body mass and stature.

There are associated limitations, in that there are large variations in injury tolerance among a given population. These subjects are generally obtained from an older population, have significant handling, storage, and disposal challenges, and are very expensive. Further, they are unable to measure internal load without substantial modifications that may affect tissue tolerance. They are also unable to exhibit a physiological response, meaning there is no muscle tone or internal pressure applied. Substantial variations exist among specific population groups such as males and females, the elderly and middle-aged, and children and adults [38] which poses a significant issue. This frequently leads to a wide variation in the anthropometric and mechanical properties of specimens, and results in generating large injury risk corridors. Nonetheless, data collected from PMHS testing is frequently used in the defence, automotive, and sports injury sectors to validate artificial surrogates and determine the associated injury response criteria.

1.7.3 Anthropomorphic Test Devices (ATDs)

Anthropomorphic Test Devices (ATDs, or 'crash test dummies') are frequently used for evaluating injury risk in the automotive and defence industries. They are designed to be biofidelic, *i.e.*, respond similarly to the human response for a given loading condition, and are equipped with instrumentation to collect data in a repeatable and reproducible manner in impact scenarios. A significant challenge associated with determining human risk of injury is that it varies for individuals of different stature, age, and sex, and is also highly dependent on the applied force, loading direction, and load rate. As such, ATDs on the market are designed with segment mass and size to represent different demographics, as well as instrumentation to collect kinematic and kinetic data for common injuries. The most common device is the 50th percentile male ATD, designed to represent the average male. Scaled versions of this device exist to represent the two

extremes: the 5th percentile female (most vulnerable) and the 95th percentile male (most robust), in the hopes of capturing most of the population within these extremes. Specialized military ATDs have been developed in response to the unique loading conditions that are associated with short-duration, high-rate impact events (*e.g.*, WIAMan, Diversified Technical Systems, Novi, United States). These have not yet received widespread adoption and are designed for specific loading events that did not consider behind shield blunt trauma.

Alongside injury criteria, these devices are useful in assessing injury risk. Measures collected using an ATD are compared to the injury criteria, established through research on PMHS to provide an estimation of the risk associated with the applied load. While these devices are designed to be biofidelic by representing the geometry, mass, mass distribution, kinematics and kinetics of the human body, they are also designed to be repeatable and durable, so they cannot represent the human body response. Some limitations of these devices include anatomically incorrect components, lack of muscle tone and other soft tissue properties representative of humans, and the inherent limitations associated with using engineering materials to represent biological material properties (*e.g.*, viscoelastic properties and dissipating energy through failure).

As ATDs can only collect measurement in discrete locations, historically the focus has been on the areas of severe injury locations such as the head, thorax, and lower extremities. As only approximately 4.1% of injuries occur in the upper extremity during automotive collisions [39], the upper extremity of ATDs have not received much attention. Therefore, there are only three viable ATD options that contain embedded instrumentation in the area of interest: the SID-II, the Thor 50th Male and the WorldSID 50th Male.

The Hybrid III (Humanetics Innovative Solutions, Farmington Hills, United States) ATD family (representing the 5th Female, 50th Male and 95th Male) are the most widely referenced

anthropomorphic test devices in safety standards as they are designed for frontal automotive collisions. The SID-IIs (Small Side Impact Dummy) is a full body ATD representative of the 5th percentile female and is based on the Hybrid III frontal ATD and upgraded to meet the needs of side impact measurements. It contains instrumentation in the head, spine, abdomen, pelvis, shoulder, elbow, femur, knee and tibia. In side impact testing, the shoulder complex can transmit relatively high forces to the thorax, but the human tolerance to such loading is not well established [35]. As such, the focus of the upper limb measurements was how it transfers force to the thorax. The instrumentation in the upper extremity is therefore inadequate for the present application, containing only a shoulder load cell (measuring forces in three directions) and elbow load cell (measuring moments in two directions), and shoulder and arm linear accelerometers.

Kemper and colleagues (2005, 2013) assessed the biofidelity of the SID-IIs (*i.e.*, the small side impact dummy) in comparison to PMHS [40] [41]. This included whole bone three-point bending tests on humeri at static and dynamic loading rates, as well as a series of compression tests performed at dynamic rates, with matched testing on the SID-IIs upper limb segment [40]. PMHS arms exhibited a considerable toe region (*i.e.*, a considerable amount of deflection under very low force before any substantial increase in force) which the SID-IIs arm did not, so it did not fall within the response corridors of the 5th percentile female [41].

The Thor 50th Male, Test device for Human Occupant Restraint is primarily used as a frontal impact dummy. It has improved biofidelity in comparison to the Hybrid III [42] and contains instrumentation in the head, spine, abdomen, pelvis, upper arm, femur, knee, tibia and foot. It contains load cells in the clavicle and upper arm to measure energy transfer through the arm to the thorax. It contains no instrumentation in the forearm of the upper extremity and is therefore not a suitable ATD for BSBT applications.

The Worldwide harmonized Side Impact Dummy (WorldSID) 50th Male is intended to be unique from other test devices and is a technically advanced side impact dummy [43]. It has two options available for the upper extremity: the half arm or the full arm. The full arm is instrumented to measure upper and lower arm loads (6-axis), elbow moments, elbow angular displacements, and 3-axis acceleration at the elbow and wrist. It can be modified to remove instrumentation and replaced with structural components. The full arm anthropometry is based on the UMTRI (University of Michigan Transportation Research Institute) anthropometry set and is constructed of a metallic instrumented bone structure with a soft flesh and skin covering [44]. It has been rated on the International Standards Organization (ISO) classification as having 'good' biofidelity with good repeatability and reproducibility; however, these tests did not include the full arm [43]. There are currently no defined injury criteria and injury risk functions for the WorldSID 50th Male, as only preliminary WorldSID injury criteria have been used to make comparisons to other ATDs [44].

1.7.4 Finite Element Models (FEMs)

Experimental testing of cadaveric specimens is limited in that it is expensive, laborious, and generally only a single injurious exposure can be conducted. Automotive and defence manufacturers employ finite element modeling (FEM) to conduct early design and safety assessments as they offer a useful method for evaluating injury risk. Models have many advantages such as allowing for a variety of experimental variables to be investigated and at relatively low cost. The model geometry is subdivided into simple shapes in order to compute the stresses and strains throughout the structure. Once a model is built it must be validated with known

experimental data to ensure it outputs accurate predictive data. They are typically analyzed using a computer-based solver (*e.g.*, Ansys LS-Dyna, San Jose, CA, USA).

A critical component of a human body model is the selection of appropriate material properties. Often, bone is divided into gross regions (*i.e.*, cortical *vs.* cancellous) and each region is assigned a bulk property. This is typically conducted due to the complex computation nature of dynamic tests. Materials are typically elastic-plastic, so the properties required to define the materials are the density, elastic modulus, Poisson's ratio, yield stress, and tangent modulus. The elastic-plastic material model of bone can be evaluated by investigating the force, time duration and impulse of the simulation in comparison to the experimental data.

Advanced predictive numerical models offer advantages over PMHS and ATD testing in that they are developed using anthropometric and material data of imaging from humans and have the potential to serve as omni-directional dummies [45]. Highly detailed models are required for predictive capabilities to evaluate new situations that include changes in loading rate and mode. There exist several detailed numerical whole-body human models that have been undergoing continual improvements for the purposes of predicting injury in automotive crashes. Examples of these models include the H-model [46], HUMOS [51], THUMS [47], and GHBMC [50].

The H-model represents the 50th percentile male human body and was conceived primarily to assess skeletal injury risk resulting from car crashes. The upper extremity of the H-model (H-UE) mainly consists of deformable and damageable bones and flesh padding [46]. Active and passive muscle forces are modeled with bar elements using the Hill muscle model. Nonlinear contact interfaces model the cartilage layers on shoulder and elbow joints.

The Total Human Model for Safety (THUMS, Toyota Motor Corporation and Toyota Central R&D Labs., Inc., Aichi, Japan) is the most advanced open-sourced upper extremity model

currently on the market. The model represents the 50th percentile adult male (AM50 Occupant Model), with a height of 173 cm and weight of 77.3 kg [47], and is based upon the dataset obtained from CT scans of a 39-year-old male with a BMI of 25.8. It has been heavily validated with automotive properties [48]. Previous validation work of the upper extremity includes single bone validation studies of the humerus, as well as validation of the forearm as a biomechanical system [48] [49]. There are also anatomical simplifications of the upper extremity that affect the biofidelity of the model, such as the lack of soft tissue in the hands, elbow joint capsule, and articular cartilage in the joints [49]. The THUMS model has undergone several studies to improve its biofidelity.

The Global Human Body Model Consortium (GHBMC, Rochester Hills, MI, USA) male 50th percentile model has a weight of 77.1 kg and a height of 175.3 cm [50]. To date, there has been no known validation work conducted specifically for the upper extremity. One recent study evaluated the response of the shoulder to lateral impacts, but the forearms of the model were removed [50]. Full body validation work has been conducted, along with regional validation of the head, neck, thorax, abdomen and pelvis/lower extremity. The upper extremity portion of the GHBMC does not include forearm musculature.

The Human Model for Safety (HUMOS) is based on the 50th percentile European adult male, with a standing height of 173 cm and a weight of 80 kg [51]. It has not received much research attention and still requires additional validation.

1.8 Injury Risk to the Upper Extremity

Injury tolerance levels for the upper extremity have been evaluated for a number of reasons, including slip and fall prevention, sports injury prevention, and automotive safety (Figure 1.6). However, the fracture tolerance of bones changes depending on direction of loading [52]. Joint orientation must also be considered when developing injury criteria, as the variability of the magnitude and direction of the joint's force vector can influence injury mechanisms and patterns [53, 54, 55]. Therefore, in order to develop a thorough understanding of injury risk to this region, PMHS testing must be conducted at a range of loading conditions on different anatomical locations of the arm.

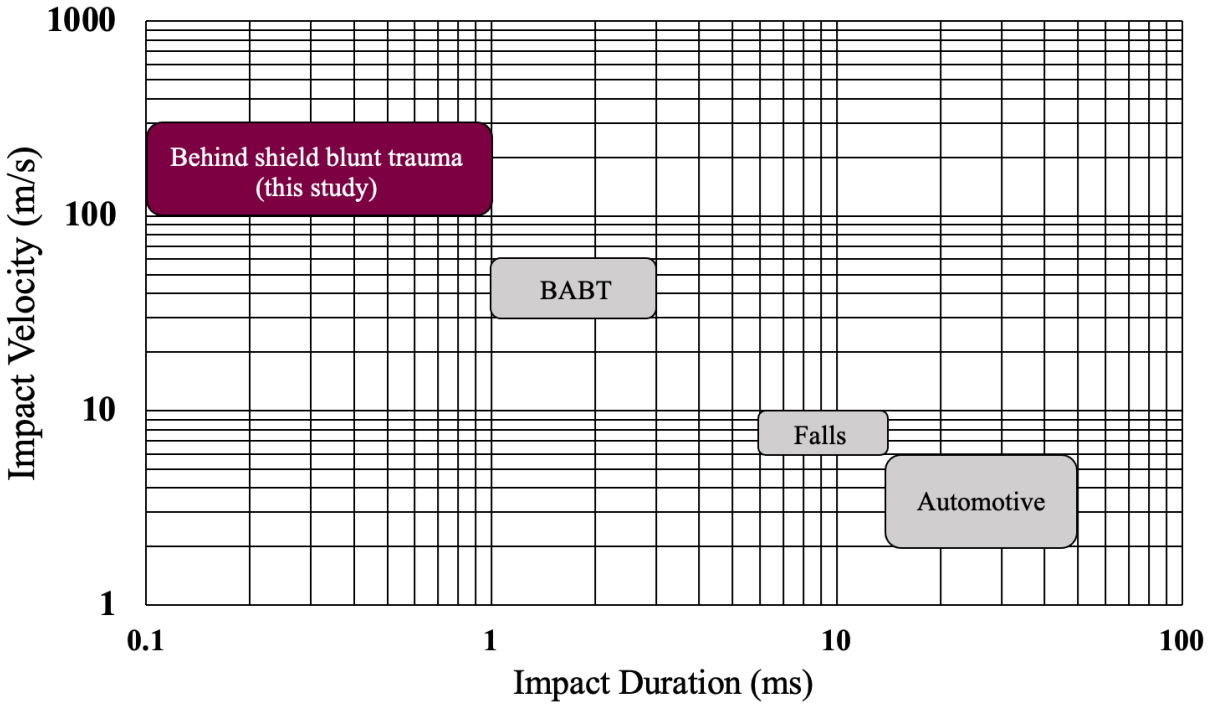

Figure 1.6: Impact duration and velocity of various injurious loading events.
Behind shield blunt trauma occurs over a much shorter duration and has a much higher impact velocity than previously studied events with established injury criteria.

Loading as a result of shield deflection occurs over a very short time duration, which will affect the injury threshold. The strength of bone increases with increased strain rate [56]. This principle is well established, as one of the oldest studies on strain rate dependence was performed by McElhaney and colleagues [57]. The rate at which PMHS are loaded has been shown to affect fracture threshold on the whole-bone level as well, with tibias average fracture tolerance increasing by 24% when impact speed increased from 6 to 12 m/s [58].

A review of each of the four anatomical regions that will be evaluated for fracture threshold because of shield deflections was conducted, to develop an understanding for the potential injury outcome and threshold. To date, no studies have been performed to evaluate injury to this region as a result of ballistic impacts, so the thresholds outlined are estimations based upon lower energy dynamic or quasi-static tests. The outcomes of these studies as they stand in terms of injury thresholds cannot be directly applied to behind shield blunt trauma due to differences in impact energies, durations and loading orientation. The focus of the current work was investigating bone failure (*i.e.*, fracture). An estimation of these limits for each anatomical region will be used as the basis for conducting pilot testing throughout the present study.

1.8.1 Hand

Limited research has been conducted on investigating the fracture tolerance of the hand, most of which applies to developing safety standards for ergonomic purposes. In a recent study by Carpanen *et al*., drop tests were conducted on 21 PMHS specimens, at impact speeds ranging from 2 to 4 m/s (2019). This study aimed to evaluate the injury tolerance of the interphalangeal and metacarpophalangeal joints during lateral, dynamic impacts (simulating a crushing injury) and found a corresponding 50% injury risk at 4.2 kN and 3.0 kN, respectively [59]. Sosa and Alessa

(2021) conducted impact testing on unprotected hands on the metacarpals, where impacts were conducted at approximately 3.2 m/s using a 32 mm hexagonal shaped impactor, intended to emulate manufacturing workplace injuries [60]. The average peak reaction force for the metacarpals was 1,639 N, in which 71% of impacts resulted in a fracture [60]. While both studies conducted dynamic impacts to the prone hand with the intent of discovering injury limits, they used a much slower loading rate than would be expected during shield deflections. The MCP joints (*i.e.*, knuckles) are likely the most susceptible to injury, as they are in close proximity to the back-face of ballistic shields, but the injury threshold may be higher than 4 kN.

1.8.2 Wrist

The majority of the research published in this area has been conducted to address injuries from falling onto an outstretched hand. This semi-axial impact scenario is not relevant to transverse BABT injury outcomes; however, the amount of bone resisting injury in these two orientations is similar. While oriented differently, the carpal bones and distal radius are vulnerable in the transverse impact scenario and may be informed by the semi-axial impact tolerance. Spadaro *et al*. identified the fracture limit to be 2,410 ± 913 N for the scaphoid bone in forward fall orientations, and 1,640 ± 980 N for the distal radius [61]. This testing was conducted on 21 intact forearm PMHS in which a platen impacted the dorsiflexed wrist.

More recently, Reeves *et al*. investigated the dynamic wrist response in the axial orientation of paired forearms and found the mean fracture force to be 6,565 ± 866 N, much higher than Spadaro *et al*.'s findings [62]. The impacts were conducted at a velocity of 3.9 m/s and energy of 35.6 J as compared to Spadaro *et al*., who tested in quasi-static conditions, at a gradual increasing load of 4.2 x 10-4 m/s. Reeves *et al*. also isolated tendons from four of the forearm musculature

and investigated the effects of initial muscle activation on fracture force, in which a higher failure threshold of 8,665 ± 5,133 N was reported in specimens with muscle force applied prior to testing. They suggested in the absence of significant findings that the muscle forces applied in their investigation may have been negligible relative to the large external impact force [62]. There was a large variation in fracture forces in the wrist, likely due to variations in the sex and anthropomorphic size of cadavers used and uncertainties associated with muscular activation.

The dynamic impact tolerance of the wrist in the transverse impact orientation is expected to be somewhere in between these two findings, as BSBT testing in dynamic conditions is expected to be much higher than Reeves *et al*. These studies provide a basis for the expected fracture tolerance of the wrist; however, the orientation and impact conditions vary substantially from behind shield impacts and therefore cannot be directly applied.

1.8.3 Forearm

Impacts to this region of the upper extremity have received the most attention in research to date. Several previous studies have investigated the fracture threshold for the forearm when struck in the frontal plane (on the prone surface directed anteriorly), a similar orientation to that experienced during BSBT. However, this research has primarily been conducted to investigate injury outcome as a result of side airbag deployment, in which the impact impulse is different due to differences in loading rate (approximately 4.42 m/s [54]) and duration (greater than 45 ms [63]). The distribution of the impact is also larger and less focal in comparison to BSBT. Saul and colleagues (1996) assessed the potential for forearm fracture due to deployment of air bags using a Hybrid III ATD [64]. The Hybrid III arm was instrumented with accelerometers at the wrist, elbow and shoulder and strain gauges to allow measurement of the accelerations and moments on

the upper extremity. Measures from this study included distal resultant bending moments of up to 105.4 Nm and proximal resultant bending moments of up to 131.1 Nm. The elbow resultant acceleration was as high as 131.1 g's.

The tolerance of the human forearm under dynamic bending load at two different impact speeds, 3.3 m/s and 7.6 m/s, has been investigated [65]. Impact velocity affected mean impact force, in which 2,083 N was measured for the high velocity impacts and 1,860 N for the low velocity impacts (though not significantly, $p = 0.486$). Given that the shield impact velocity is much higher than this study, there would likely be a substantial effect on peak force. The mean failure bending moment for the high velocity impacts was 99 ± 39 Nm. The male specimens had a significantly higher mean fracture force in comparison to female specimens, of 2,368 N for males and 1,377 N for females. However, this value was highly correlated to bone mineral density, bone mass, and forearm mass [66].

The effect of loading rate was also studied by Begeman *et al*., who examined the difference between static and dynamic impacts on the forearm (1999) [84]. In dynamic bending, a drop weight was used to load the arm at approximately 3 m/s. Fracture of ulna or radius occurred with an average peak force of 1,370 N and an average moment of 87 Nm. Static fracture load and moment tolerances were approximately 20% lower than dynamic tolerances. It is therefore expected that the forearm will fail as a result of bending, should sufficient displacement to this region occur and is expected to be in the 90 Nm range in behind shield blunt trauma loading scenarios.

Duma and colleagues conducted a series of investigations into the fracture tolerance of the upper extremity. They started with dynamic three-point bending tests using a 9.48 kg impactor resulting in impact velocities of 4.42 m/s [54]. The purpose was to investigate the influence of impact direction on the forearm and found the supinated position to be 21% stronger (91 Nm) than

the pronated position (75 Nm). The injury criterion for the forearm of the 50th percentile adult male was determined to be 108 Nm [54]. Injury risk functions for the 5th percentile female forearm were also investigated at the humerus, wrist and elbow. Forearm risk functions predicted a 50% risk of injury at 58 Nm of bending of the forearm. These studies also observed that when the arm was in the pronated position, the radius fractured after the ulna, and while in the supinated position, both bones fractured at approximately the same time. They also noted that while the arm was in the supinated position it carried approximately 17-21% (depending on male *vs.* female) more load than when in the pronated position.

Hardy and colleagues (1997, 1998) used cadavers to investigate two different types of airbag systems, where the forearms were positioned in the path of a deploying airbag. They used the peak distal forearm speed and the average distal forearm speed as forearm-fracture predictors [52]. The peak distal forearm threshold speed was established as 15.2 m/s, while average distal forearm speed was 11.7 m/s [67].

These studies illustrate the importance of developing injury criteria for the expected orientation, loading rate and magnitude of impacts. However, no investigations to date have investigated forearm response at rates typical of behind shield blunt trauma, so these data cannot be applied to shield standards.

1.8.4 Elbow

Impacts to the elbow have been investigated for transverse impacts typical of side airbag deployment, in which a pendulum impacted the elbow of PMHS in the sagittal plane [53]. A variety of elbow orientations were investigated, and the average force to fracture the olecranon was 4.1 kN and the distal humerus was 3.8 kN. Of note, Amis and Miller identified that the locations of

fracture were dependent on the elbow joint flexion/extension angles [53]. Duma *et al*. observed that elbow injuries can not only be caused by an axial force but also by a force acting vertically relative to the horizontal forearm (elbow shear force) [63]. They determined that there is a 50% risk of injury when 1,680 N is applied to a 5th percentile female [68].

Another study by Duma *et al*. compared moments in the elbow due to hyperextension to both fracture and dislocation potential. Results included a 50% risk of elbow fracture with a bending moment of 56 Nm, and 100% at 186 Nm, while a 50% risk of dislocation occurred at 93 Nm and 100% risk of dislocation at 194 Nm [63]. These were developed with respect to 5th percentile female PMHS, so are limited in both the studied population and types of impacts applied.

A summary of relevant injury tolerance studies to the upper extremity is included in Table 1.3.

Table 1.3: Summary of Relevant Previous Injury Tolerance Studies of the Upper Extremity
The failure threshold (when produced in the respective study) for the midsized male at the anatomical regions of interest are summarized. The loading rate is also included when indicated.

Anatomical Location	Study	Loading Information	Failure Threshold
Elbow	Duma *et al.*, 2004	Dynamic	50% risk at 56 Nm
	Duma *et al.*, 2001	Dynamic	50% risk at 1,680 N
	Amis and Miller, 1995	Dynamic	4,100 N (olecranon), 3,800 N (distal humerus)
Forearm	Pintar and Yoganandan, 2002	Dynamic, 7.6 m/s	2,083 N
	Duma *et al.*, 2002	Dynamic, 4.42 m/s	126 Nm
	Begeman *et al.*, 1999	Dynamic	1,370 N or 87 Nm
	Bass *et al.*, 1997	Dynamic, 3 m/s	50% risk at 67 Nm
Wrist	Reeves *et al.*, 2014	Dynamic, 3.9 m/s	6,565 ± 866 N
	Duma *et al.*, 2003	Dynamic	50% risk at 1,700 N
	Greenwald *et al.*, 1998	Dynamic	2,821 ± 763 N
	Chiu and Robinovitch, 1998	Dynamic	1,780 ± 650 N
	Spadaro *et al.*, 1994	Quasi-static, 4.2 $x10^{-4}$ m/s	2,410 ± 913 N (scaphoid), 1,640 ± 980 N (distal radius)
Hand	Sosa and Alessa, 2021	Dynamic, 3.2 m/s	1,639 N (metacarpal failure force)
	Carpanen *et al.*, 2019	Dynamic, 2 and 4 m/s	50% risk at 4,200 N (interphalangeal), 50% risk at 3,000 N (metacarpophalangeal)

1.9 Behind Shield Blunt Trauma Project Status, November 2019

A previous study by Bolduc *et al*. reproduced a realistic scenario representing a barricaded shooter during a hostage rescue operation, and collected the impact duration, peak force and impulse from a uniaxial load cell behind a shield [69]. This is the only known study that has

evaluated ballistic shield impact testing for the purposes of behind shield force transfer. Two different ‘stand-off distances,’ a term used to describe the distance between the back of the shield and the force sensor, were tested (20 mm and 40 mm), resulting in peak forces from 16 kN to 4 kN. Although an important first step in characterizing the deformation rate of ballistic shields, the setup used in this study produced overly rigid boundary conditions. Developing boundary conditions expected of the upper extremity when holding a shield are necessary.

The WorldSID 50th Male ATD upper limb has been previously modified by our group (outlined in Steinmann *et al*., 2021) to evaluate force at four critical locations: the hand, wrist, forearm and elbow (Figure 1.7). In this study, a PCB piezoelectric uniaxial washer style force sensor (model 201B05, PCB Piezotronics, MTS Systems Corporation, Depew, NY, USA) with a capacity of 22.25 kN was added to the elbow, wrist and hand. The hand was modified to maintain consistent orientation relative to impact, to ‘grip’ the handle as a point of fixation, and to mount instrumentation on the dorsal side. The integrated 6-axis load cell was assumed to collect forces at the forearm location, and the PVC flesh was removed to allow for this additional instrumentation and to increase repeatability of impacts [70].

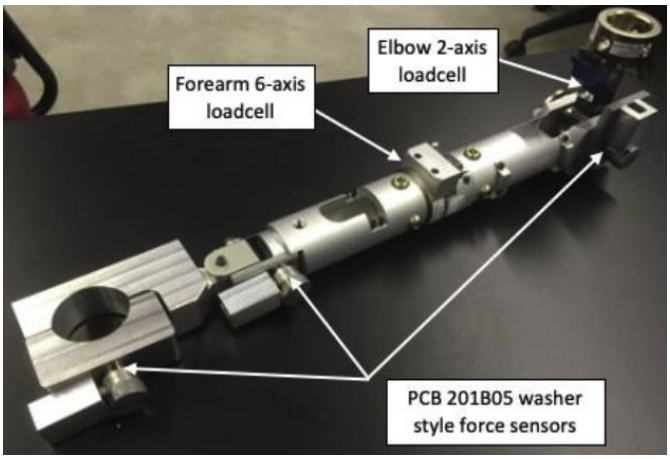

Figure 1.7: Final modified WorldSID ATD from our February 2020 ballistic testing [70]. The new hand, wrist and elbow structures were fully assembled with impact caps and cable protection channels.

This modified ATD was used for testing at Defence Research and Development Canada (DRDC) – Valcartier Research Centre for investigating two types of composite ballistic shields, both rated Level III in NIJ 0108.01 [20]. Ballistic testing was conducted using the modified ATD to measure the impact forces behind ballistic shields using a 7.62 x 51mm ball projectile (9.6 g) fired at 850 m/s nominal velocity, in accordance with testing a Level III protective material as outlined in NIJ 0106.01 [70]. This testing was limited to the elbow and hand, as the forearm load cell experienced mechanical damage during testing and there were limited shields (and thus shots) available. Results from this study indicated that although both shields were successful in preventing projectile penetration, they had substantially different back-face velocities (181 ± 35.5 m/s *vs.* 275 ± 13.9 m/s) and deformations (1.8 ± 0.3 cm *vs.* 3.8 ± 0.3 cm). The forces measured in this study (2.3-5.3 kN) were in line with those reported in the previously mentioned study (4-16 kN) [69]; however, greater characterization is required for all anatomical locations of interest. Further, there was a ‘wrap-around’ of the shield back-face deformation onto the force sensors,

which may have artificially reduced the peak force of the impact by not recording the entirety of the event.

Additional modifications to the revised ATD are required; the requirements for the modified ATD are as follows. The ATD must collect uniaxial load data at four locations in the upper extremity: the hand, wrist, forearm and elbow due to their close proximity with ballistic shields and unique anatomy and boundary conditions. This instrumentation must be capable of collecting forces up to 16 kN, with impact durations ranging from 1-3 ms [69] [70]. As the deformation behind a shield is unpredictable, a large force sensing area is required, as well as the ability to detect impacts if they are slightly offset. The exact peak deformation point was challenging to predict given the propagation of the bullets through ballistic shields and created a larger back face signature than expected. The PCB force sensors previously used had a small sensing area (0.685 in.) so it would be beneficial to increase the size to capture the full impact event. Finally, the ATD must be able to mechanically withstand the focal impacts expected of shield deformation and has previously demonstrated inadequacy in this [71].

1.10 Study Rationale

To investigate the fracture threshold of upper extremities exposed to high-rate impact loading as a result of shield deflections, a modified ATD is required to characterize upper extremity loading during ballistic shield impacts. Due to complexities surrounding tissue testing, loads representative of ballistic shields deforming must be applied to post-mortem human surrogate (PMHS) in a laboratory-based setting, so establishing a mechanism to do so is required. Upper extremities representative of the 50^{th} percentile male due to their prevalence in the Canadian

Armed Forces [72] need to be acquired as no existing injury limits fill the need for this unique loading scenario. Shield behind armour blunt trauma (BABT) can result in injuries to the elbow, forearm, wrist and/or hand, so paired PMHS sectioned at the mid-humerus allow for investigation of injury potential while limiting cadaveric material required. Although injury criteria have been developed for these locations for automotive safety, workplace injury mechanisms, injuries as a result of falling on an outstretched hand and sports injury prevention, resultant injury is highly dependent on joint orientation, loading conditions and anthropomorphic size. The upper extremity injury threshold for BABT applications is largely uninvestigated and is expected to vary from fracture threshold research that has already been conducted in this area. A finite element model that accurately predicts fracture resulting from behind shield blunt trauma would be useful to employ for evaluating future shield designs. Results from the PMHS experimental portion of this work can assist in validating an existing model for these high-rate impacts.

1.11 Objectives and Hypothesis

The objectives of this thesis were:

1. Modify an existing WorldSID ATD upper extremity and employ it during ballistic testing to quantify loading behind a shield as a result of ballistic impacts at four vulnerable locations: the hand, wrist, forearm and elbow;
2. Experimentally determine four corresponding injury criteria for the upper extremity specific to behind shield blunt trauma; and
3. Investigate the applicability of the THUMS upper extremity for behind shield blunt trauma injury prediction by comparing the response to experimental results.

The corresponding hypotheses were:

1. The injury criteria would be substantially different than previously reported criteria in these anatomical areas due to the unique loading conditions and orientation of the upper extremity while supporting a ballistic shield. Anatomical area (and therefore boundary condition) will also have a substantial effect on injury criteria.
2. The THUMS as it stands will not accurately predict injury to the upper extremity, but with modifications could be employed to test the fracture pattern and location, load, and load duration resulting from behind shield blunt impacts.

1.12 Thesis Overview

This thesis is written as a sandwich thesis. Chapter 2 includes the experimentally obtained characterization of behind-shield blunt trauma loading to the ATD upper extremity. Chapter 3 includes the experimental study that was conducted on cadaveric upper extremities to develop injury criteria for the hand and forearm in response to shield BABT, with a comparison to WorldSID ATD measured outputs. Similarly, Chapter 4 assesses the response of the wrist and elbow, which used the contralateral limbs and has a modified experimental setup in comparison to Chapter 3. Chapter 5 describes the methods that were used to modify and assess the response of an existing finite element model of the isolated upper extremity (the THUMS) to evaluate its response to behind shield blunt trauma. Chapter 6 summarizes the conclusions of the thesis, as well as discusses potential future work related to these studies.

Chapter 2 – Behind Shield Blunt Trauma: Characterizing the Back-face Deformation of Shields with a Focus on Upper Limb Loading

Overview: *In this chapter, the augmented WorldSID ATD was employed to measure the back-face deformation that occurs when ballistic shields absorb a projectile in accordance with test standards to address Objective 1. This chapter has been published in Annals of Biomedical Engineering (2023, V51, pages 1331–1342, DOI: https://doi.org/10.1007/s10439-023-03141-0). The proper permission from the copyright holder (Springer Nature) has been obtained to include the publication in this thesis (License #5618250048981).*

2.1 Abstract

Shield back-face deformation (BFD) is the result of composite ballistic shields deflecting or absorbing a projectile's energy and deforming towards the user. BFD can result in localized loading to the upper extremity, where the shield is secured to the user. An augmented anthropomorphic test device upper extremity was used to quantify this applied load. Four locations along the upper extremity were tested—the hand, wrist, forearm, and elbow—for investigating differing boundary conditions and their effect on resultant load. Varying stand-off distances, the distance between the back of the shield and the force sensor, were investigated. Digital image correlation was also conducted to measure the dynamic displacement of the shield. The mean peak

back-face velocity of the shield was 208.4 ± 38.8 m/s, while the average affected area was 1,505 ± 158.3 mm^2. Impulse was not significantly affected by anatomical location for the same stand-off distance; however, as stand-off distance decreased, the measured force significantly increased ($p < 0.05$). Notably, impact duration did not differ significantly for any of the impact scenarios. This is the first step in developing injury criteria for this region resulting from behind shield blunt trauma, and these data will be used for developing injury thresholds in post-mortem human surrogates.

2.2 Introduction

Behind-armour blunt trauma (BABT) refers to bodily injuries that may occur as a result of the rapid deformation caused by projectiles striking protective equipment [1]. Portable ballistic shields, used by defence personnel for diffusing dangerous situations, are supported by a user's arm to protect themselves and those around them against projectile penetration. When a bullet strikes a composite ballistic shield, the shield plastically deforms along the woven pattern of the structure to absorb the impact energy, a process termed back-face deformation (BFD). The high rate deformation of the shield resulting from projectile penetration may cause injury to the upper extremity due to its proximity to the shield, as has been seen in body armour and helmet BABT [23]. Currently, there are no known standards that limit the allowable force transferred to the upper extremity through shield BABT, only standards pertaining to projectile penetration [2].

As BFD often occurs for body armour, standards exist that define a maximum allowable static post-impact indentation, taken as a pass/fail criterion [20]. The most widely referenced standard was developed by the National Institute of Justice, NIJ 0101.06 [20], specifying the

allowable BFD of protective materials for five types of protection classifications (types II–IV), based on the types of ammunition a material must protect against. The National Institute of Justice standard specifies a maximum of 44 mm of static post-impact indentation into clay backing. It has been widely established that this indentation standard is inadequate [23, 26], as it is unknown how exactly it correlates to injury [27, 28]. It was also developed concerning injury potential to the torso and was assessed using animal surrogates, the results of which were scaled to humans [1]. There are many limitations to this standard and its application to shields. This clay does not match the response of living soft tissue during impact and is almost entirely plastic, while impact is a dynamic event. Most importantly, this standard cannot be directly applied to ballistic shields which are in contact with a different anatomical area, likely with different injury thresholds and boundary conditions.

Four anatomical locations along the upper extremity may be particularly vulnerable to injury as a result of this type of impact: the hand, wrist, forearm, and elbow. Due to confidentiality surrounding the defence sector, it is unknown how prevalent these injuries are; however, the complex geometries and varying boundary conditions along the upper extremity present an interesting opportunity for investigating injury risk to these regions. Upper extremity fractures are generally classified as AIS (Abbreviated Injury Scale) 2–3, indicating a moderate severity of injury [31]; however, these injuries can lead to the user dropping the shield, putting themselves and others at greater risk of exposure to injury or even death. Development of BFD-limiting shield standards is therefore critical.

Although injury criteria have been developed for these locations for automotive safety [66], prevention of injuries resulting from falls on the outstretched hand [62], and sports injury prevention [73], these mechanisms typically occur over a longer duration (greater than 50 ms) and

have an impact velocity less than 5 m/s. As injury is known to be highly dependent on the direction of loading [53] [55], loading conditions [67] [58], and anthropometric size [66], these thresholds cannot be directly applied to this loading condition (over 20 m/s for less than 1 ms) [70]. The upper extremity injury threshold for high rate loading typical of BFD is largely uninvestigated and is expected to vary from fracture threshold research that has already been conducted in this area. To develop injury limits from this loading scenario, post-mortem human surrogates (PMHS) need to be tested under loading conditions representative of the BFD of shields. To do so, this impact event must be properly characterized in terms of the duration, magnitude, and profile shape. The long-term goal of this research is to conduct injurious testing on human surrogates. There are many challenges associated with PMHS testing, including variation among specimens which limits repeatability, and the vast preparation and expense associated with these types of tests. For repeatability purposes, the events should first be characterized with a mechanical surrogate.

Behind-armour blunt trauma has been previously studied in the context of torso injuries [27, 28], and head injury [74, 75]; however, limited investigation has been conducted into injury risk for BFD of ballistic shield impact conditions [69, 70]. Protecting against BABT is becoming increasingly relevant as efforts are made to reduce the weight and thickness of protective armours to allow for greater mobility.

Two known previous studies have investigated ballistic shield deformation [69, 70].The first investigated the BFD of ballistic shields to develop an operational test protocol aimed to address the level of shield protection required to prevent forearm and hand bone fractures [69]. They proposed optimizing stand-off distance (*i.e.*, the distance between the back of the shield and a force sensor) as a design parameter in future shield iterations. In practice, of shields currently in use, stand-off distance can vary from 0 to 50 mm. Findings from this study indicated that

decreasing the stand-off distance from 40 to 20 mm increased the peak force from 4 to 16 kN [69]. This work highlighted the high forces resulting from BFD of ballistic shields but was limited to a single rigid boundary condition. Previous work from our group characterized the effect of composite ballistic shield type and stand-off distance on back-face loading for two more realistic boundary conditions, at the elbow and hand, using a modified Worldwide Harmonized Side Impact Dummy (WorldSID) 50th percentile (Humanetics Innovative Solutions, Farmington Hills, MI, USA) male Anthropomorphic Test Device (ATD) [70]. The molded polyvinyl chloride (PVC) flesh hand was replaced with a modified hand structure to facilitate attachment of force sensors and the ability to 'grip' a handle. These impacts resulted in average peak forces up to 5.1 kN over 0.39 ms [70]. However, this testing used small force sensors that may not have captured the full impact event, and a direct comparison between boundary conditions (anatomical location) was not possible due to differing shields (and thus resulting BFDs) used in these impacts. As such, further investigation is required to study the effects of shield deformation on upper extremity loading.

It has also been shown previously that the shape of an impact influences the injury outcome [76]. Therefore, capturing the impact profile of the load applied to the upper extremity over time is important. Researchers have critiqued the use of the final BFD of armour as not representative of the dynamic deformation that occurs throughout the impact event [26, 77]. Digital image correlation (DIC) is useful for characterizing the BFD profile, as it is a powerful non-contact optical technique that may be used to measure three-dimensional deformations. It informs the dynamic deformation, velocity, acceleration, and volume of the BFD and has been used in previous BABT studies [76]. In order to assess the potential injury mechanisms resulting from rapid shield BFD, the shield BFD needs to be characterized so it may be correlated to injury criteria.

This study aimed to investigate the composite shield response from ballistic impacts on the upper extremity, using an augmented WorldSID ATD upper limb. The ATD was employed to investigate the effects of anatomical location and stand-off distance on back-face loading using level III ballistic shields. The goal of the data collected herein is to characterize the dynamic loading that the upper extremity would experience, to inform future work developing injury limits on PMHS.

2.3 Materials and Methods

The WorldSID 50th percentile ATD (representing the anthropometry of an average male) upper limb was previously modified to facilitate measurement of the localized, high-rate forces typical of BABT impacts [70]. These modifications included the addition of a structural hand to facilitate mounting of force sensors (as they required a flat mounting surface per manufacturer installation instructions), as well as facilitating clamping to a 38.1 mm diameter handle. Further modifications were made in the present study to facilitate the addition of larger force-sensors at the hand, forearm and elbow (model 200C20, PCB Piezotronics, MTS Systems Corporation, Depew, NY, USA, 38.1 mm sensing diameter). These force sensors had a fast response time (up to 0.025 ms) and a high measurement range (up to 88.96 kN), making them a suitable measurement system for this application. Depending on the impact location, the inclusion of WorldSID-manufactured structural components rather than the embedded forearm (model W50-71070S11, Humanetics Innovative Solutions, Farmington Hills, MI, USA) and elbow (model W50-71060S11) load cells were used to avoid mechanical damage (Figure 2.1a). For the wrist impact location, a smaller (16.51 mm) force sensor (model 201B05, PCB Piezotronics, MTS Systems

Corporation, Depew, NY, USA) was used due to the limited area of this shot location. An NI-PXIe-1082 Data Acquisition system (National Instruments, Austin, TX, USA) with a NI TB-4330 terminal block that sampled data from the strain-based integrated load cells at 100 kHz, as well as a PXIe-4480 module to sample data from the PCB force sensors at 1 MHz were used for data collection.

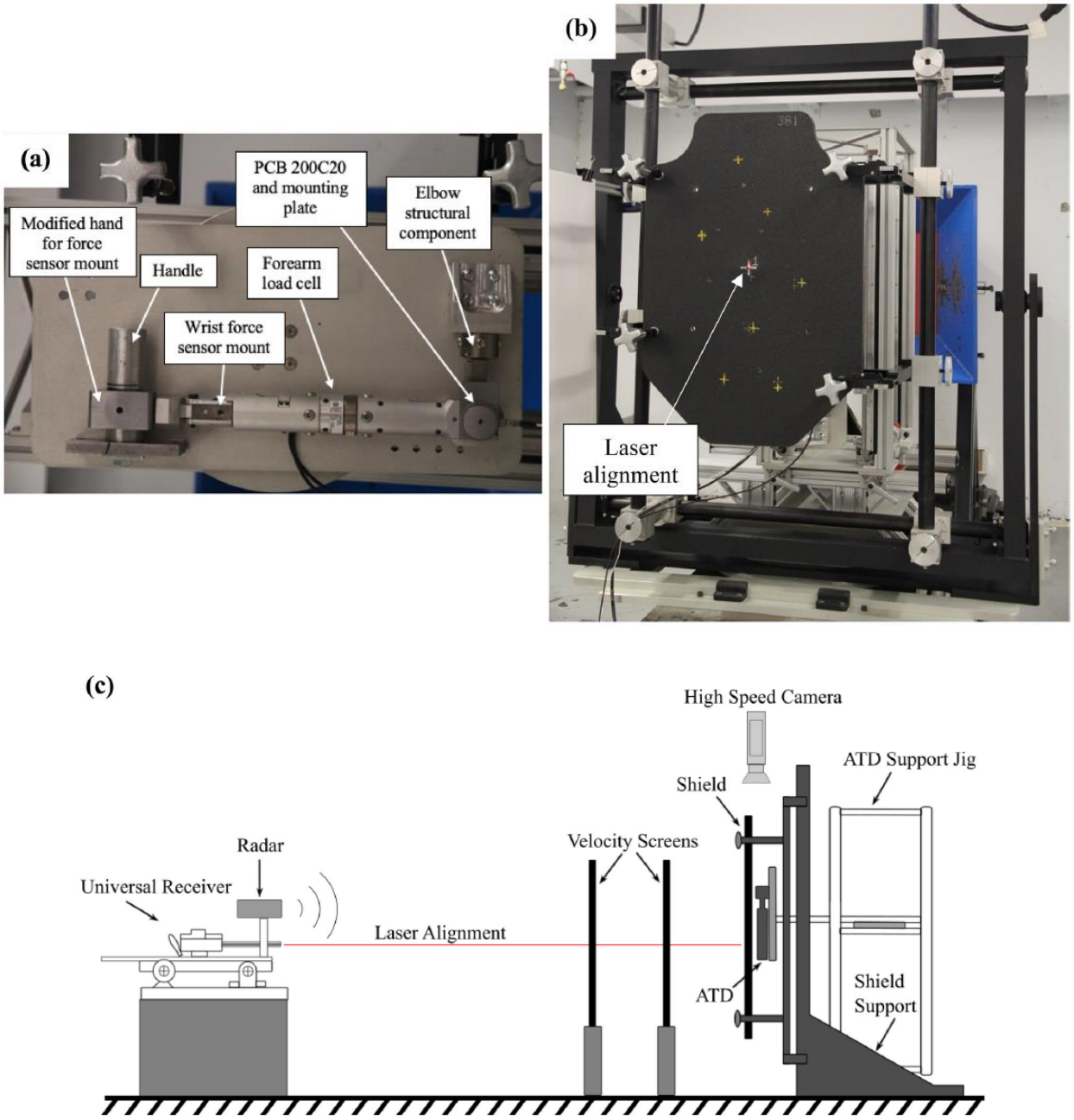

Figure 2.1: (a) Modified WorldSID ATD to facilitate shield BABT data collection, with the handle and humerus mount secured to the baseplate, (b) photograph of the ballistic testing setup with the Level III shield, and (c) schematic of the testing setup.

For each shot, the WorldSID ATD was positioned such that the elbow joint formed a 90°-angle joining the humerus and forearm, confirmed by laser level. The arm was secured to the testing jig at the mid-humerus, and at the hand via the handle that was secured to the baseplate. The entire baseplate was mounted to an ATD support jig, that allowed for lateral translation post-impact.

Ballistic testing was conducted using the augmented ATD to measure the impact forces behind a flat composite ballistic shield, rated Level III in NIJ 0108.01 (Figure 2.1b). All shields that were used were from the same lot number. The trauma-attenuating backing, handles, and supporting hardware were all removed for ease of alignment in the testing jig and high-speed camera recording visibility. The shields were 508 mm wide and 762 mm tall and tapered at each of the four corners. The shield was mounted in front of the arm on an independent testing jig to ensure there was no global shield movement during each impact and was clamped at four locations along the perimeter of the shield. This allowed for the stand-off distance to be controlled for each test. The forearm was positioned in a vertical orientation, and all hardware was checked to ensure rigid attachment.

A 7.62 mm NATO ball projectile (9.6 g) was fired at 838 ± 15 m/s, in accordance with the testing procedure for Level III protective materials. The bullet was fired from a universal receiver test barrel (Wiseman 09- 2016(08), Bill Wiseman and Co. Inc., College Station, TX), with a length of 559 mm and a right-hand twist rate of 1:305 mm (Figure 2.1c). Shots were aligned using a laser sight through the universal receiver with the centre of the force sensor at the predetermined impact location. The bullet travelled 15 m down the test range, and velocity was measured using a Doppler radar (model BR-198 3502, Infinition Inc., Trois-Rivières, QC) and confirmed using two photoelectric screens (model 53131 A, Oehler Research Inc., Austin, TX) that were spaced 1 m

apart. Two high-speed video cameras captured the event to characterize the response of the shield, one overhead video and one video parallel to the shot path (Fastcam SA-X type 324 K-M2, Photron USA Inc., San Diego, CA, USA) at 30,000 fps with a 384 x 264-bit resolution. An additional high-speed camera of the same type was positioned parallel to the shot path and in front of the ballistic shield to measure the yaw of the bullet (36,000 fps, 1024 x 288 resolution) after each shot, and if the angle of the bullet exceeded 5° the shot was discarded from further analysis. The video footage was analyzed in Photron FASTCAM Viewer Software (Photron USA Inc., San Diego, CA, USA) to calculate the BFD and velocity profiles, while all force data were analyzed in Matlab (MathWorks, Natick, MA, USA).

In-plane delamination from a singular shot typically extended in an approximately 60 mm circular radius along the back-face of the shield (determined from pilot testing). To minimize the effects of adjacent shots, each shot location was placed a minimum of 150 mm apart from any previous shots, 120 mm away from the shield edge, and 100 mm away from the shield-manufactured holes created for supporting the shield via the arm. This allowed for six shots per shield to be tested while still being considered independent from previous shots. Shot order was randomized. A seventh shot was also obtained from each shield to investigate the effect of an edge shot on the deformation observed in the shield. The shot-to-edge distances for these shots was 122 ± 7 mm (mean ± SD).

Differing stand-off distances, *i.e.*, the initial spacing between the back-face of the shield and the front face of the arm-mounted force sensor were investigated for each location to evaluate its effect on arm loading. These distances ranged from 10 to 20 mm, as determined from the amount of BFD from initial pilot tests. A limited number of shots and shields available meant the number of repetitions at each shot location varied (Table 2.1).

Table 2.1: Impact Matrix
The load cells were integrated WorldSID 50th Male instrumentation, while the PCB force sensors were modifications to collect force at the impact location.

Anatomical Location	Data Collected	Stand-off Distances Tested (mm)	Repetitions
Hand	PCB 200C20, elbow 2-axis load cell, forearm 6-axis load cell	15	4
		20	4
Wrist	PCB 201B05, elbow 2-axis load cell, forearm 6-axis load cell	20	3
Forearm	PCB 200C20, elbow 2-axis load cell	15	4
		20	4
Hand	PCB 200C20, forearm 6-axis load cell	10	3
		15	4
		15, edge shot	4
		20	4

High speed video of the ballistic testing was assessed to determine shield back-face velocity and the thickness of the shield after deforming. For each shot, three to five still frames extracted from the high-speed video were imported to Fiji ImageJ (Fiji, version 1.53f51, National Institutes of Health, Bethesda, MD, USA) and processed using the MTrackJ plugin. The peak of deformation was identified within each frame and the frame rate (30,000 fps) determined the interval between still images, allowing for the calculation of back-face velocity between successive frames. The velocity was then averaged between the overhead and parallel videos for each shot to reduce error associated with obstruction of view caused by prior BFD patterns.

Three extra shots at the conclusion of the testing procedure were allocated for the purposes of digital image correlation (DIC) to evaluate the evolution of the deformation profile and confirm the back-face velocity calculated from the high-speed video analysis. There was no ATD

positioned behind the shield for the DIC testing. Two high-speed video cameras (Fastcam SA-X, type 324K-M2) at 40,000 fps with a 512 x 512 resolution were used. The orientation of the cameras were aligned per manufacturer suggestions, and a cross-section of the model was acquired to measure the profile and obtain the peak values. For these tests, the polyurea (black protective coating on the shield) was removed to avoid a false profile, as this was shown to detach from the shield during previous ballistic tests. The shields were painted with a thin layer of white paint to create a uniform surface for image capture. Black speckling was then applied to the shield to provide landmarks for tracking the back-face deformation. The images were analyzed using GOM Correlate Pro software (version 2018) and two orthogonal sections were used to track the deformation profile of the BFD. The DIC analysis allowed for the study of the shield deformation independent of what was in contact with it (*i.e.*, the arm) in order to isolate the response of the shield itself.

Two of the shields were X-rayed post-test to investigate the extent of the bullet fragment travel distance within the shield, and check whether the spacing between shots was sufficient. The DIC and X-rays informed the calculation of energy of the BFD of the shield (Eqs. (1) to (3)) [78].

$$E_{BFD} = E_{impact} - E_{deformation} \quad \text{Equation (1)}$$

$$E_{BFD} = \frac{1}{2} m_{bullet} \cdot {v_{bullet}}^2 - \frac{1}{2} m_{deformation} \cdot {v_{deformation}}^2 \quad \text{Equation (2)}$$

$$E_{BFD} = \frac{1}{2} m_{bullet} \cdot {v_{bullet}}^2 - \frac{1}{2} \rho_{affected} \cdot A_{affected} \cdot {v_{deformation}}^2 \quad \text{Equation (3)}$$

In the above equations, EBFD is the energy of the BFD, as calculated from the energy of the deformation subtracted from the input energy of impact. The m_{bullet} and v_{bullet} represent the

mass and velocity of the bullet, respectively. Similarly, $m_{deformation}$ and $v_{deformation}$ represent the mass and velocity of deformation of the shield during impact. The mass of the deformation of the shield is simplified to the product of the affected density (q) and the affected area ($A_{affected}$), as determined from the X-ray images taken at the completion of the testing sequence.

The forearm and elbow ATD data were dual-pass filtered using a second-order Butterworth low-pass filter with a cut-off frequency of 1,250 Hz, in accordance with industry testing standards [41] [30]. An analysis of the frequency domain informed the filtering technique of the PCB data, in which a second-order Butterworth low-pass filter with a cut-off frequency of 40 kHz was used. Impact duration was considered to have begun when the PCB force sensor (at the impact location) increased to 5% of the peak force and concluded when the force fell below 5% of the peak force. All impact profiles were aligned by peak force. The jig travel distance after each impact was also recorded. A one-way Analysis of Variance (ANOVA) with posthoc Tukey test was conducted on peak force, duration of impact, and impulse to compare among impact locations and stand-off distances, with a significance threshold of $\alpha = 0.05$.

2.4 Results

Thirty-six shots in total were conducted for this study. High-speed video confirmed impacts were centered on the force sensor (Figure 2.2). The intact shields weighed 7,092.8 ± 87.6 g (mean ± standard deviation). Removal of the handle, hardware, and trauma attenuating backing reduced the shield weight by approximately 800 g. The average bullet velocity immediately prior to impact was 840.9 ± 4.7 m/s. The back-face velocity did not vary significantly among stand-off distance ($p = 0.87$) and across all impacts and was 208.4 ± 38.8 m/s (mean ± standard deviation). The

combined yaw of the bullet was 1.44 ± 0.69°, with the maximum yaw 2.91°. The average jig travel distance post-test was 3.94 ± 4.92 mm. Maximum forces at the location of impact ranged from 2,026 to 18,979 N, with durations between 0.180 and 0.730 ms (Table 2.2).

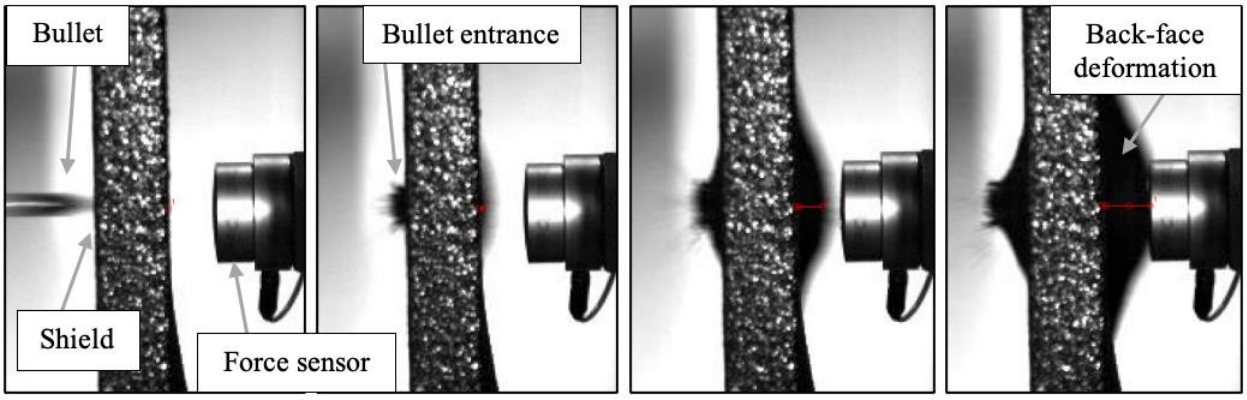

Figure 2.2: Pictures from the high-speed video footage of shot 12 (15 mm stand-off hand shot).

Table 2.2: Summary of collected data from the force sensors at the locaiton of impact (mean ± standard deviation).

Anatomical Location	Stand-off Distance (mm)	Maximum Force (N)	Impact Duration (ms)	Impulse (Ns)
Hand	15	9,326 ± 3,141	0.440 ± 0.145	1.187 ± 0.322
	20	3,750 ± 874	0.483 ± 0.204	0.646 ± 0.486
Wrist	20	5,274 ± 1,571	0.542 ± 0.140	0.552 ± 0.324
Forearm	15	6,931 ± 792	0.493 ± 0.138	1.106 ± 0.155
	20	3,753 ± 956	0.515 ± 0.272	0.498 ± 0.201
Elbow	10	18,979 ± 3,229	0.180 ± 0.045	1.303 ± 0.303
	15	5,833 ± 1,054	0.623 ± 0.160	1.036 ± 0.168
	20	2,026 ± 492	0.730 ± 0.307	0.517 ± 0.168

When comparing the peak force at each anatomical location at the 20 mm stand-off distance, only the wrist location was significantly higher than the elbow (p = 0.004, Figure 2.3a). The hand and forearm were higher than the elbow, although not significantly (p = 0.1 for both).

When comparing the peak force at the elbow among stand-off distances, each incremental decrease in stand-off distance produced significantly higher results ($p < 0.05$). The peak forces at the hand and forearm were significantly less at the 20 mm standoff distance compared to the 15 mm stand-off distance ($p = 0.02$ and $p = 0.001$, respectively, Figure 2.4). At each anatomical location, the force followed the same general shape throughout the duration of the impact among stand-off distance. At the elbow, the difference between the peak force at the 10 mm stand-off distance in comparison to the 15 mm stand-off was much greater than the 15 mm in comparison to the 20 mm. Interestingly, the forearm force–time traces were very similar for both the 15 mm and 20 mm impacts.

(a)

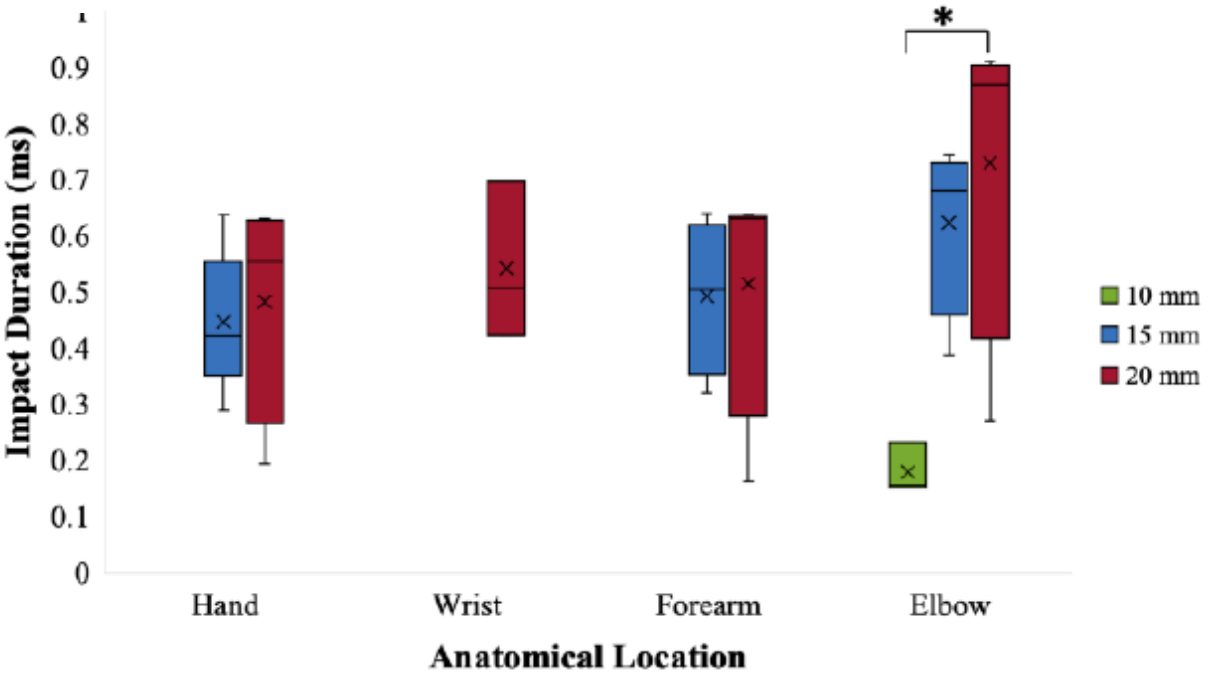

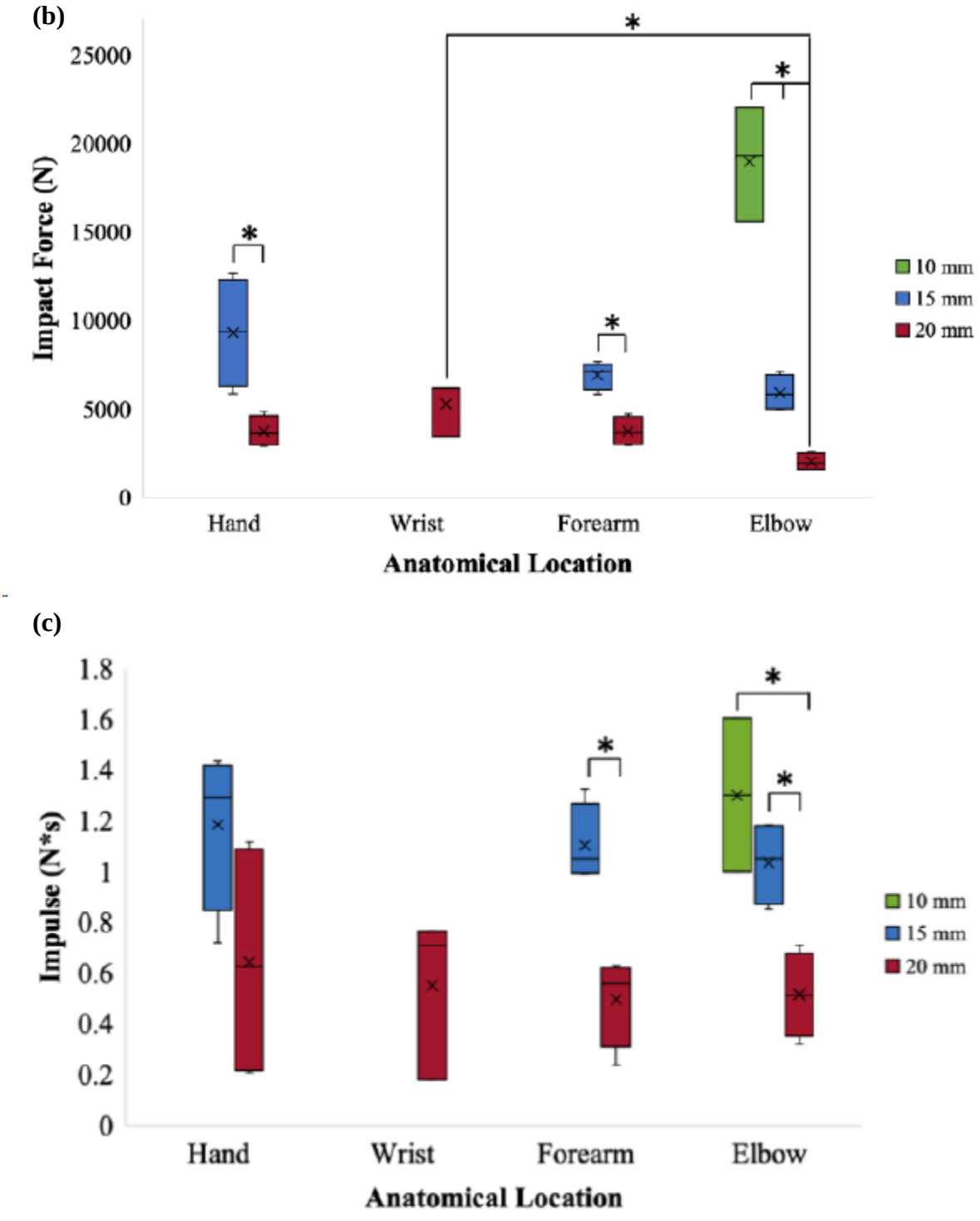

Figure 2.3: The (a) impact duration, (b) peak force, and (c) impulse with respect to stand-off distance at each anatomic location. Note '*' denotes a significant difference, α = 0.05.

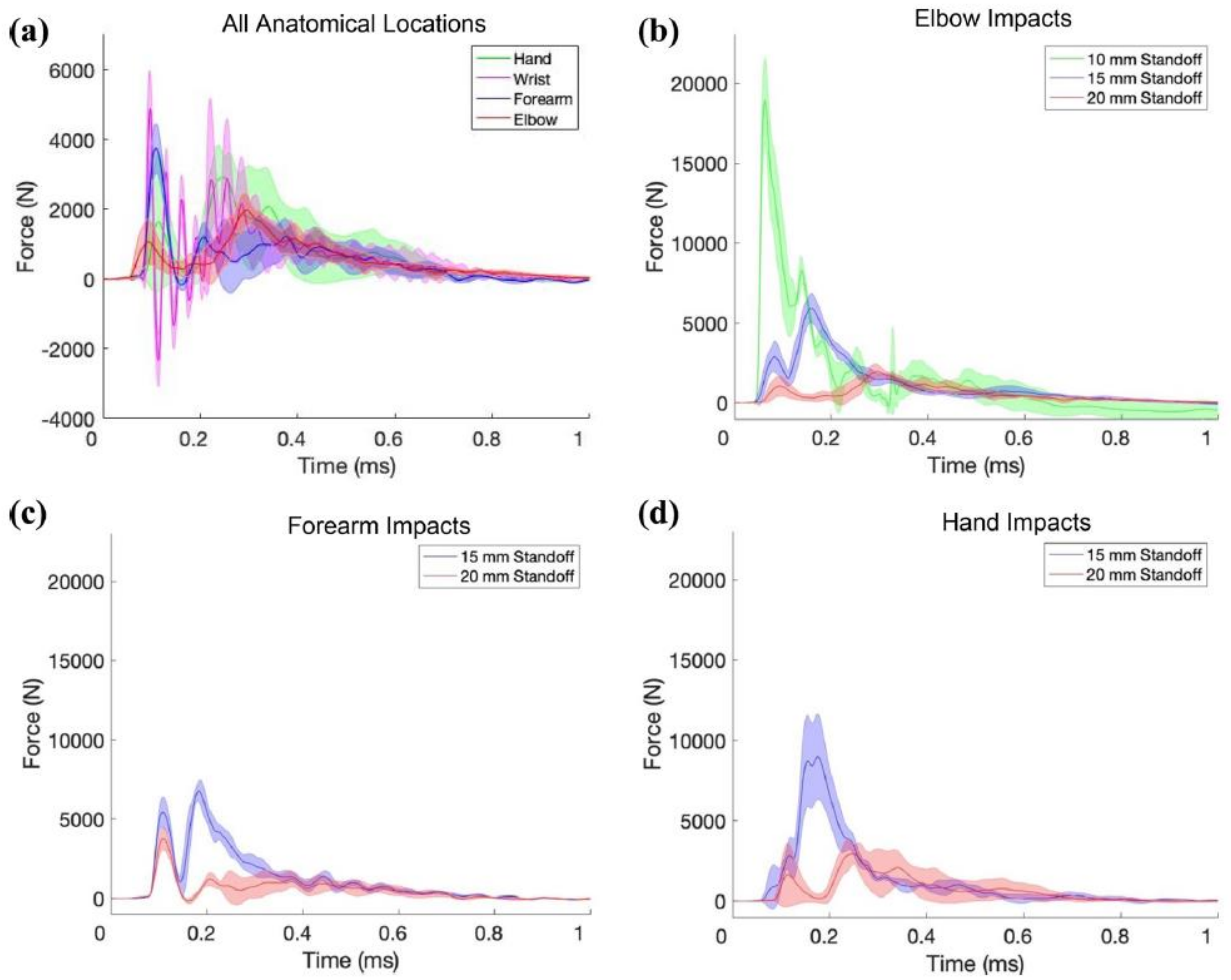

Figure 2.4: Force-time traces, aligned by peak force for (a) each anatomical location, (b) for each stand-off distance at the elbow, (c) for the forearm, and (d) for the hand.
The line represents the mean of each repeated impact, and the shaded region represents the standard deviation of the repeated trials.

No significant findings were noted when comparing impact duration among anatomical locations (Figure 2.3b). The elbow did tend to have a slightly longer impact duration than the hand and forearm, though not significantly (p = 0.5 and 0.6, respectively). The average impact duration among all impacts was 0.509 ± 0.217 ms. The impact duration at the elbow 20 mm stand-off was significantly higher than 10 mm (p = 0.02). When comparing the impulse at each anatomical

location at the 20 mm stand-off distance, results were also statistically insignificant (Figure 2.3c). The elbow impulse was significantly less at 20 mm when compared to the 10 mm stand-off (p = 0.003) and when compared to the 15 mm stand-off (p = 0.02). For the forearm impulse, the 20 mm stand-off was also significantly higher than the 15 mm stand-off (p = 0.001).

For elbow impacts, the peak force measured at the elbow location was 18,979 ± 3,229 N, while the forearm load cell recorded 105.8 ± 8.2 N. The forearm moment generated during impacts was highest for impacts to the elbow and was highest at the 10 mm stand-off distance (10.1 Nm). The 15 mm stand-off distance forearm impacts created the greatest elbow moments (11.5 Nm). When investigating the effects of the shield edge shots, the peak force (9,160 ± 534 N) was significantly higher than for same impact condition mid-shield (*i.e.*, a non-edge shot), 15 mm stand-off elbow impacts (p = 0.002). The impulse was also significantly higher (p = 0.003), but the duration did not differ significantly (p = 0.3).

Based on the result of the DIC, the back-face velocity was 199.65 ± 9.37 m/s, which is consistent with the value determined from the high-speed video camera still image analysis. The polyurea coating was removed for the DIC shots (Figure 2.5a). The evolution of the deformation profile associated with BFD during impact was tracked for two orthogonal sections (Figure 2.5b), and the corresponding deformation profile in the z-axis at four different times were plotted for Sect. 1 (Figure 2.5c). The time resolution between measurements was not sufficient to get the exact times for each profile. During impact, some data points were not trackable (the grey region of the DIC contour mapping in Figure 2.5b), therefore deformation could not be tracked exactly at the maximum deformation. Therefore, one point was tracked, which was as close as possible to the point of impact (by analyzing the first two images of the DIC where the deformation begins) and provided close values to the section results. It was not possible to completely track the apex of the

deformation for all shots (DIC shot 2 and 3) because the paint on the ballistic material was starting to delaminate. Therefore, a second order polynomial regression was used to extrapolate the maximum, which aligned very closely with the DIC data.

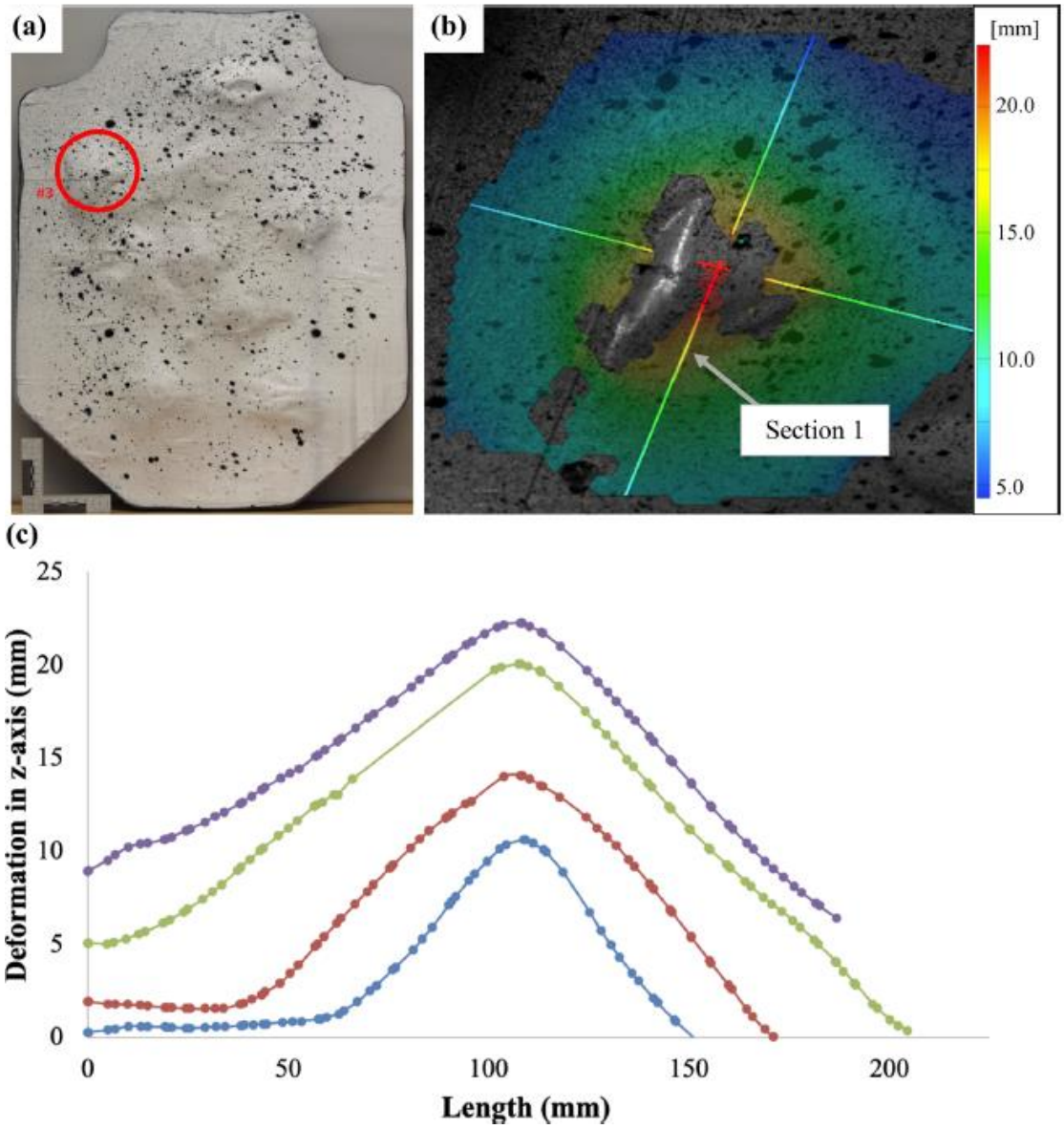

Figure 2.5: Digital image correlation.
(a) Shot location, and spray pattern for the third shot of the DIC, (b) DIC deformation contours with Section 1 highlighted (the length along the shield in which the deformation was tracked), and (c) the tracked deformation from Section 1 at four different time-points during the deformation process, aligned by peak height.

Two shields were X-rayed after testing was completed for a total of 13 shots (Figure 2.6). Two of the shots were from the 10 mm stand-off, five from the 15 mm stand-off (one of which was an edge shot), and five from the 20 mm stand-off. As expected, the bullet fragments were displaced mainly along the orientation of the fibers in the horizontal and vertical directions. This resulted in a square-like pattern of displacement of the fragment inside the shield. The average affected area for all shots collected from the X-ray images (*i.e.*, post-test) was approximately $1{,}504.5 \pm 158.3$ mm^2 and did not vary significantly among stand-off distance ($p > 0.3$). The energy exerted through BFD was approximately 2,982 J. This was calculated by considering the average bullet impact velocity, approximating the areal density (75% of the shield density, 13.742 kg/m^2) of the affected area in the shields post-impact, and the resultant BFD velocity as collected from the DIC.

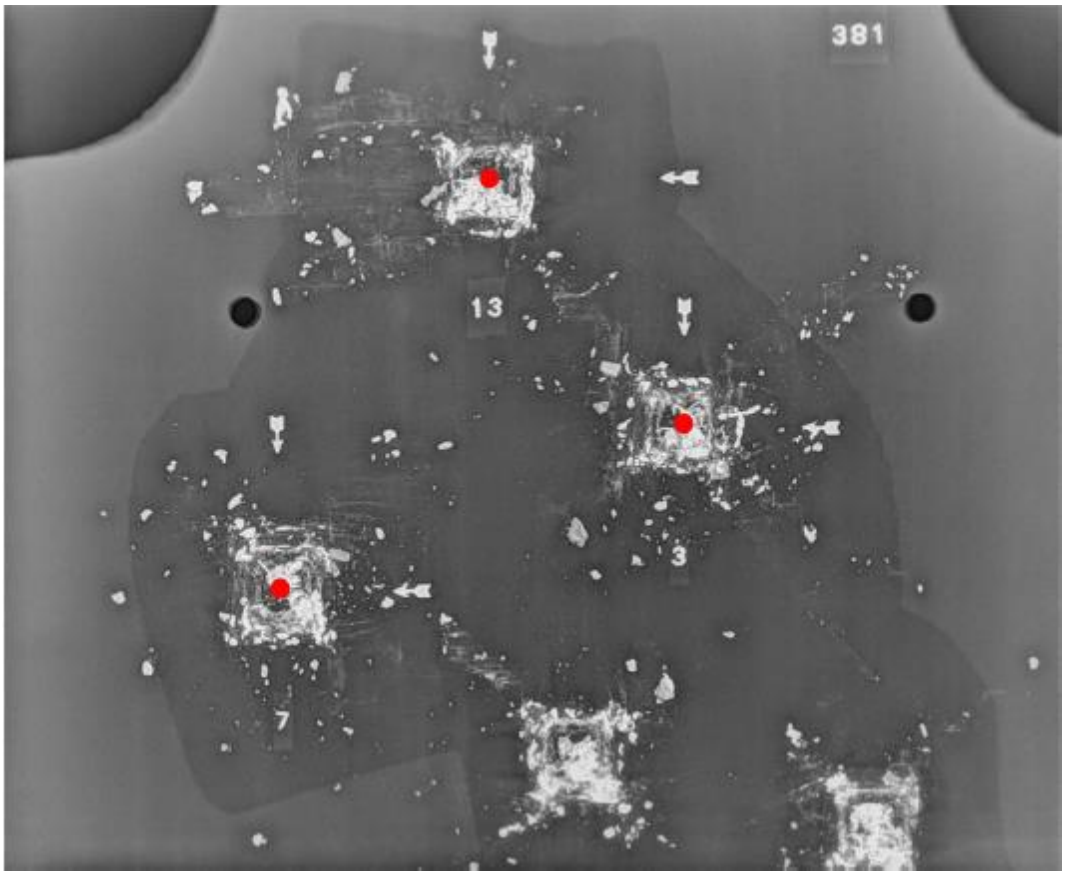

Figure 2.6: X-ray of one shield tested.
This shows the scatter of the bullet within the shield post-test. The white arrows and red dots indicate the bullet point of impact (bullet entry) of each shot.

2.5 Discussion

The generation of force–time curves for quantifying the back-face deformation of shields is the first step in developing biomechanical assessments for this type of loading. The forces generated during these impacts were up to 19 kN over fractions of a millisecond (0.156 ms). Therefore, this impact event is much different than blunt ballistic impacts studied in the context of the thorax, in which forces generated were reported as over 7 kN over several milliseconds [27] or for the head, in which forces over 10 kN were recorded [79]. This is the first study to investigate

both the effects of stand-off distance and anatomical impact location on shield BABT to the upper extremity. The augmented ATD allowed for the capture of this unique loading event at four locations along the upper extremity and this study represents the most robust characterization of the BFD of shields to date. The high magnitude of force data collected at the location of impact, and correspondingly low load and moment data collected elsewhere highlight the focal nature of these impacts.

For each impact location, as stand-off distance decreased peak impact force unsurprisingly increased. This observation is consistent with findings from previous studies [69] [79], where the same trend was observed. Stand-off distance should be considered when developing test standards pertaining to the allowable BFD of shields as well as in future design iterations of shield supports, as this study highlights its potential as an injury mitigating measure. The forces measured in the present study (2.0–18.9 kN) were in line with those reported in a previous study by Steinmann and colleagues (2.3–5.3 kN), with the current study providing a more robust investigation of the effects of anatomical location and stand-off distance [70]. The data collected from the present study was also less variable than previous work. This is likely due to variations in shields used for testing as well as a force-sensing area capable of detecting the entire impact event, while representing boundary conditions realistic of upper extremity impact geometry.

Although there was a small amount of wraparound of the shield on the larger force sensors, there was more wrap-around of shield delamination on the smaller force sensors, as seen in the high-speed video capturing the event. Although the hand, elbow, and forearm impact locations did not have a substantial effect on peak force, the wrist impact location (5,274 ± 1571 N) was significantly higher than the elbow (2,026 ± 492 N), meaning boundary conditions likely do have some effect on force outcome. This finding is surprising as the wrist was the only impact location

that used a smaller sensing area and recorded higher impact forces than the rigid hand. Further investigation of this event is therefore required. Furthermore, while both the hand and the elbow were cantilevered to the forearm, a greater force was experienced at the hand for the same standoff (3,750 N *vs.* 2,026 N). This demonstrates the effect of the much more rigid boundary condition at the hand due to the presence and attachment to the in-line handle.

The majority of attention for upper limb ATDs has been a result of investigations from the automotive industry. To date, most research attention for upper limb ATDs has focused on the automotive industry, and current upper extremities have limited instrumentation, for example, the Hybrid III and Euro-SID 2 ATD's do not include instrumentation in the forearm. The WorldSID ATD is currently the most advanced upper extremity on the market in terms of available embedded instrumentation. The biofidelity and validation of the WorldSID for this application remains unknown; however, match-pair testing with this surrogate and PMHS in the future will allow for assessment of the biofidelity of this augmented ATD and discern whether it is an appropriate tool for assessing injury risk. Unfortunately, due to the focal nature of these impacts, the integrated load cells could not be used, as previously demonstrated by Steinmann *et al*. they cannot mechanically withstand BSBT impacts [70]. The soft tissue also needed to be removed to allow for additional instrumentation at the points of interest. This likely did have some effect on the short duration of the impacts produced in this study and the impacts may be attenuated from soft tissue on PMHS. The results presented also highlighted the extremely focal nature of these impacts, which required characterization through DIC. The DIC provided a more accurate method of determining the back-face velocity of the shield as well as presented interesting results of the shield deflection over time.

Impulse, which is thought to drive bone fracture [80], did not vary among anatomical location. The injury mechanisms involved in BSBT are drastically different from automotive impacts, due to variations in the impact velocity, pulse duration, and peak force applied. The mean forearm fracture force has been reported as 2,368 N for males in dynamic 3-point bending [66]; however, higher velocity impacts are expected to result in higher mean fracture forces, [67] [58] and therefore potentially elevated injury thresholds. There is a gap in the literature where no dynamic injury criteria for ballistic impacts exist for the upper extremity, which will need to be developed for shield standards in the future. This study is the first step in characterizing that risk, which will be used for development of injury criteria on PMHS. The PMHS will be oriented in the same manner as the current study (secured at the mid-humerus and hand on the mounting plate) to replicate boundary conditions, and the BSBT loading conditions developed in this study will be applied.

The primary limitation of this work was the number of tests that could be conducted. Although the shots were presumed to be independent based on the static post-test delamination, there is scatter in the fragmentation within the shield as seen on X-ray images collected post-test. These images supported the assumption that the shots were independent of one another, as physical bridging of the deformation was not observed in the shields. Further, trends of increasing force with shots conducted later in a testing sequence were not observed to indicate any cumulative damage effects.

A secondary limitation was the boundary conditions of the ATD arm. Although ATDs are designed to be biofidelic in the direction of impact, they are generally stiffer than biological specimens [81], so the effects of anatomical location boundary conditions, while not noted herein, may be significant in PMHS. These differences in kinematics will be investigated in a future

PMHS study under these BSBT conditions. Simplifications to the testing setup were also made to ensure a repeatable testing protocol at differing anatomical locations, which included fixing the shield independently of the ATD. However, the deformation of the shield occurred faster than the rearward movement of the shield, which was verified using high-speed video, so this likely did not have a substantial effect. Further, additional instrumentation and facilitating mounting of that instrumentation may have produced overly rigid conditions that are not typical of the WorldSID ATD or biological upper extremities. The ATD upper extremity was mounted at the mid-humerus and hand on a plate that was on linear bearings, allowing for bending only at the elbow and wrist. This meant that some components of the arm could not move relative to one another, but instead as an entire segment. However, due to the short duration of these impacts, limited motion of the upper extremity was expected during the impact events. The global motion of the arm was also very small (3.94 ± 4.92 mm), as measured at the end of each test. Further, the impact event occurred over a very short duration, so it is likely there was insufficient time for post-kinematic motion to have an effect. The lightweight and fast bullet was also impacting a heavy and rigid system, where much of the impact energy would have been dispersed. Effort was made to allow for post-kinematic translation of the upper extremity and supporting structures; however, the force generation does in part depend on the compliance of the structure behind the shield. This is evident by the significantly lower forces recorded in this study in comparison to a previous, rigid jig [69] and should be taken into consideration.

Next, there were challenges associated with conducting the DIC, such as delamination of the white painted surface and loss of tracked points during impact because the event occurred very quickly. The DIC was also conducted at the end of the testing sequence, meaning these shots may

have experienced greater delamination due to the proximity to the edge of the shield and any accumulated degradation from the other shots.

The time-to-peak of the force data was approximately 9 µs. As such, the frame rate of the high-speed video (30,000 fps) was likely too low to capture the entirety of the BFD profile of the shield, as the velocity was based on only four frames. Thus, the shield velocity should be treated as an estimate. The limited number of tests also meant that the number of repetitions at some locations were restricted (*e.g.*, wrist location). The objective was to characterize all four anatomical locations; however, a secondary goal was to develop impact corridors with varying stand-off distances that could be used for future testing on PMHS. As such, the elbow location was tested at three stand-off distances while the wrist location was only tested at the 20 mm stand-off distance. The peak force data collected also had large coefficients of variation (CoV, range 11–34%), which may have limited statistical findings and may be problematic in future standards. This variation is indicative of a high level of variability that was inherent in BSBT testing, as the variation in shield material properties and the effects of repeated shots is unknown.

This work represents the first robust analysis of shield deformation as it pertains to BABT. Impacts at four discrete locations along the upper extremity were characterized as a result of the BFD of a Level III composite ballistic shield. The BFD of the shield (peak force and duration of impact) and the anatomical region to protect differed from documented BABT studies involving helmets and body armours, so standards specific to shields' interaction with the arm are required. The force–time curves generated using the ATD will provide a basis for developing injury limits resulting from BSBT by applying these curves to PMHS. The DIC also presents the shape of the impact that occurs as a result of shield deformation, which will inform the impacting shape on PMHS studies. This work also represents the first step in developing standards and defining the

optimal stand-off distance and allowable impulse due to BFD of shields, to optimize the protective capabilities of shields while minimizing weight.

Chapter 3 – Injury Risk for the Hand and Forearm Under Shield Behind Armour Blunt Trauma Loading

Overview: *This chapter details the experimental testing of post-mortem human subjects of loads representative of behind shield blunt trauma to the hand and forearm, to address Objective 2. This chapter is currently under revision at the Annals of Biomedical Engineering, and upon acceptance and publication, the proper permission from the copyright holder will be obtained to include the article in this thesis.*

3.1 Abstract

Ballistic shields protect users from a variety of threats, including projectiles. Shield back-face deformation (BFD) is the result of the shield absorbing energy from a projectile and deforming towards the user. Back-face deformation can result in localized blunt loading to the upper extremity, where the shield is secured to the user and may cause injury through behind armour blunt trauma (BABT) mechanisms. Post-mortem human subject (PMHS) responses are critical to identify the injury risk in these high-rate scenarios and are used to quantify the injury tolerance. Two vulnerable locations along the upper extremity were investigated – the hand and forearm – using eight PMHS to identify the fracture threshold resulting from shield BABT loading conditions. Impacts delivered to the hand at 16.4 ± 0.8 m/s resulted in failure loads of 3,818 ± 897 N, while the forearm impacts delivered at a similar velocity of 16.9 ± 1.9 m/s had lower failure

loads at 2,972 ± 711 N. The corresponding 10% risk of hand and forearm fractures (as measured on a modified WorldSID Anthropomorphic Test Device) were identified as 11.0 kN and 8.1 kN, respectively, which should be used when evaluating future designs of composite ballistic shields. This study is the first known investigation of the upper extremity to this high loading rate scenario and provides the foundation for future biomechanical research in the area of behind-shield blunt trauma.

3.2 Introduction

Behind-armour blunt trauma (BABT) refers to bodily injuries that may occur due to the rapid deformation from projectiles striking protective equipment [1]. Ballistic shields, used by defence personnel for diffusing dangerous situations, are supported by a user's arm to protect against projectile (*i.e.*, bullets) penetrating through a shield. Currently, there are no known standards that limit the allowable force transferred to the upper extremity through shield BABT, only ones pertaining to projectile penetration [1]. Behind-armour blunt trauma has been previously studied in the context of torso injuries [27] [28] and head injury [75] [74]; however, limited investigation has been conducted into BABT injury risk for ballistic shield impact conditions [82] [70] [69].

As back-face deformation has been recognized as an injury mechanism for body armour, standards have been developed that define a maximum allowable static post-impact indentation into a block of clay (representing the torso), taken as a pass/fail criterion [20]. The most widely referenced standard was developed by the National Institute of Justice, NIJ 0101.06 [20], which specifies a maximum of 44 mm of allowable indentation in a clay backing material. This was developed concerning injury potential to the torso and was validated on goats, the results of which

were scaled to humans [1]. It can therefore not be directly applied to shields, which are in contact with a different anatomical area, likely with different injury thresholds. Two anatomical locations along the upper extremity may be particularly vulnerable to injury from behind shield deformation: the hand and forearm, which are frequently in close proximity to the back surface of the shield. Due to privacy surrounding the defence sector, it is unknown how prevalent these upper extremity injuries are. However, the complex geometries of the hand and forearm, their differing boundary conditions, and the contact with the shield warrants an investigation for the injury risk to these regions.

Behind armour blunt trauma is becoming increasingly relevant as manufacturers strive to reduce the weight and thickness of protective armours to allow for greater mobility. The back-face deformation loading from ballistic shields has been previously characterized in a ballistic testing facility at differing stand-off distances, defined as the distance from the back of the shield to the front of the arm in two previous studies [70, 82]. Several stand-off distances are employed in commercial shields, which range from 0 to 50 mm. Stand-off distance influences the amount of shield deformation applied to the upper extremity, thus altering the severity of the impact.

A Worldwide Harmonized Side Impact Dummy (WorldSID, Humanetics Innovative Solutions, Farmington Hills, MI, USA) 50th percentile Anthropomorphic Test Device (ATD) upper limb was previously enhanced with additional instrumentation and employed to quantify loads at the hand and forearm for shield BABT [70, 82]. Ballistic testing was conducted on Level III shields in accordance with NIJ standard 0108.01 with the WorldSID secured to a custom testing jig positioned behind the shields. In the first study, two different Level III shields were tested, and findings indicated that the back-face response varies dramatically between shield models, even when both had the same protective rating [70]. The measured loads from this study ranged from

2.1 kN to 5.3 kN, while the dynamic back-face deformation of the shield ranged from 1.8 to 3.8 cm, with impact velocities between 6.5 and 163.6 m/s and durations between 0.39 and 1.16 ms [71]. This study was limited in its findings in that the number of impacts conducted was small, and the force-sensing area might not have captured the entirety of the event. An improved WorldSID ATD and supporting jig were developed, with increased force sensing area and greater stability while allowing for translation post-impact [82]. A different kind of Level III ballistic shield was employed to further gather data on the shield response and corresponding load at the hand and forearm when subjected to ballistic testing. As a result of these impacts, the ATD hand recorded forces ranging from 3.8 kN to 9.3 kN over durations of 0.483 ms to 0.440 ms. At the forearm, impact forces were recorded ranging from 3.8 kN to 6.9 kN over durations of 0.515 ms to 0.493 ms. Although these findings were not significantly different from one another as measured on the ATD, the post-mortem human surrogate (PMHS) response has yet to be evaluated. The dynamic back-face deformation of the shield ranged from 4 to 22 mm, with shield impact velocities ranging from 91 to 302 m/s [82]. Results from these studies indicate the specific deformation of ballistic shields is highly dependent on the model tested, and a consistent standard is needed to outline allowable loading transferred to users. First, PMHS limits under a representative behind shield blunt trauma load curve must be determined.

Injury criteria have been developed for the upper extremity related to automotive safety [63] [83] [54], falls prevention [62], and sports injury prevention [73]. Injuries in these scenarios have shown that the resultant injury is highly dependent on joint orientation [83] [54], loading conditions (*i.e.*, rate and duration of impact) [67] [58], and anthropometric size [53]. Several studies have investigated the fracture threshold for the forearm, when struck in the frontal (coronal) plane by side airbags, a similar orientation to that experienced during shield BABT. Impact

velocities ranging from 3 to 7 m/s have been studied, resulting in mean impact forces of 1.4 to 2.1 kN and mean failure bending moments of 94 to 108 Nm [54] [66] [84]. The effect of impact direction on the forearm has also been studied, and findings suggest the supinated position to be 21% stronger (91 Nm) than the pronated position (75 Nm) [54]. Limited research has been conducted on the fracture tolerance of the hand and focused on workplace crushing injuries. Previous dynamic hand impacts have been conducted ranging from 2 to 4 m/s, with peak fracture thresholds ranging from approximately 1.6 to 6.5 kN [59] [60].

While automotive impacts occur in the same orientation as shield BABT, they tend to occur over a longer duration (29.1 ms for automotive *vs.* 0.18 ms for shield BABT) and generally have a smaller magnitude (1.7 kN *vs.* 19.0 kN) [82] [63]. These previously mentioned studies were also conducted using a much slower loading rate than would be expected during shield deflections. The upper extremity injury threshold for high rate loading typical of shield BABT is largely uninvestigated and is expected to vary from fracture threshold research that has already been conducted in this area. These prior thresholds therefore cannot be directly applied to shield standards to protect the hand and forearm from fracture without investigation into the rate effects.

The objective of the present study was to develop injury risk functions for the 50th percentile male upper extremity (the hand and the forearm) due to loading representative of behind shield blunt trauma. The loading measured on the augmented WorldSID 50^{th} percentile ATD upper limb previously employed in a ballistic testing study [82] was used to inform the loading profile applied to PMHS in a laboratory setting to determine the failure thresholds at these loading rates. The results of this were translated to the augmented WorldSID 50th percentile ATD upper limb to propose a safety standard for allowable loading that limits hand and forearm fractures resulting from behind shield blunt trauma. Limits measured on the ATD are proposed herein in order to

evaluate shields for their efficacy in limiting hand and forearm fractures resulting from shield BABT independent of shield model or deformation.

3.3 Methods

3.3.1 ATD Impacts

All testing was completed in a pneumatic impacting apparatus that has previously been used in many impact studies (Figure 3.1a) [58] [85] [86]. The specimens were secured to a jig that had been used in ballistic testing with the augmented WorldSID 50th Male ATD (representing the anthropometry of an average male) to collect load data resulting from shield BABT at varying stand-off distances (defined as the distance between the back-face of the shield and the front of the ATD). The WorldSID ATD was designed for side impacts, and its upper extremity is the most technically advanced for this purpose on the market. It contains a 6-axis forearm load cell and a 2-axis elbow load cell, and modifications including the addition of a structural hand and extra instrumentation were previously conducted to collect loading typical of shield deformation. Details can be found in [82]. The force curves generated from this previous study involved positioning the ATD behind Level III ballistic shields and impacting at four discrete locations along the ATD: the hand, wrist, forearm and elbow. This same jig and ATD were also employed in the pneumatic impacting apparatus to conduct controlled laboratory-based assessments that replicated the average data collected in ballistic tests at the hand and forearm. Translation was permitted in the testing jig post-impact, which was the same as during the ballistic testing (facilitated by using the same supporting jig to hold both the ATD in the ballistic work and the ATD and PMHS in the present work). As with ballistic testing, the flesh of the ATD was removed in the impacting

apparatus to allow for the addition of instrumentation to the modified hand and forearm and ensure a repeatable response over multiple tests.

Impacts were applied by accelerating a 434 g projectile down a 7.62 cm (3") diameter tube by compressed air, travelling approximately 86 cm towards the testing chamber. The design of this projectile was focused on the creation of a durable and repeatable impactor that was lightweight and collected the applied force during impact. The projectile was equipped with two force sensors (model 201B05, PCB Piezotronics, MTS Systems Corporation, Depew, NY, USA), each with a maximum capacity of 22.24 kN, mounted in parallel below the impact cap of the projectile to measure the applied force (Figure 3.1b). This allowed for a combined capacity of 44.48 kN. The impact cap (Figure 3.1c) was designed such that the shape of the impact cap matched that of the apex of the deforming shield during ballistic impacts, and the stiffness was based on the affected area and material properties of the shield during ballistic testing [82]. To maximize the strength while keeping it lightweight, the impacting cap was embedded with a spherical periodic diamond lattice and 3D printed out of an aluminum alloy (AlSi10Mg) using direct metal laser sintering.

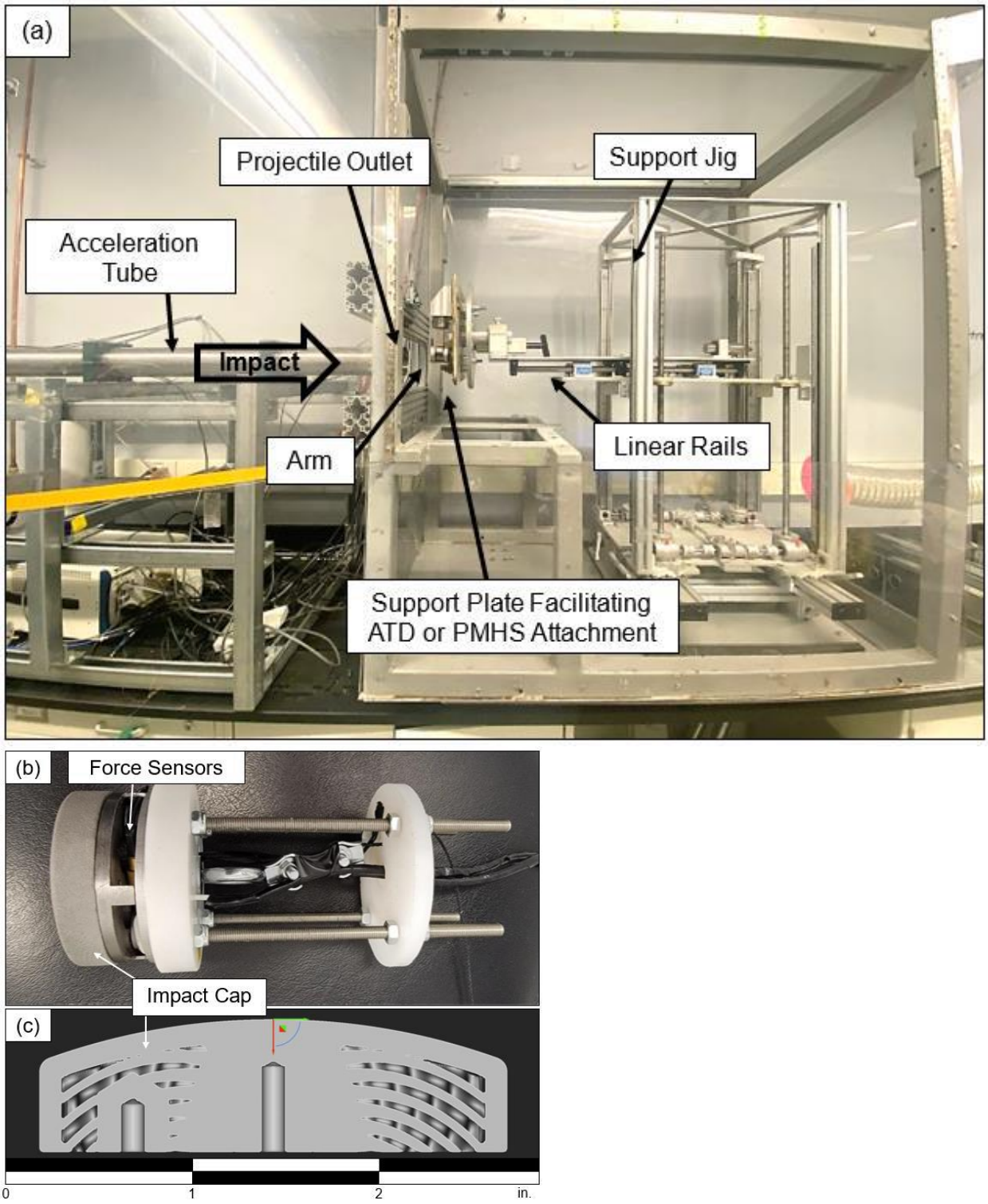

Figure 3.1: Components of the projectile and impacting apparatus used for testing.
The (a) impacting apparats detailing the support jig, and (b) the instrumented projectile used for testing, and (c) a cross-section of the impact cap.

The forearm ATD data were dual-pass filtered using a second-order Butterworth low-pass filter with a cut-off frequency of 1,250 Hz, in accordance with industry standards [30, 41]. High-speed videos were collected (IL3 100-L, Fastec Imaging Corporation, San Diego, CA) at 1,250 frames per second, at 8-bit resolution depth, parallel to the shot path. The shutter speed was 160 s. Two optical sensors (PZ-V31P, Keyence Corporation, Osaka, Japan) were mounted over the exit from the acceleration tube to collect the instantaneous impact velocity of the projectile immediately prior to impact with the arm. The testing procedure was controlled, and data were collected (at 1 MHz) using a custom-written LabVIEW (National Instruments, Austin, TX) program and a PXIe-1082 Data Acquisition System (National Instruments, Austin, TX, USA). The two projectile impact cap force sensors were sampled at 1MHz. A smoothing filter was applied, and data points were summed at each time point. From this data, the peak force, impact duration and impulse were identified. Impact duration was considered to have begun when the force increased above 5% of the peak force and concluded when the force fell back below 5% of the peak force.

Target testing parameters were derived from the data previously collected on the augmented WorldSID 50th Male ATD under ballistic behind-shield conditions [82]. Lab-based impact testing was conducted on the same ATD upper limb in the pneumatic impacting apparatus to determine appropriate parameters [82]. The pneumatic impacting apparatus could not match the velocity of the shield deforming for most of the prior tests conducted (up to 208 m/s) due to device constraints, so was varied within the capabilities of the test apparatus while targeting the applied force and minimizing impact duration.[3] As impact force did not differ significantly between the

[3] See Appendix B for details surrounding determining the impact velocity.

hand and forearm impact locations on the ATD, the average of all trials was used as the target impact force (Table 3.1). Thus, the parameters that were targeted were peak force for the 10 mm (18,979 N), 15 mm (7,397 N), and 20 mm (3,098 N) stand-off distances. The impact duration was also intended to be as short as possible, which averaged approximately 0.511 ms in ballistic impacting scenarios and 0.840 ms in the lab-based replications. Both ballistic and lab-based replications were conducted without the soft tissue analog of the ATD, so it was expected that PMHS impact durations would be longer due to differences in stiffness between the two surrogates and the addition of soft tissue. Data were extrapolated out of the ballistic impacting scenarios by fitting a polynomial to the ballistic data and conducting lab-based replications that fit this curve.

Table 3.1: Target parameters as collected in ballistic tests [82] as compared to parameters generated in the laboratory-based assessments, presented as mean ± standard deviation of the three repeated trials in the pneumatic impacting apparatus.

Stand-Off Distance	10 mm	15 mm	20 mm
Target Average Peak Force, Ballistic Data (N)	18,979	7,397	3,098
Peak Force, Lab (N)	17,370 ± 64	6,979 ± 351	3,105 ± 29
Force Difference (%)	0.2	5.0	0.4
Target Impact Duration, Ballistic Data (ms)	0.730	0.623	0.180
Impact Duration, Lab (ms)	0.848	1.130	0.523
Impact Duration Difference (%)	13.9	44.9	66.8

3.3.2 Specimen Preparation

This research was approved by the Hamilton Integrated Research Ethics Board (HiREB, Project ID 9459). Eight fresh-frozen post-mortem human subjects (PMHS) upper limbs (mid-humerus to fingertips) were obtained for testing from male donors within the 30th-70th percentile

in terms of height and weight in the Canadian Forces [87]. Specimens between 1.73 and 1.80 m tall and 79 and 95 kg were selected. Average male donors were selected as this is the first known study to investigate the upper extremity response at these higher rates, and the army population in Canada is still 86.2% male [72]. The average age of the donors selected was 72 ± 15 years. There were no reported musculoskeletal diseases for any specimens. All specimens were Computed Tomography (CT) scanned (GE Revolution CT ES, Boston, MA, USA, 0.625 mm slice thickness) prior to testing to check for existing injury and measure bone mineral density. Bone mineral density was computed from the CT scans at the distal 1/3 radius through the use of a calibrated phantom placed in the field of view (consisting of two materials of known density, facilitating the development of a linear relationship between Hounsfield Units and density). A full set of anthropometric measurements was also taken (Table 3.2).

Table 3.2: Anthropometric data for PMHS tested.[4]
The letter following the specimen ID and hyphen denotes a right (R) or left (L) arm. The forearm length was measured from the lateral epicondyle to the ulnar styloid process by palpation, while the circumference was measured at the midpoint of that length. The bone mineral density was measured at the 1/3 distal radius.

				Upper Extremity			
Specimen ID	**Age (years)**	**Body Mass (kg)**	**Stature (cm)**	**Segment Mass (kg)**	**Forearm Length (cm)**	**Circumference (cm)**	**Bone Mineral Density (g/cm^3)**
211357-L	80	91.4	173	2.5	27.7	22.9	1.207
210891-R	59	81.7	180	2.6	26.5	24.5	1.171
210897-L	74	85.9	173	2.3	21.3	23.3	1.490
211127-R	75	79.4	180	1.7	27.0	19.1	1.180
220316-R	71	84.4	180	3.3	25.6	23.6	1.207
230246-L	49	83.5	173	1.6	24.1	23.4	1.217
221296-L	70	83.0	180	1.9	27.2	22.8	1.272
230522-R	99	84.5	178	1.9	28.8	20.9	1.052

For each specimen, the tissue surrounding the humerus was resected to reveal 50 mm of bone. The exposed bone was potted in square aluminum pots (2.5 in. by 2.5 in., with a ¼ in. wall thickness) to a depth of approximately 15 mm with SimplexTM P bone cement (Stryker MedEd, Mahwah, NJ, USA) and 25 mm with dental cement (Denstone Type III, Kulzer, Hanau, Germany) for a total potting depth of 40 mm. Specimens were consistently aligned using anatomical landmarks and then left to cure for 30 minutes.

The long axis of the forearm (defined as the line connecting the lateral epicondyle and ulnar styloid process) was kept at a 90°-angle to the long axis of the humerus using laser levels. This was consistent with how the ATD was positioned during ballistic testing. Impact locations were identified by anatomical landmarks along the upper extremity *via* palpation.[5] The forearm impact

[4] See Appendix C for a full set of anthropometry metrics specific to the upper extremity for these specimens.
[5] See Appendix D for exact impact locations.

location was selected as the halfway point between the lateral epicondyle and the ulnar styloid process, while the midpoint of the third metacarpal was targeted for hand impacts. The hand was positioned around a handle such that the handle was proximal to the proximal interphalangeal joints of the fingers, with the metacarpals positioned in front of the handle (in line with the impactor). Aside from the mid-humerus potting and the tensor union between the hand and the handle, the limb was not in contact with the plate behind it. Prior to testing, each specimen hand was affixed to the testing handle using tensor bandages in a consistent wrapping method that left the impact location exposed (marked with a marker) to ensure a gripping posture was simulated (Figure 3.2). Post-impact translation was facilitated by linear rails in the testing jig, allowing for the jig to travel away from the direction of impact, as was used in the ballistic testing.

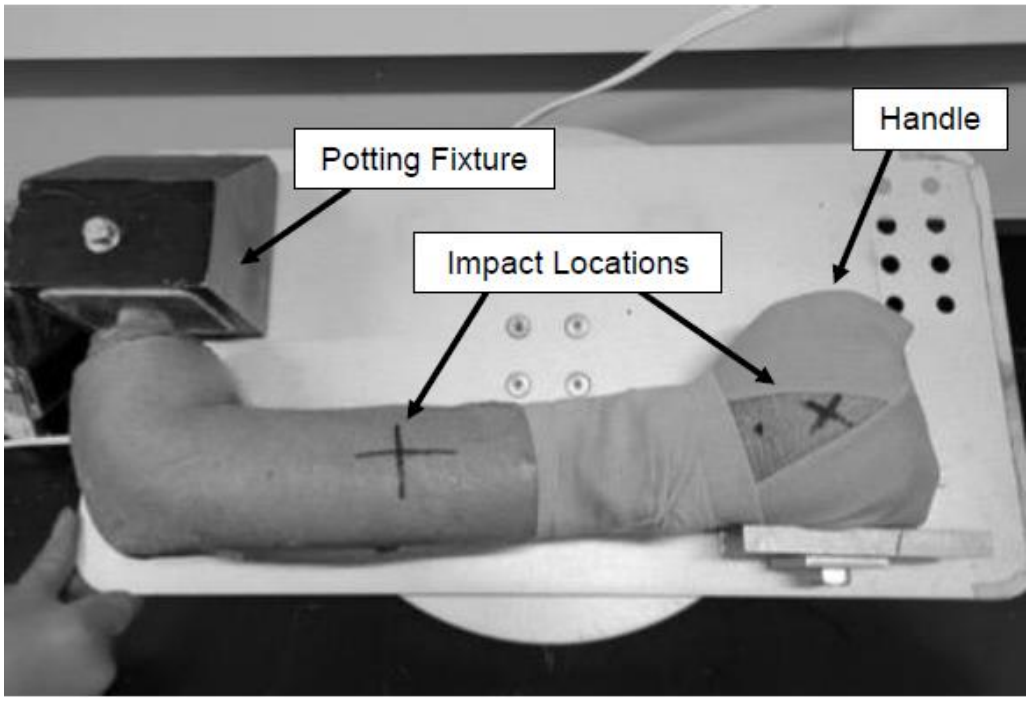

Figure 3.2: The tensor bandage wrap method. The forearm and hand impact locations are identified.

3.3.3 PMHS Impacts

As each limb was impacted at two anatomical locations, the order of impacts was randomized so that any sequencing effects would be nullified. For the second location on each specimen, the previously damaged location was wrapped in tensor bandages to minimize any effect of the fracture on structural boundary conditions. Peak force of the injury-inducing impacts was considered the force required to fracture, and the time at which fracture occurred.

One specimen (211357-L) was used to establish testing procedures in an effort to identify the conditions required to generate an injury threshold. The specimen was impacted at conditions representing decreasing stand-off distances (through increasing the impact velocity) in a stepwise manner, starting with the 20 mm stand-off distance. After each test, the specimen was x-ray imaged (anterior-posterior and lateral views). If no fracture was observed, the specimen (for that impact location) was re-impacted at a higher energy level. Fractures were generated at both locations under conditions representing the 0 mm stand-off distance. This therefore formed the basis for the impact parameters that were used for the remainder of the specimens (target of 17 m/s). After testing was complete, CT imaging was conducted of all upper extremities. From these scans, the fracture type and location were determined.

3.3.4 Statistical Analysis

A one-way Analysis of Variance (ANOVA) with posthoc Tukey test was conducted on peak force, duration of impact, and impulse to compare between the hand and the forearm, with a significance threshold of $\alpha = 0.05$. A Weibull survival analysis was performed with respect to peak impact force (*i.e.*, injury risk curves) for the hand and forearm [59] [88]. Force was the focus of the analysis given its direct translation to ATD safety assessments. Data were right-censored if the

measured value was less than the injury threshold. This means, any impacts that did not generate a fracture were right-censored. The log-normal and log-logistic distributions were also investigated in comparison to the Weibull, and the best fit according to the Akaike Information Criterion (AIC) was selected.[6] The Maximum Likelihood Estimation (MLE) was used to find the scale and shape parameters with the highest likelihood of occurring based on the failure test data collected from the impact testing [89]. This model determined the scale (α) and shape (β) parameters of the two-parameter Weibull probability function with the highest likelihood of occurring based on the given dataset. The likelihood of failure was then plotted by generating the cumulative distribution function against the measure of fracture force. The relationship that was developed between the ATD and PMHS impacts under the same impact conditions was also used to determine the acceptable amount of loading on the ATD prior to injury in shield BABT conditions. 10% of the fracture threshold of the PMHS was established and using the developed relationship between the ATD and the PMHS allowed for identifying the impact conditions that would have generated this value on the ATD. This 10% ATD value is proposed as the acceptable limit.

3.4 Results

There were no pre-existing injuries identified on the CT scans. The volumetric bone mineral density at the 1/3 distal radius was 1.25 ± 0.11 g/cm^3 (mean ± standard deviation), which was within a normal range [90].

[6] Details of this determination can be found in Appendix E.

Ballistic testing impacts replicating the peak force associated with the 10-, 15-, and 20-mm stand-off distances (orange, Figure 3.3) were replicated in our pneumatic impacting apparatus (green, Figure 3.3). This aligns with stand-off distances employed while shields are in use. Due to instrumentation capacity limitations on the WorldSID ATD (maximum 88 kN), a power function was used to extrapolate parameters for stand-off distances below 10 mm. The replicated impacts were then applied to the pilot specimen (blue, Figure 3.3); these data points reflect the impact force averaged across both impact locations. As expected, the difference in stiffness between the ATD and PMHS, as well as the presence of soft tissue, substantially reduced the applied force (*i.e.*, the ATD force was approximately 90% higher than the PMHS force under the same impact conditions).

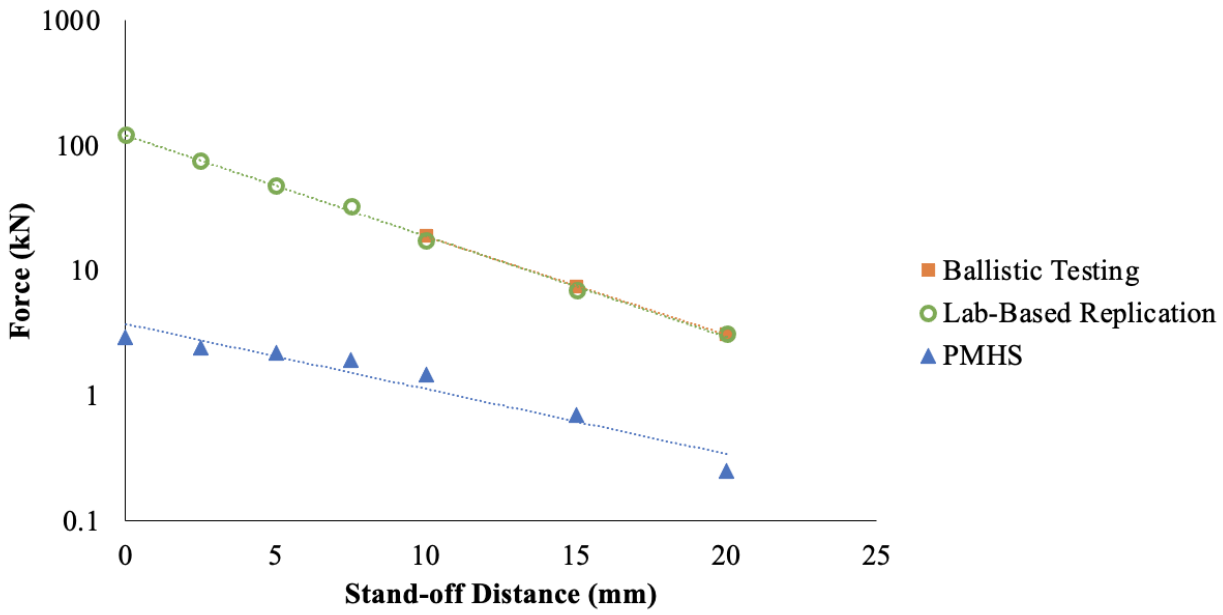

Figure 3.3: A comparison of the average values of the data collected.
'Ballistic Testing' is the previous ballistic impacts conducted on the WorldSID ATD [82]. 'Lab-Based Replication' is the data collected on the same WorldSID ATD in the pneumatic impacting apparatus (the solid green circles were extrapolated out of the testing range), while 'PMHS' is the same impact condition as the 'Lab-Based Replication,' conducted on the pilot specimen.

The hand and forearm of the pilot specimen both fractured at conditions representing a 0 mm stand-off distance. These impact conditions were then repeated on the remaining seven specimens. The failure impact velocity for all hand impacts was 16.4 ± 0.8 m/s (mean ± standard deviation), while the impact duration was 6.2 ± 4.0 ms, and the impulse was 5.3 ± 1.7 N*s (Table 3.3). The failure impact velocity for all forearm impacts was 16.9 ± 1.9 m/s (mean ± standard deviation), while the impact duration was 9.8 ± 3.9 ms, and the impulse was 6.8 ± 1.2 N*s (Table 3.4). There were no statistical differences between the hand and forearm parameters for velocity (p = 0.52). The impact duration was longer for the forearm impacts in comparison to the hand, though not significantly (p = 0.25), and the impulse was also slightly larger for the forearm impacts (p = 0.16). The fracture force of the hand and forearm was approaching significance (p = 0.06), with the hand being stronger than the forearm.

Table 3.3: Hand impact failure data.
The impact order denotes whether the hand was impacted before (1) or after (2) the forearm. The number of previous impacts the specimen underwent prior to fracture is also included. The pilot specimen is italicized.

Specimen ID	Impact Order	Impact Velocity (m/s)	Fracture Force (N)	Impact Duration (ms)	Impulse (N*s)	# Previous Impacts
211357-L	*1*	*16.3*	*3,333*	*3.5*	*3.7*	*6*
210891-R	2	14.9	3,617	5.7	2.7	0
210897-L	2	17.0	3,023	4.4	4.6	0
211127-R	1	16.7	3,490	6.1	5.4	1
220316-R	2	16.7	3,436	15.2	8.5	1
230246-L	2	15.5	5,007	3.0	5.8	0
221296-L	1	16.7	5,448	3.5	6.1	0
230522-R	1	17.3	3,189	8.4	5.3	0
Mean ± Standard Deviation		**16.4 ± 0.8**	**3,818 ± 897**	**6.2 ± 4.0**	**5.3 ± 1.7**	

Table 3.4: Results from the forearm impacts.
The impact order denotes whether the forearm was impacted before (1) or after (2) the hand. The number of previous impacts the specimen underwent prior to fracture is also included. The pilot specimen is italicized.

Specimen ID	Impact Order	Impact Velocity (m/s)	Fracture Force (N)	Impact Duration (ms)	Impulse (N*s)	# Previous Impacts
211357-L	*2*	*14.9*	*2,449*	*10.1*	*6.5*	*7*
210891-R	1	17.7	2,318	4.7	5.2	1
210897-L	1	19.3	2,286	10.6	6.7	0
211127-R	2	17.3	3,184	6.7	5.4	1
220316-R	1	14.7	3,210	8.0	6.6	1
230246-L	1	14.7	2,837	7.4	6.8	0
221296-L	2	18.1	3,928	10.3	8.7	0
230522-R	2	18.1	3,878	6.9	5.4	0
Mean ± Standard Deviation		**16.8 ± 1.8**	**3,011 ± 656**	**8.1 ± 2.1**	**6.4 ± 1.1**	

The force-time traces for both anatomical locations followed a similar trend, with an obvious peak followed by a dip (fracture), then a more gradual decline for the rest of the test (Figure 3.4).

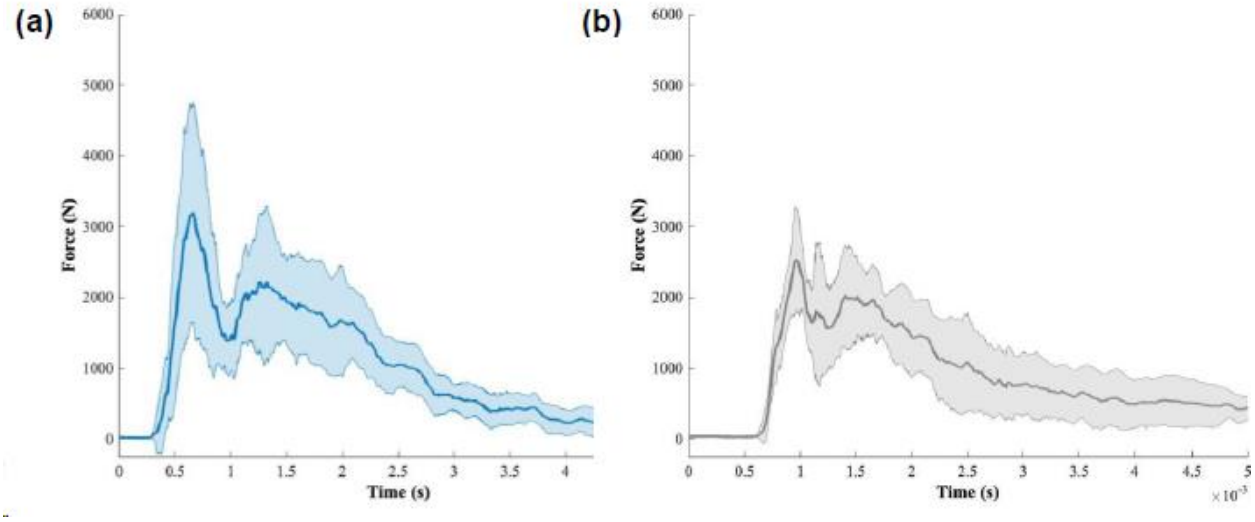

Figure 3.4: Force-time curves of the (a) hand, and (b) forearm impacts causing fracture. The line represents the mean, while the shaded region represents one standard deviation. Impacts were aligned by the approximate rise time.

The fracture force of the hand (3,818 ± 897 N) was higher than the forearm (3,011 ± 656 N, p = 0.06, Figure 3.5). These fracture data generated substantially different injury risk curves (Figure 3.6). The hand fracture risk, P(x), formula is given by Equation (1), while the forearm fracture risk is given by Equation (2).

$$P_{hand\ fracture}(x) = 1 - e^{-(\frac{x}{5{,}162.7})^{1.3402}} \qquad \text{Equation (1)}$$

$$P_{forearm\ fracture}(x) = 1 - e^{-(\frac{x}{3{,}400.3})^{1.4389}} \qquad \text{Equation (2)}$$

This would result in a 10% and 50% risk of hand fracture at approximately 963 N and 3,927 N, respectively. The 10% and 50% risk of forearm fracture would be approximately 712 N and 2,636 N, respectively.

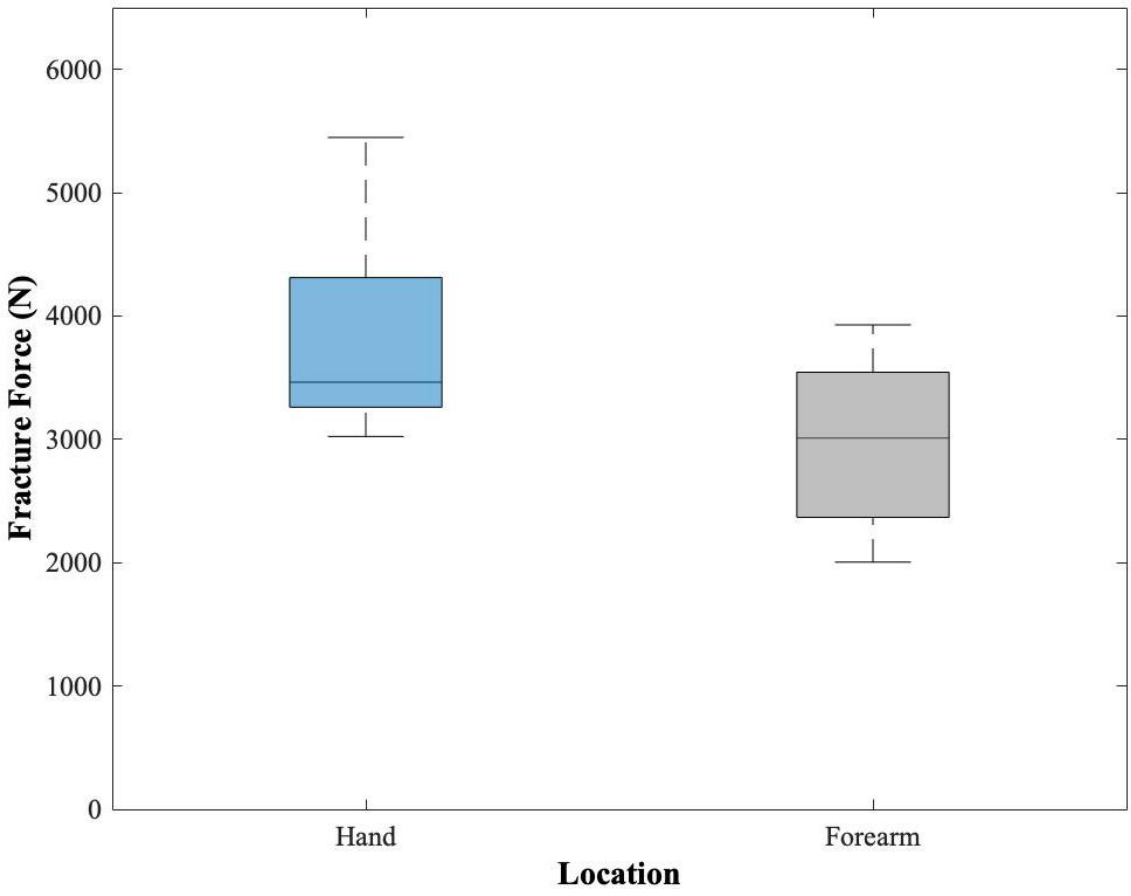

Figure 3.5: Fracture force data for both the hand and forearm 50th percentile male PMHS.

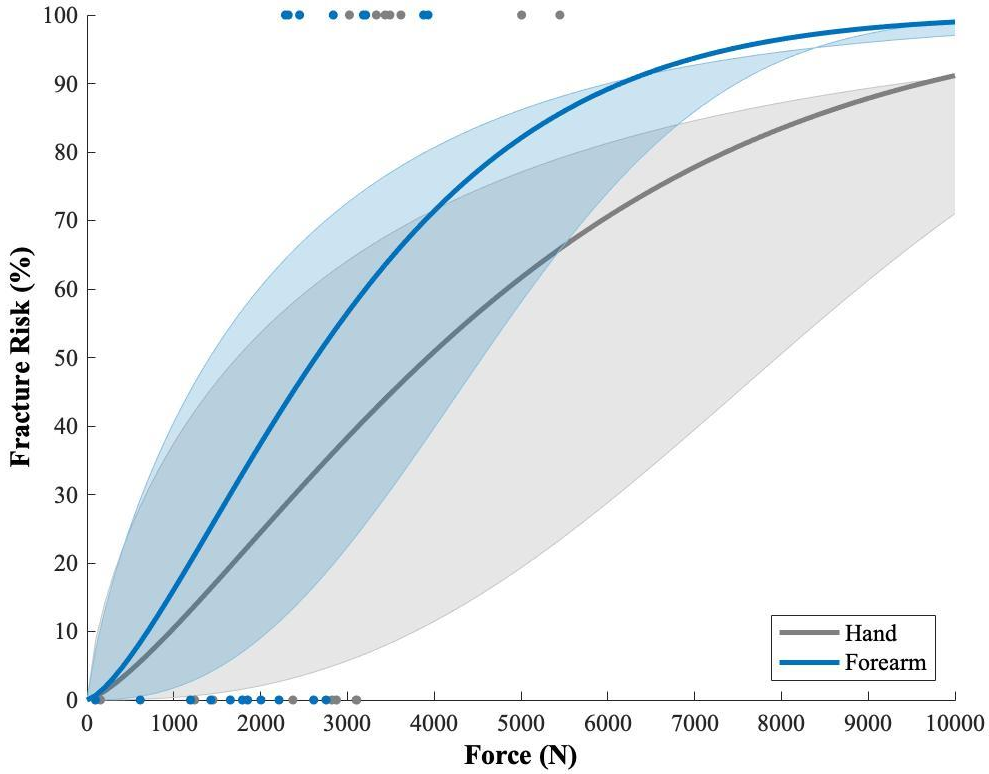

Figure 3.6: Injury risk curves for the hand and forearm, under behind shield blunt trauma loading conditions.
The shaded region represents the 95% confidence intervals of each curve.

For future shield safety assessments, the probability of sustaining an upper extremity fracture from these events needs to be related to a mechanical surrogate. A 10% limit is recommended in this application, as this is in accordance with defence standards seen elsewhere in the body [30] and in automotive upper extremity thresholds [29]. This would result in a measured applied force of 11.0 kN (hand) and 8.1 kN (forearm) on the modified WorldSID ATD. This threshold was determined from the relationship developed describing the PMHS and ATD responses under the same impact conditions.

For the forearm impacts, only two specimens sustained fractures of the radius only, while six incurred fractures of both the radius and the ulna (

Table 3.5). The forearm was impacted at a point that corresponded to approximately 47% of the total ulna length, yet both the radius and ulna fracture locations were normally slightly distal to this point, with the radius fracture location at approximately 55 ± 8% of the radial length and the ulnar fracture location at approximately 50 ± 7% of the ulnar length (as determined from the x-ray images). The hand fractures were primarily on the second, third, and fourth metacarpals (*i.e.*, surrounding the impact location); however, some were noted at locations remote to the impact site (two sustained fractures of the 5th metacarpal). Representative hand and forearm fractures are shown in Figure 3.7a and Figure 3.7b, respectively.

Table 3.5: Description of the fractures sustained during testing.

Specimen ID	Hand Fracture Description	Forearm Fracture Description
210891-L	Nondisplaced second distal metacarpal fracture	Mildly displaced mid radius fracture
210897-L	Minimally displaced angulated second, third and fourth mid to distal metacarpal fractures	Comminuted mildly displaced mid radius and mid ulna fractures
211357-L	Nondisplaced comminuted second mid metacarpal fracture; nondisplaced third mid metacarpal fracture	Minimally displaced mid radius fracture; nondisplaced mid ulna fracture
211127-R	Comminuted second, third, and fourth metacarpal head fractures	Nondisplaced mid radius and ulna fracture
220316-R	Nondisplaced comminuted second distal metacarpal fracture	Comminuted displaced mid radius and mid ulna fractures
230246-L	Minimally displaced distal fourth metacarpal head fracture; nondisplaced distal fifth metacarpal head fracture	Comminuted displaced mid radius (extending to proximal radius shaft) and mid ulna fractures
221296-L	Minimally displaced distal fourth metacarpal fracture; second and third metacarpal head fractures with no displacement	Displaced comminuted mid radius shaft fracture
230522-R	Comminuted displaced third, fourth, and fifth metacarpal fractures	Comminuted displaced mid radius fracture; comminuted displaced mid ulna fracture

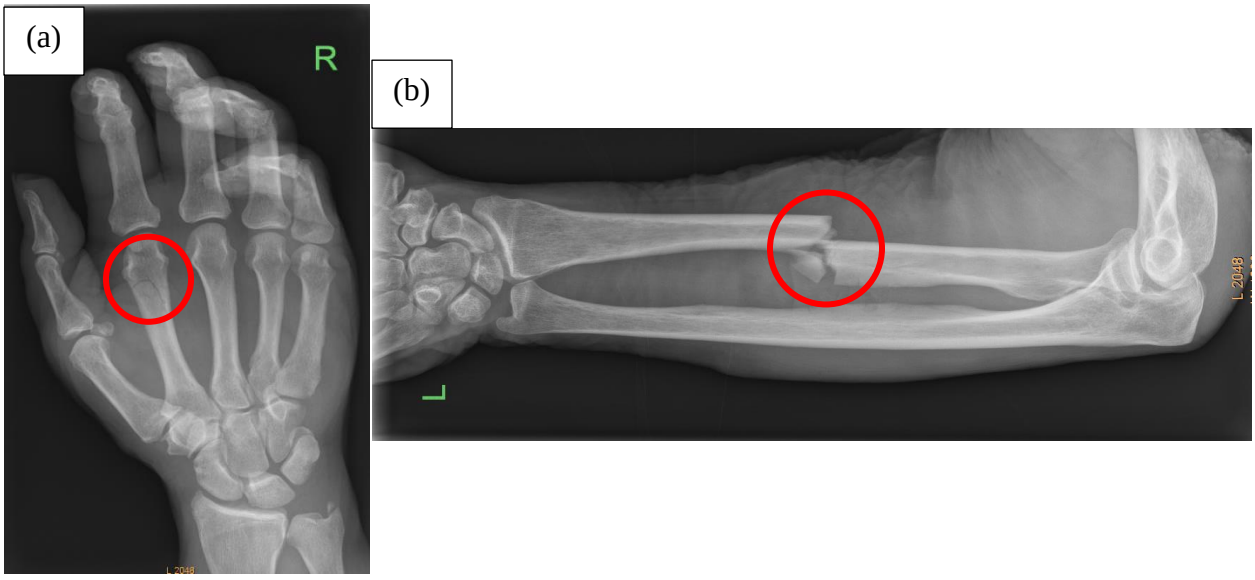

Figure 3.7: X-ray images showing fractures of the (a) hand of specimen 220316, and (b) the forearm of specimen 221296. The fractures are indicated (red).[7]

3.5 Discussion

This study represents the first known investigation into the fracture tolerance of the upper extremity due to shield BABT. It used realistic impacts applied on an ATD to generate injuries in PMHS. Results from this study will provide the foundation towards a protective standard for behind shield blunt trauma.

The mean peak fracture force for the hand impacts was 3,818 ± 897 N, in the range of previously reported injury thresholds for this region (range: 1,639 – 6,500 N [59] [60]); however, a direct comparison is challenging due to the differing impact velocities, impactor shapes and sizes and the location on the hand that was impacted. One hand impact (220316-R) resulted in a very high impact duration (15.0 ms, whereas all other impacts ranged from 3.4-6.1 ms). Upon inspection

[7] All additional x-rays can be seen in Appendix F.

of the high-speed video after impact, the hand and jig did not initially recoil as all other impacts did, making the projectile in contact with the arm longer, possibly due to alignment issues causing friction in the jig post-impact. The current study had substantially higher metacarpal fracture forces than have previously been reported (1,639 ± 451 N [60]). This could be due to a variety of factors, including the smaller impactor (32 mm hexagonal-shaped flat impactor *vs.* the 63.5 mm hemispherical impactor used in this study), the higher impact rate (approximately 3.2 m/s *vs.* our 16.2 m/s), and/or the differing boundary conditions. The shape of the Weibull curve was also much flatter for the hand, with two high-force data points influencing this. The donor ages were not particularly different, and these specimens had not undergone repeated impacts, so it is challenging to determine the reason for these two higher data points.

The higher hand forces are unsurprising as the hand represents a more rigid boundary condition than the forearm, which would exhibit beam-type bending. The peak average forearm fracture force in this study was 2,972 ± 711, also higher than previously reported levels (*e.g.*, 2,368 ± 812 N [66] and 1,386 ± 198 N [84]). One specimen (L210891-R) did not appear to fracture on impact (2,318 N); however, in the subsequent impact the arm sustained less force (2,004 N), meaning it had likely undergone damage at the earlier impact, but no fracture was detected on the x-ray. As such, we used the higher impact force as the fracture force. While automotive impacts occur in the same orientation as shield BABT, they tend to occur over a longer duration (29.1 ms for automotive *vs.* 0.18 ms for shield BABT) and generally a smaller magnitude (1.7 kN *vs.* 19.0 kN) [82] [63]. There was also a lower impact velocity used in previous studies (range: 3 – 7.6 m/s) as compared to this study (16.8 m/s), which again highlights why it is critical to have injury metrics specific to high-rate conditions. The complex boundary conditions used in this study prevent a bending moment of the forearm from being calculated and compared to previous literature.

A stepwise approach was used to generate these impacts, where the forearm load was quantified using an ATD mounted to a jig on linear rails in a ballistic testing facility, and these impacts were recreated in a controlled laboratory setting to determine injury limits. Finally, they were applied to PMHS mounted on the same jig in matched-paired testing. Unfortunately, the impact velocity could not be matched due to equipment constraints; however, the difference in force was less than 5%, and the duration of impact remained small (0.834 ms in the laboratory in comparison to 0.509 ms in ballistic impacts). Error would have been introduced in extrapolating out of the tested region during the ballistic investigations but was necessary to generate failure-inducing impacts on the PMHS. The relationship generated between the PMHS and ATD was only based upon three data points, and as such may have affected the relation function at higher impact rates. The ATD flesh was removed for all impact conditions, and as such the compliant PMHS experienced a longer duration of impact in comparison to the stiffer ATD when impacted under the same conditions. The present study was advantageous as it represents much more realistic boundary conditions than have previously been produced, in that the humerus and hand were both fixed but allowed for movement at the elbow and wrist, similar to what is observed by soldiers in the field. This is in contrast to the typical three-point bending of the isolated ulna and radius that is typically employed (*e.g.*, [54]).

There were limitations to the study. In PMHS studies, the physical condition of the specimens is generally lesser due to advanced aging than that of the intended user group. This is particularly relevant to individuals in the military who are generally much younger; however, as bone tissue quality decreases with age, the data presented herein likely presents a conservative estimate of the fracture tolerance of younger specimens. A very homogenous population was also selected (in terms of height and weight) to better represent the target user, but it is important to

recognize that an injury threshold developed using 50th percentile donors may not adequately protect all users. Further, there is a lack of muscle tension and physiological response in PMHS testing. These events occur over a very short duration (0.509 ± 0.217 ms [82]), which is insufficient time for a muscular response in a living person, therefore the lack of muscle activation during impact is not a limiting factor in the use of cadaveric specimens in this study [91]. However, the initial tension of the tendons and muscles at the time of impact (from supporting the shield) may have affected the injury tolerance threshold and should be considered in future studies. However, efforts were made to wrap the hand to mechanically simulate a gripping posture, and PMHS still represent the most accurate depiction of biological tissues. Nonetheless, the more relaxed soft tissue may have affected the tissue threshold presented.

The ATD flesh was removed for all impact conditions, and as such the complaint PMHS experienced a longer duration of impact in comparison to the stiffer ATD when impacted under the same conditions. Removal of the surrogate flesh was conducted to facilitate the addition of instrumentation that could withstand these kinds of loads and provide a durable and repeatable test surrogate that would not degrade with multiple impacts. Shield BFD is a much more focal impact than blunt automotive impacts that ATD flesh is designed for, making damage highly likely as seen in previous embedded instrumentation loading [71]. Additional tests with the ATD flesh under these conditions would be an interesting future investigation to quantify the damping it provides, the available repeatability, and compare with PMHS stiffness.

The force was also extrapolated outside of the collected range due to instrumentation constraints within the ATD. This likely introduced some error into this analysis, which may have introduced some error. Specimens that did not sustain a fracture (based on x-ray examination) at lower energy levels were tested again at a higher energy level. These repeated loads may have

affected the biomechanical response and decreased the fracture tolerance of these dynamic impacts due to the potential for micro-cracks that may not have been detected in x-ray examination. However, specimens that underwent more than one hand impact (3 specimens) *vs.* fractured on the first impact (5 specimens) did not differ significantly ($p = 0.37$) in fracture force. The same was true for forearm impacts, in which specimens that underwent more than one forearm impact (4 specimens), when compared to specimens that fractured on the first impact (4 specimens), did not differ significantly ($p = 0.34$) in fracture force. The pilot data were also in the range of fracture data collected, so it was included in the failure dataset even though there may have been potential accumulated damage. There was also no obvious effect of order between test sites ($p > 0.34$), and as such, the hand and forearm tests can be considered independent of one another.

Lastly, the impact velocity delivered to the PMHS in this study (approximately 16 m/s) was lower than previously reported ballistic shield responses (up to 302 m/s, [82]) but was in the lower range of another study (6.5-163.6 m/s, [71]). This highlights the vast differences in shield responses within the same ballistic protection rating class (Level III). Given that injury limit has been shown to be influenced by impact speed (*e.g.*, [58]), the lower impact velocity likely resulted in reduced failure thresholds and represents a conservative limit, providing enhanced protection for the intended demographic.

Debilitating injuries to the upper extremity can result in loss of functionality, which have significant implications in the defence sector. These injuries can cause the user to drop the shield which would potentially put them and others at great risk of injury. Future shields should consider a back-face deformation force measurement of less than 11.0 kN to the hand and 7.2 kN to the forearm of a modified WorldSID ATD as acceptable in order to minimize this risk of injury. A

new standard is recommended to not only protect against projectile penetration but also to limit back-face deformation force transfer to limit the risk of forearm and hand fractures.

This study was the first of its kind to present the upper extremity response to impacts representative of behind shield blunt trauma. It highlighted the fact that current shields that are passing standards regulations are not adequate in limiting hand and forearm fracture risk. This study will inform a standardized protocol in which the applied force from shield BABT provides context for interpreting injury risk. The data presented herein can be used when assessing future shields to determine the probability of fracture occurring as a result of behind-shield blunt trauma and will ultimately lead to greater protective measures for our armed forces.

Chapter 4 – Injury Risk Functions for the Midsized Male Wrist and Elbow as a Result of Behind Shield Blunt Trauma

Overview: *This chapter details the experimental testing of post-mortem human subjects of loads representative of behind shield blunt trauma to the wrist and elbow, also to address Objective 2. This chapter has been submitted to the Journal of Biomechanical Engineering, and upon acceptance and publication, the proper permission from the copyright holder will be obtained to include the article in this thesis.*

4.1 Abstract

Ballistic shields protect users from a variety of threats, including projectiles. Shield back-face deformation (BFD) is the result of the shield deflecting or absorbing a projectile and deforming towards the user. Back-face deformation can result in localized blunt loading to the upper extremity, where the shield is secured to the user. Two vulnerable locations along the upper extremity were investigated – the wrist and elbow – on eight post-mortem human subjects (PMHS) using a pneumatic impacting apparatus for investigating the fracture threshold as a result of behind shield blunt trauma (BSBT). Impacting parameters were established by subjecting an augmented WorldSID Anthropomorphic Test Device (ATD) positioned behind a ballistic shield to ballistic impacts. These data were used to form the impact parameters applied to PMHS, where the wrist most frequently fractured at the distal radius and the elbow most frequently fractured at the radial

head. The fracture threshold for the wrist was 5,663 ± 1,386 N (mean ± standard deviation), higher than the elbow at 4,765 ± 893 N (though not significantly, $p = 0.15$). The failure impact velocity for wrist impacts was 17.7 ± 2.1 m/s, while for the elbow, the failure impact velocity was 19.5 ± 0.9 m/s. An approximate 10% risk of fracture threshold was identified on the modified WorldSID ATD, where measured impacts less than 10.8 kN at the wrist and 12.5 kN at the elbow would be considered effective at limiting injury from BSBT. To inform a protective standard to limit wrist and elbow fracture resulting from behind shield blunt trauma, a 10% injury limit as measured using the augmented WorldSID ATD was developed.

4.2 Introduction

Injuries resulting from behind-armour blunt trauma (BABT), caused by the rapid deformation of protective equipment from projectiles, can be severe and debilitating [1]. Ballistic shields are used by defence personnel while diffusing dangerous situations and are supported by a user's arm to protect against projectile penetration. While these shields are effective at stopping the projectile itself, they can deflect and cause injury to areas along the upper extremity that are in contact with the shield. There are existing standards that pertain to projectile penetration [2]; however, there are no known standards for ballistic shields that limit the allowable back-face deformation a shield may exhibit or detail the amount of allowable force transfer to the upper extremity. Due to privacy surrounding the defence sector, it is unknown how prevalent these injuries are in operation; however, injuries to the head [74] and chest [27] have been reported from similar behind armour blunt trauma mechanisms. Investigation into the types of behind shield blunt trauma loads have been measured by a modified Anthropomorphic Test Device (ATD) arm [70]

[82] and risk of forearm and hand fracture identified from these types of loads [92]. The wrist and elbow are also in contact with ballistic shields when supported by users and combined with the complex geometry and minimal soft tissue coverage of these anatomical areas makes injury to these locations likely. As such, injury risk must be quantified to these areas as a result of behind shield blunt trauma (BSBT).

Injury criteria have been developed for the upper extremity for automotive safety [63] [83] [54], falls prevention [62], and sports injury prevention [73], and the tolerance has been shown to be highly dependent on joint orientation [83] [54], loading conditions [67] [58], and anthropometric size [53]. Transverse impacts to the elbow typical from side airbag deployment have been previously investigated, in which a pendulum impacted the elbow of post-mortem human subjects (PMHS) in the sagittal plane of the humerus [53]. A variety of elbow postures (ranging between 0 to 145° of flexion) were investigated, and the average force to fracture the olecranon was 4.1 kN and the distal humerus was 3.8 kN. In practice, the elbow is in contact with the back face of a ballistic shield, in which the deformation may strike the user while the elbow is in deep flexion. As such, these established injury limits may not apply due to the differing orientation, loading direction, and rate of load application.

The majority of research conducted on the wrist has been focused on injuries from falling onto an outstretched hand. This primarily axial impact scenario is not relevant to transverse BSBT injury outcomes, where the back face of the shield strikes the posterior aspect of the wrist with the joint in a neutral posture. While oriented differently, the carpal bones and distal radius are still vulnerable in a transverse impact scenario. The carpals are short bones, so their ability to withstand stress in these two different orientations may be similar due to the relatively similar geometry in different directions. The fracture limit of the scaphoid bone has previously been identified as 2,410

± 913 N, and 1,640 ± 980 N for the distal radius [61]. Testing rate has been shown to have a substantial effect on failure force, as a recent study testing at 3.9 m/s found a failure threshold of 6,565 ± 866 N [62], more than double that of the previously-mentioned quasi-static conditions [61].

The upper extremity injury threshold for high-rate loading typical of behind shield blunt trauma is largely uninvestigated and is expected to vary from fracture threshold research that has already been conducted in this area due to the increased loading rate and different direction of impact. This is consistent with findings with our previous study that investigated the fracture threshold at the forearm and hand under BSBT conditions [92]. The complex geometries of the wrist and elbow, close proximity to the back of a ballistic shield, and differing boundary conditions they assume while holding a shield necessitate an investigation of injury risk to these regions.

The purpose of this study was to investigate the fracture threshold of the wrist and elbow of the 50th percentile male upper extremity due to behind shield blunt trauma. Results were then translated to an instrumented ATD for the purposes of developing a safety standard for evaluating future designs of ballistic shields.

4.3 Methods

4.3.1 Specimen Preparation

This research was approved by the Hamilton Integrated Research Ethics Board (HIREB, Project ID 9459). Eight post-mortem human subjects (PMHS) sectioned mid-humerus were obtained from donors that fell within the 30th-70th percentile of males in terms of height and weight [87]. Midsized male donors were selected as the focus as the majority of the military

population is male, and as this is the first study of its kind, addressing the most common size aims to protect as many users as possible [72]. There were no reported musculoskeletal diseases for any specimens. All specimens were scanned using Computed Tomography (CT) prior to impacting to screen for pre-existing bone injury and abnormalities, and adequate bone mineral density (where a bone mineral density of less than 80 mg/cm^3 is considered osteoporotic [13] and would be excluded from this study). A full set of manual anthropometric measurements were also taken (Table 4.1). Bone quality was examined by measuring the apparent density at multiple locations: the mid-slice of all eight carpal bones, the ultra-distal radius and ulna, 1/3 distal radius and ulna, as well as the center of the trochlear notch on the olecranon and the center of the capitellum on the humerus. Measures were obtained using Mimics 25.0 image processing software (Materialise, Belgium), where ash density was quantified by developing a linear relationship between the Hounsfield Units and water and hydroxyapatite phantoms that were included in each scan.

Table 4.1: Anthropometric data for PMHS.
The letter following the specimen ID and hyphen denotes a right (R) or left (L) arm. The forearm length was measured from the lateral epicondyle to the ulnar styloid process by palpation, while the circumference was measured at the midpoint of that length. The reported bone mineral density was measured at the 1/3 distal radius. The italicized specimen was used for pilot testing.

				Upper Extremity Measurements			
Specimen ID	**Age (years)**	**Body Mass (kg)**	**Stature (cm)**	**Segment Mass (kg)**	**Forearm Length (cm)**	**Forearm Circumference (cm)**	**Bone Mineral Density (g/cm^3)**
211357-R	*80*	*91.4*	*173*	*2.5*	*28.4*	*23.5*	*1.136*
210891-L	59	81.8	180	2.6	26.3	24.3	1.362
210897-R	74	85.9	173	2.5	26.9	24.0	1.246
211127-L	75	79.5	180	1.9	25.8	22.8	1.272
220316-L	71	84.4	180	2.5	25.6	26.5	1.155
230246-R	49	83.5	173	1.8	25.2	22.3	1.210
211296-R	70	83.0	180	2.1	28.2	19.6	1.226
230522-L	99	87.5	178	2.0	27.5	28.2	1.144

In an effort to consistently identify the location of elbow impacts among specimens, the long axis of the forearm (defined as the line connecting the lateral epicondyle and ulnar styloid process) was kept at a 90°-angle to the long axis of the humerus using laser levels. The elbow impact location was identified as the center of the lateral epicondyle of the humerus. The wrist impact location was defined as 1 cm distal to the line connecting the ulnar and radial styloid processes (Figure 4.1). The PMHS were secured such that the hand was wrapped around a testing handle using tensor bandages to replicate a gripping posture. A 3-D printed component sat behind the distal radial ulnar joint to prevent extension of the wrist. It had a semicircle indentation that was larger than the width of the wrist to allow for distributed wrist support without generating any point loading. A second 3-D printed component was placed underneath the proximal 1/3 of the forearm to support its weight during impact testing.

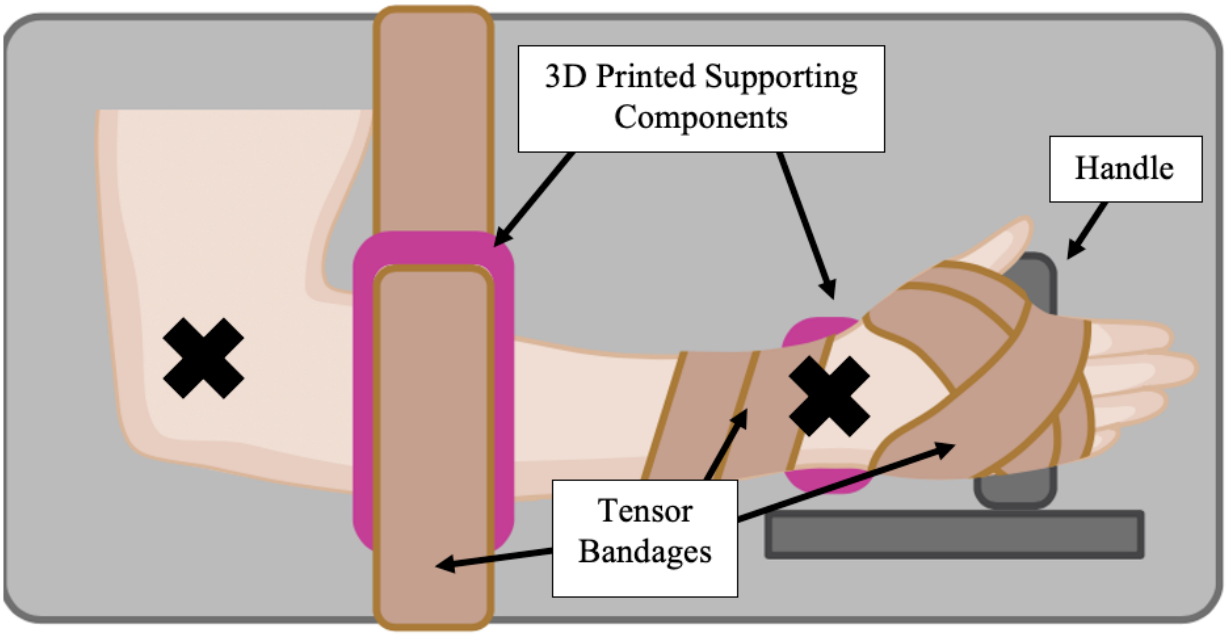

Figure 4.1: Schematic of impact locations of the wrist and elbow.
Locations are denoted by the black 'x'. The hand was wrapped around the handle in a consistent method for each specimen, as well as to secure the forearm to the back of the plate, while avoiding the location of impact.

4.3.2 Experimental Testing Protocol

The Worldwide Harmonized Side Impact Dummy (WorldSID, Humanetics Innovative Solutions, Farmington Hills, MI, USA) 50th percentile male ATD upper limb was previously enhanced with additional instrumentation and employed to quantify loading from BSBT [82]. Impact conditions from three decreasing stand-off distances (*i.e.*, the distance between the back of the shield and the front of the arm) conducted during ballistic testing in accordance with shield performance standards [2] were replicated in a laboratory-based setting that facilitated the testing of PMHS. The force and duration of impacts as measured using the ATD upper extremity exposed to BSBT were targeted on the replicated impacts [82]. All laboratory-based testing was completed in a pneumatic impacting apparatus that has been used in many previous studies [70] [93]. The same support apparatus was used in the ballistic testing as was used in the laboratory-based

replications, and the soft tissue surrogate of the ATD was removed to facilitate additional instrumentation.

Data were extrapolated out of the ballistic impacting scenarios (forces ranging from 3,098 N to 18,979 N over approximately 0.511 ms as measured on the ATD) by fitting a polynomial to the ballistic data and conducting lab-based replications on the ATD to fit the curve within these parameters. The pneumatic impacting apparatus could not match the velocity of the back face of the shield deforming (approximately 208 m/s) due to device constraints, so force and impact duration were targeted by tuning the mass of the projectile and pressure of the pneumatic system.

Impacts were applied by accelerating a 434 g projectile down a tube by compressed air towards the testing chamber. The projectile was equipped with two force sensors (model 201B05, PCB Piezotronics, MTS Systems Corporation, Depew, NY, USA) with a maximum capacity of 22.24 kN each, mounted into the front end of the impactor to measure applied force. The shape and stiffness of the projectile impact cap matched that of a deforming ballistic shield [82]. Data from the two force sensors were collected at 1 MHz and summed at each time point before a moving average filter was applied. From this, the peak force, impact duration and impulse were identified. Impact duration was considered to have begun when the force increased above 5% of the peak force and concluded when the force fell back down below 5% of the peak force.

High-speed video was collected using a high-speed camera (IL3 100-L, Fastec Imaging Corporation, San Diego, CA) at 1,250 frames per second, at 8-bit resolution depth, parallel to the shot path to study the kinematic results. The shutter speed was 160 s. The testing procedure was controlled, and data were collected, using a custom-written LabVIEW (National Instruments, Austin, TX) program and a PXIe-1082 Data Acquisition System (National Instruments, Austin,

TX, USA). Two optical sensors (PZ-V31P, Keyence Corporation, Osaka, Japan) were mounted over the projectile exit from the acceleration tube to collect instantaneous impact velocity.

Once the required impact parameters were established on the ATD, the same conditions were applied to PMHS. One specimen (211357, the 'pilot specimen') was used to identify the conditions required to generate a fracture, by increasing the impact velocity and thereby the impact energy with each test. Between tests, the specimen was x-ray imaged to assess for fracture. If no fracture was observed, the specimen was re-impacted at a higher energy level, intended to represent a decreased stand-off distance. Peak force of the impacts resulting in fracture was considered the force required to fracture. Each specimen was impacted at two anatomical locations, in an effort to maximize the value from each specimen and which were presumed to be independent, but the order of impacts alternated between the wrist and elbow to nullify any possible sequencing effects. If specimens fractured upon impact, bandages at the wrist and elbow were added post-fracture in an effort to maintain stability and reduce any sequencing effects. After testing was complete, CT imaging was conducted to determine fracture type and location.

4.3.3 Statistical Analysis

A two-tailed t-test was conducted to compare fracture force, impact velocity, impact duration and impulse between the wrist and elbow impacts. A one-way Analysis of Variance (ANOVA) with post hoc Tukey test was conducted on peak force to compare wrist and elbow impact locations with the forearm and hand, as reported previously in [92]. A significance threshold was set at $\alpha = 0.05$ for all tests. Linear regression and correlation analyses were conducted to assess the effects of donor age, height, body mass, bone mineral density, and impact velocity on force at fracture.

A survival analysis was performed with respect to peak impact force collected from each test at both the elbow and wrist to generate injury risk curves resulting from BSBT for these locations [59] [88]. Data were right-censored if the impact did not cause an injury, with the response as 1 for fracture tests and 0 for non-fracture tests. The Weibull regression model is:

$$P(x) = 1 - e^{-(\frac{x}{\lambda})^{\kappa}}$$

where P is the probability of injury, x is the predictor variable, and λ and κ are the scale and shape parameters, respectively.

A relationship was also developed to relay the injury risk curves generated onto the augmented WorldSID ATD that had previously been instrumented for measurement of BSBT in a ballistic range. The 10% and 50% injury risk from the PMHS survival curve generated was inputted into the scaling relationship that was developed between the ATD and PMHS to generate a useful injury threshold. The ATD measured higher responses in comparison to the PMHS (due primarily to the increased stiffness) and served as a repeatable measurement tool to evaluate shield efficacy in the future. The same was conducted for the hand and forearm impacts that were tested on the contralateral limb [92], in order to identify the most vulnerable anatomical location, and limit fracture from behind shield blunt trauma with confidence.

4.4 Results

There were no pre-existing injuries identified on the CT scans. The volumetric bone mineral density obtained from the CT scans at the 1/3 distal radius was 1.215 ± 0.081 (mean ± standard deviation), and all specimens fell within the normal range, meaning osteoporosis was not deemed a contributing factor [61].

In the wrist, the distal ulna and radius fractured frequently, with the distal radius fracturing in six and the distal ulna fracturing in three specimens (Table 4.2). Interestingly, the carpal bones were only fractured in two of the eight wrist impacts conducted, and the proximal metacarpals only damaged in one wrist impact. For elbow impacts, the radial head was fractured in all impacts. The distal humerus only fractured in five of the eight tests conducted.

Table 4.2: Fracture descriptions.
Note the italicized specimen is the pilot specimen.

Specimen ID	Wrist Fracture Description	Elbow Fracture Description
211357-R	Nondisplaced comminuted distal radius fracture.	Nondisplaced distal humeral fracture; radial head fracture.
210891-L	Comminuted pisiform fracture, radial styloid fracture.	Nondisplaced radial head fracture.
210897-R	Comminuted pisiform fracture with mild displacement of a tiny osseous fragment. Nondisplaced trapezium chip fracture.	Nondisplaced radial head fracture; nondisplaced distal humerus fracture.
211127-L	Minimally displaced second, third, and fourth proximal metacarpal fractures.	Nondisplaced distal humerus fracture; minimally displaced radial head fracture.
220316-L	Comminuted distal radius and distal ulna fractures.	Nondisplaced lateral epicondyle fracture; nondisplaced radial head fracture.
230246-R	Nondisplaced distal radius and distal ulna fractures.	Comminuted nondisplaced distal humeral fracture involving the trochlea/capitate; radial head fracture.
221296-R	Comminuted distal radius fracture, distal ulnar styloid fracture.	Radial head fracture.
230522-L	Comminuted distal radius fracture.	Minimally displaced radial head fracture.

The fracture threshold for the wrist was 5,663 ± 1,386 N (mean ± standard deviation), higher than the elbow at 4,765 ± 893 N (though not significantly, $p = 0.15$). All fracture force data

(including that produced by the pilot impacts) fell within two standard deviations of the mean, so was included in the statistical analysis. The failure impact velocity for wrist impacts was 17.7 ± 2.1 m/s (mean ± standard deviation), with an impact duration of 2.9 ± 0.5 ms and an impulse of 6.81 ± 2.17 N*s (Table 4.3). For the elbow, the failure impact velocity was 19.5 ± 0.9 m/s (mean ± standard deviation), while the impact duration was 5.2 ± 2.8 ms and the impulse was 7.13 ± 3.56 N*s (Table 4.4). The impact velocities for the elbow fracture tests were significantly higher than the wrist velocity fracture impacts ($p = 0.048$), but anatomical location did not significantly affect the impact duration ($p = 0.08$) or the impulse ($p = 0.99$).

Table 4.3: Wrist impact failure data.
The impact order denotes whether the wrist was impacted before (1) or after (2) the elbow. The number of previous impacts the specimen underwent prior to fracture is also included. The pilot specimen is italicized.

Specimen ID	Impact Order	Impact Velocity (m/s)	Peak Force (N)	Impact Duration (ms)	Impulse (N*s)	# Previous Impacts
211357-R	*1*	*20.7*	*6,054*	*3.1*	*6.6*	*7*
210891-L	1	19.8	6,028	2.2	6.6	2
210897-R	2	14.9	3,445	5.0	4.5	2
211127-L	2	16.3	4,578	3.5	7.3	1
220316-R	1	19.8	5,953	2.5	7.1	1
230246-R	2	17.0	7,979	3.3	10.7	0
221296-R	1	16.3	6,664	2.9	6.2	0
230522-L	2	16.7	4,296	3.5	7.2	0
Mean ± Standard Deviation		**17.7 ± 2.1**	**5,663 ± 1,386**	**3.3 ± 0.9**	**7.2 ± 1.6**	

Table 4.4: Elbow impact failure data.
The impact order denotes whether the elbow was impacted before (1) or after (2) the wrist. The number of previous impacts the specimen underwent prior to fracture is also included. The pilot specimen is italicized.

Specimen ID	Impact Order	Impact Velocity (m/s)	Peak Force (N)	Impact Duration (ms)	Impulse (N*s)	# Previous Impacts
211357-R	*2*	*19.3*	*3,600*	*3.6*	*8.0*	*7*
210891-L	2	19.6	4,876	1.1	1.9	3
210897-R	1	17.7	6,256	9.0	14.1	2
211127-L	1	20.7	4,189	4.0	5.0	2
220316-R	2	20.2	5,185	8.1	6.8	1
230246-R	1	19.3	4,960	4.0	6.9	0
221296-R	2	19.4	5,345	7.7	9.2	1
230522-L	1	19.3	3,711	3.8	5.1	0
Mean ± Standard Deviation		**19.5 ± 0.9**	**4,765 ± 894**	**5.2 ± 2.8**	**7.1 ± 3.6**	

When comparing among all impact locations (including those from [92]), the hand fracture threshold was significantly less than the wrist ($p = 0.0047$), and the wrist was significantly higher than the forearm ($p < 0.0001$, Figure 4.2). The elbow was also significantly higher than the forearm ($p < 0.01$). These data suggest the forearm is the most vulnerable to injury as a result of BSBT.

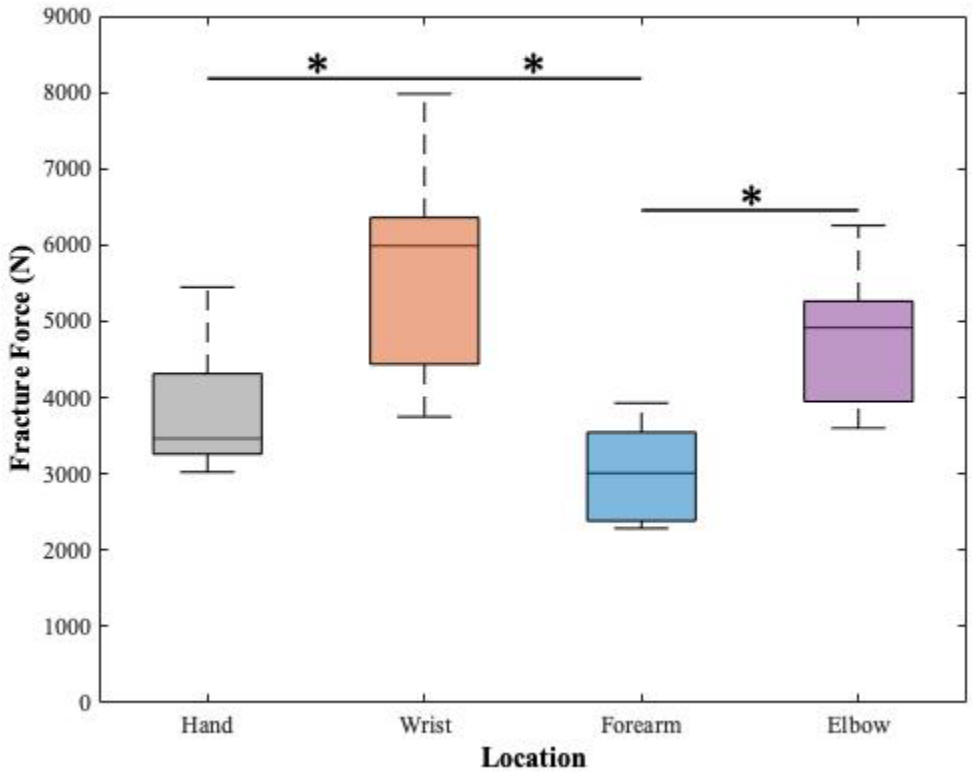

Figure 4.2: A comparison of all anatomical locations tested for BSBT, combining present results with those of a previous hand/forearm study [92]. The '*' denotes a significant finding, with a significance threshold (α) set at 0.05.

These data were fit with injury risk curves (Figure 4.3). The scale (λ) and shape (κ) parameters for the wrist were 6,860.1 and 1.1342, respectively. This resulted in a 10% risk of fracture as 943 N and 50% risk of fracture as 4,966 N. For the elbow, the scale (λ) was 5253.6 and the shape (κ) was 1.4256, resulting in 10% risk of fracture as 1,084 N and 50% risk of fracture as

4,063 N. When translating these 10% injury risk parameters to the WorldSID ATD from a relationship developed between the ATD and PMHS, this would be 10.8 kN measured for the wrist and 12.5 kN for the elbow.

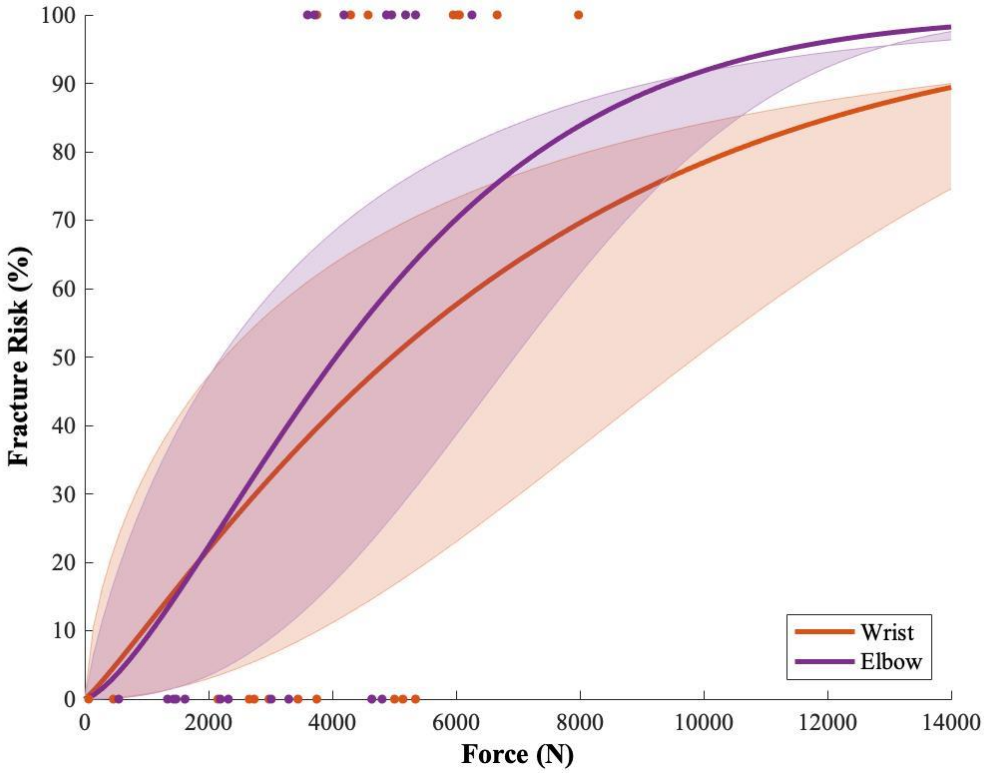

Figure 4.3: The wrist (orange) and elbow (purple) fracture injury risk curves generated from this study.
The shaded regions represent the 95% confidence intervals of the curves.

When investigating the effects of impact duration, impact velocity, donor height, bone mineral density, age, or body mass on the fracture force, only donor age had a moderate correlation with fracture force (an R^2 of 0.51 for the wrist and 0.23 in the elbow), with younger donors having a higher fracture threshold. Surprisingly, BMD at the distal 1/3 radius location did not have a linear

correlation (R^2 of 0.0008 in the wrist and 0.1691 in the elbow). The effect of BMD measured at the mid-slice of the scaphoid (0.22 ± 0.05 g/cm^3, mean ± standard deviation) and the lunate (0.28 ± 0.07 g/cm^3) also did not show a strong correlation with fracture force in the wrist (R^2 of 0.14 in the lunate and 0.02 in the scaphoid).

4.5 Discussion

This study investigated the risk of wrist and elbow fracture, which when combined with previous work on hand and forearm risk [92], completes the investigation of the fracture tolerance of the upper extremity when subjected to BSBT. Realistic loading conditions that were previously collected using a modified WorldSID ATD in the same testing apparatus in a ballistic loading scenario [82] were applied to PMHS in this study. The statistically significant differences in fracture threshold among different anatomical areas indicates that boundary conditions are an important factor to consider in PMHS testing, and different locations need to be considered when establishing an injury threshold for an entire limb. Using one specimen to impact two anatomical locations is advantageous to investigate the effects of different anatomical locations while controlling for factors like bone quality and age. This is further supported by testing different anatomical locations on the contralateral limb (the hand and forearm) [92]. Results from the present study will be an essential component in evaluating future shield designs to ensure they are both protective of projectile penetration and minimize risk of upper extremity fracture.

The wrist fracture force identified in this study (5,663 ± 1,386 N) was somewhat lower than one previous study identifying the fracture force in the axial orientation (6,565 ± 980 N) [62]. However, this was investigated in conditions representing a forward fall, delivered with a heavy

projectile (6.66 kg) at a lower impact velocity (3.9 m/s), and used ballast masses to simulate the effective mass of specimens. This may have been partially responsible for the higher impact forces than were reported herein. The most frequent location of fracture in this previous study was the distal radius [62], findings that are consistent with this study. Most other studies that have investigated the carpal bones or distal radius and ulna fracture threshold have also been conducted in the forward-fall orientation (*e.g.*, [94] with lower failure forces, 3,896 N). It is therefore challenging to directly compare results from this study with the previously reported studies. As in general, higher-rate impacts result in greater fracture thresholds (*e.g.*, [92], [58]) it may be that the present impact scenario (energy and orientation) is more vulnerable to injury from impacts directed on the dorsal wrist as opposed to axial impacts.

The elbow fracture force in this study (4,765 N) is higher than previously reported when impacted in the sagittal plane, with previously reported mean forces of 4,100 N for the olecranon and 3,800 N for the distal humerus [53]. This was again a different orientation that used a 20 kg impacting mass, making it challenging to compare results. However, the experiments conducted in the previous study that had the elbow positioned in 0° to 80° flexion generated radial head fractures [53], consistent with findings from this study. Further, the higher fracture threshold in the present higher-rate study is unsurprising and may be attributable to the viscoelastic nature of bone.

The use of midsized males was selected as a baseline population group for generating injury criteria as there has been no work conducted in this orientation and loading condition to date, and the ATD used in this study represents that of a 50th male. Further, much of the Canadian Armed Forces is male (86.2%, [72]). However, there remained a substantial amount of variation in the data produced herein, despite this being a very homogenous donor population. This may

have been attributed to differing ages and variances in alignment which may have changed the loading path and highlights why a 10% injury risk is important (to account for varying individual tissue tolerance).

There were limitations to this study. Firstly, a support was placed behind the wrist in order to prevent rapid extension during impact, that may not occur in a field setting. However, musculature surrounding the wrist would provide reinforcement against extension during impact, so this was considered a reasonable boundary condition. Nevertheless, it is possible that this led to an overly rigid condition, and a more conservative injury limit. The large number of distal radius and ulna fractures in this study was surprising in comparison to carpal bone fractures. It is challenging to identify whether this is simply a weaker location or if this was caused by alignment issues with the projectile or the wrist support component. Further, the specimens used in this study were of advanced age (72 ± 15 years) and as such were not representative of a typical younger soldier population. As bone tissue quality is known to decrease with age, a younger population would likely sustain a higher force prior to failure. However, bone quality was assessed prior to impact and all specimens were within a normal range. Thus, the data presented here may represent a conservative estimate of the fracture tolerance for soldiers. The limited sample size of this study is common to cadaveric investigations. There was also a lack of muscle tension applied to the specimens as PMHS are unable to generate a physiological response. There may be initial muscle tension applied in the upper extremity for individuals carrying ballistic shields; however, the extent of this activation is unknown. This should be considered in future studies as it may have affected the injury threshold but is generally a typical limitation of injury tissue testing. Post-mortem human subjects remain the most accurate depiction of biological specimens, especially when considering this is the first study to investigate upper extremities at this rate of loading.

Specimens that did not appear to sustain a fracture during impact (as viewed by a radiologist on x-ray images) were re-impacted at a higher energy level. These repeated impacts may have affected the injury threshold of the specimens. Four specimen impacts (210897 at the wrist and 210891, 211127, 211296 at the elbow) survived a higher-force impact without sustaining a visible fracture, but the subsequent impact resulted in a lower force. In these cases, the higher force was treated as the failure-inducing impact. For the wrist impacts, five specimens underwent repeated impacts, whereas three specimens fractured on the first impact. The means of these two groups did not differ significantly ($p = 0.33$). Although impacted many times, the pilot failure force was within the range of data for the rest of the impacts, as such, it was included in the dataset. In the elbow impacts, six specimens underwent repeated impacts while two sustained fractures on the first impact. These two groups also did not vary significantly ($p = 0.48$), so were all included in the analysis. There was also a potential effect of the impact sequence, which was necessary in an effort to maximize the value obtained from these experiments. However, no trends were observed with sequencing, so it likely had minimal effect given the distance between test locations. When comparing the failure thresholds of specimens that were impacted at the wrist first *vs.* second there was no effect of order ($p = 0.32$), the same of which was noted for the elbow impacts ($p = 0.97$).

The significantly lower forearm fracture threshold in comparison to the wrist and elbow under similar loading conditions indicates it may be the most vulnerable location for injury resulting from behind shield blunt trauma. When translating these 10% injury risk parameters to the WorldSID ATD from a relationship developed between the ATD and PMHS, this would be an 11.0 kN limit for the hand, 10.8 kN measure for the wrist, 7.2 kN measure for the forearm and 12.5 kN for the elbow. It should be noted that these limits were extrapolated beyond the data used to

develop a linear relationship developed for translating the WorldSID ATD to PMHS measures due to instrumentation capability limits on the ATD.

It is important that ballistic shields protect users from both projectile penetration and injuries resulting from behind shield blunt trauma. Currently used shields that pass standards regulations on projectile penetration are not adequate in minimizing upper extremity fracture risk, as the 10% risk of fracture that is generally accepted for protective equipment exceeded measurements obtained on an ATD under ballistic testing [82]. Results from this study can be used to develop a new standard to assess whether or not shields are adequate at minimizing upper extremity fractures, providing important protection for armed forces users.

Chapter 5 – A Comparison of the THUMS AM50 Finite Element Model to Experimental Results When Subjected to Behind Shield Blunt Trauma Loading Conditions

Overview: *In this chapter, the THUMS is evaluated for its ability to predict fracture in response to high-rate impacts typical of behind shield blunt trauma. A model that matched the shape and stiffness of the projectile used in experimental testing was used for the simulation. One post-mortem human subject (from Chapter 3) was instrumented with strain gauges to measure the bone strain at failure, which was used as the critical failure strain defining when fracture occurred in the model. A comparison was made for the THUMS response and the overall PMHS experimental response under the same loading conditions and improvements were suggested for future iterations of this model to address Objective 3, should it be used for assessing shield efficacy as it relates to behind armour blunt trauma.*

5.1 Introduction

Experimental injury testing of post-mortem human subjects (PMHS) is limited in that it is expensive, laborious, and generally only constitutes a one-time-use experiment. Automotive and defence manufacturers frequently use computer simulations for design and safety assessments as finite element (FE) models offer a useful method for evaluating injury risk. Finite element computational models of the human body are designed to replicate the kinematic and

biomechanical properties of humans in a variety of scenarios. Similar to Anthropomorphic Test Devices (ATDs), they are typically designed to represent a specific demographic of the population but can be used to predict injury and provide the exact time at which injury may occur. Models have many advantages such as allowing for a variety of experimental variables to be investigated in a single 'specimen', and at relatively low cost. They also have infinite measurement points, in contrast to ATDs and PMHS, which are typically instrumented in discrete locations.

Innovative predictive numerical models are important for the design and advancement of safety systems due to the complexities surrounding PMHS and physical surrogate testing. Highly detailed models are required to evaluate new situations that include changes in loading rate and mode. In order to have confidence in their output, they need to be validated through comparison to experimental work. This could include evaluation of behind shield blunt trauma (BSBT), an injury mechanism that describes blunt trauma resulting from rapidly deforming ballistic shields [92].

There is currently a concerted effort to contribute, develop and validate whole body models that may be used for a variety of industries (*e.g.*, automotive, sports, and military) in an effort to consolidate research initiatives from many institutions [32]. Two such models, the Global Human Body Model Consortium (GHBMC, Rochester Hills, MI, USA) and the Total Human Model for Safety (THUMS, Toyota Motor Corporation and Toyota Central R&D Labs., Inc., Aichi, Japan) have received significant advancements of late to contribute to this effort and are being widely used. In the case of BSBT, it has been observed that this unique loading condition results in vastly different injury mechanisms and thresholds [92]. Further research is required to link the shield response and measurable upper extremity response in models to injury risk.

5.1.1 The THUMS Model

The Total Human Model for Safety (THUMS) is the most detailed upper extremity model currently (as of 2023) freely available. The AM50 Occupant model represents the 50th percentile adult male and is based upon the dataset obtained from Computed Tomography (CT) scans of a 39-year-old male [47]. It has a height of 175 cm and weight of 77 kg [95], and the segmented arm (distal to the isolated humerus) has 59,647 total elements. Solid elements are used for both cortical and trabecular bone in the model, while shell elements are used to model the skin.

The THUMS AM50 has been extensively validated from a whole-body perspective under automotive conditions [48]. There are anatomical simplifications of the upper extremity that may affect the biofidelity of the model under certain scenarios, such as the lack of soft tissue in the hands and elbow, and articular cartilage in the joints [49]. Previous validation work of the upper extremity includes evaluation of the intact shoulder as a biomechanical system [48]. This version has also previously been validated with quasistatic 3-point bending and dynamic lateral compression for the humerus [40]. The model performed well for the humerus 3-point bending test (*i.e.*, the force-displacement was within the PMHS corridors up until approximately 10 mm of displacement), but although it followed the same general shape for the dynamic tests, did not fall within PMHS corridors [47].

Recent work from our group has also validated the segmented upper extremity for lateral impacts to the forearm simulating automotive energies, in which it showed good agreement with literature failure forces [96]. The focus of this assessment was fracture prediction of the radius and ulna. Aside from this recent investigation, there has been limited focus on the THUMS upper extremity and its response to loading.

5.1.2 Failure Prediction

Fracture has been simulated in previous human body model simulations using two different methods, and both are available in the THUMS AM50 [47]. The first is to estimate the occurrence of injury from relevant values such as strain and deflection (*e.g.*, [97]). For example, the cortical bone strain can be measured after a simulation has concluded to determine whether certain elements would have failed, should their strain exceed a measured threshold value. This method does not require special failure or damage functions in material modeling, and thus is easy to implement and computationally less expensive. However, the kinematics or the mechanical response of an undamaged model might be different from those of actual damaged parts. The other method used is to explicitly simulate the injuries using failure or damage functions such as element deletion. This method requires a failure or damage criterion to eliminate/remove elements from calculation and must be specified in material models and is only suitable for tensile type failures [97].

It has been shown in many experimental studies that have spanned decades that the strength of bone increases with increased strain rate [56, 57, 98, 58]. The THUMS had originally modelled the cortical bone as isotropic elastic plastic material using shell elements and the trabecular bone as the same material using solid elements [45]. However, in version 6 (the version used in this study), solid elements are used for both cortical and trabecular bones [47]. The trabecular bone and cortical bone in the THUMS AM50 include strain-rate dependent properties; however, the model response needs to be assessed to ensure an accurate representation or to be further improved and refined. If it to be used as a tool for assessing injury for behind shield blunt trauma investigations, verification of output parameters at the different impact speeds should be conducted.

Post-mortem human subject (PMHS) studies of projectile impacts emulating the back-face deformation of ballistic shields on the upper extremity measured an average peak force of 3,011 ± 656 N applied to the forearm resulted in skeletal fractures [92]. Upper extremity injury criteria such as peak force [66] has been established in the automotive community in the relevant loading scenario. However, the forearm response to BSBT differs from the automotive response [92] and therefore this automotive model needs to be evaluated before use for BSBT purposes. Finite element modelling may offer a reliable tool for shield manufacturers to assess potential new designs but needs to be verified that it responds appropriately under these unique conditions.

5.1.3 Study Objective

Human body models have been previously used to assess the potential for upper extremity injury from blunt impacts as a result of side airbags for motor vehicle applications. To the author's knowledge, no finite elements model of the upper extremity has been employed to investigate its application to behind-shield blunt trauma. The purpose of this study was to assess the response of the THUMS AM50 forearm to behind shield blunt trauma impacts, with a focus on fracture through comparison with previous experimental work [92]. The overall goal was to assess its suitability for evaluating shield efficacy, by first determining if it can accurately predict upper extremity forearm fractures at BSBT loading rates.

5.2 Methods

5.2.1 Experimental Data Collection

The experimental methods for this portion of the work were detailed previously (Chapter 3) [92]. One PMHS upper extremity (230246-L) was selected for instrumentation as it was the

youngest of the specimen group (aged 46, mean age 72 years), intended to be the closest match to that of the soldier population, and the subject from whom the FE model was developed. It was instrumented with four tri-axial strain gauge rosettes (F series, Tokyo Measuring Instruments Laboratory Co., Ltd. Tokyo, Japan), two on the radius and two on the ulna to characterize the strain patterns during impact (Figure 5.1). The specimen was positioned supine (*i.e.*, exposing the anterior side of the forearm) and dissected prior to testing to expose the ulna and radius at the midpoint of the bones, measured as the halfway point between the ulnar styloid process and the lateral epicondyle. Approximately two inches of soft tissue was resected on both the ulna and radius to allow for application of two strain gauges positioned approximately 1 inch apart on the supine side (*i.e.*, the opposite side in which impact would occur). Details of the impact procedure are discussed in previous work [92]. Briefly, the specimen was secured into a pneumatic impacting apparatus and a 434 g projectile was accelerated down a tube via compressed air. Force sensors beneath the impact cap of the projectile were mounted in parallel to measure the applied force (up to 44.48 kN). It was then impacted at the forearm to failure and the strain data were recorded (at 50 kHz) and used to calculate the maximum principal strains[8] of the bone, taken as the strain at fracture. All data were recorded, and the apparatus triggered by using a LabVIEW program (National Instruments, Austin, TX, USA).

[8] Calculations and methodology for the determination of maximum principal strain can be found in Appendix G.

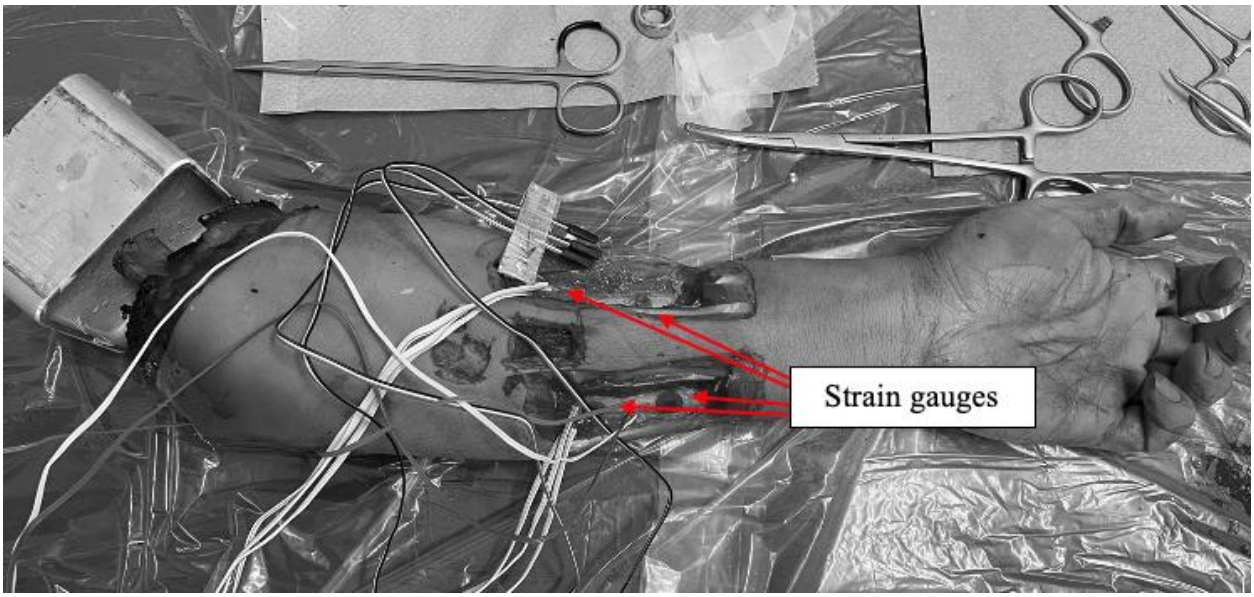

Figure 5.1: Strain gauge rosette application.
Strain gauges were applied to the anterior side of the radius and ulna.

5.2.2 Evaluating the THUMS for High-Rate Loading

The THUMS AM50 Occupant Model Version 6.1 was obtained for this study. To alleviate some of the computational demands of running a full-body model, the left upper extremity was segmented from the remainder of the model in LS-PrePost (Ansys Inc., Canonsburg, PA, Figure 5.2). All anatomical structures distal to and including the humeral head were preserved to ensure the biomechanical properties embedded within the model remained intact, and to replicate the segmentation that was conducted on the PMHS tested experimentally (Chapter 3).

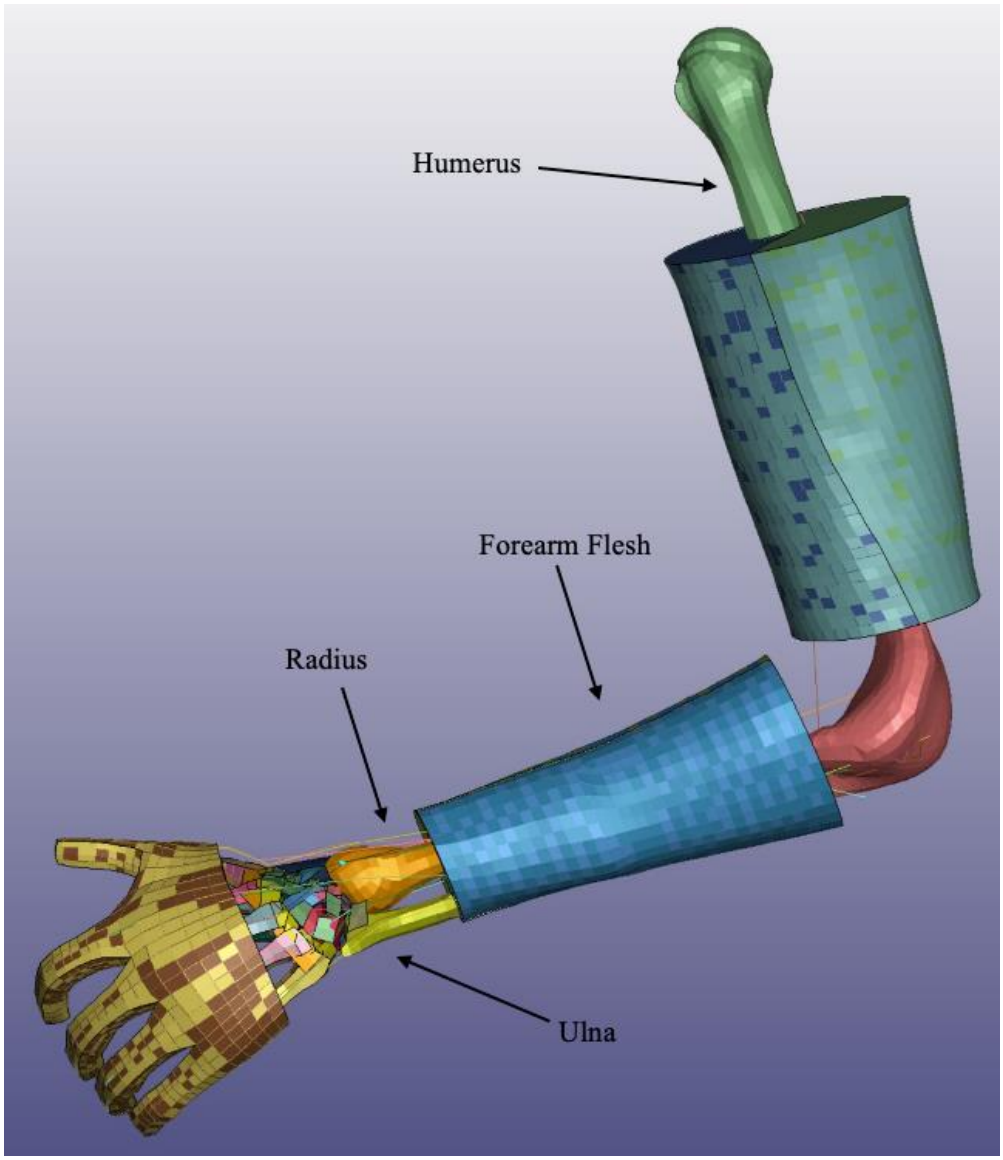

Figure 5.2: The THUMS AM50 Occupant Model Upper Limb.
The isolated THUMS upper extremity used for simulations. Note: superficial soft tissue was removed from the elbow and wrist for visualization of deeper (bony) structures.

The built-in material models were used for all structures. Radius and/or ulnar fracture was implemented using an element erosion technique, with critical plastic strain using material properties generated from the experimental data. As such, the ulnar and radial strain determined from the experimental impacts was input as the deletion thresholds within the model. When bone

strain increased above the collected experimental strain threshold, elements deleted to represent failure (*i.e.*, fracture occurred).

The experimental setup was recreated in the model, such that the humerus was constrained in all directions at the humeral head (similar to being potted in bone cement) and the aluminum handle was positioned proximal to the proximal interphalangeal joints of the fingers, with the metacarpals positioned in front of the handle. The arm was positioned in an approximate 90° humerus-to-radius/ulna position. A rigid hemispherical impact cap that matched the shape of the impacts conducted on the PMHS was used in this study. A simplified version of the projectile body was then used and modelled as a rigid material with density to match the mass of the projectile. The projectile cap and body were fastened to one another in the model such that there was no relative movement during impact. The projectile was aligned in the same manner as was conducted experimentally, in that the halfway point between the lateral epicondyle of the elbow and the ulnar styloid process on the posterior side was the target impact location. Two impact conditions were simulated – that which caused fracture of the gauged specimen (14.7 m/s, the 'subject-specific test condition'), as well as that representing the mean of all eight PMHS forearms (16.8 m/s, the 'impact representing the average') [92].

All simulations were executed using LS-RUN (Ansys, Inc., Canonsburg, PA). Applied force was measured beneath the projectile impact cap experimentally, so the interface of the impact cap with the rest of the projectile was the location of force collection in the numerical model. The model performance was evaluated using impactor force *vs.* time as well as peak force. Responses within one standard deviation of the injury curve were considered a good predictor of injury.

5.3 Results

The radius and ulna both fractured in the experimental impact. The radius fractured at two locations along the bone while the ulna only fractured at the approximate midpoint. The maximum impact force experimentally was measured as 2,837 N, slightly less than the average forearm failure force under these conditions (3,011 N) but within one standard deviation [92]. The conditions associated with the experimental failure test were a projectile velocity of 14.7 m/s, impact duration of 7.39 ms, and impulse (as measured from the area under the force-time curve) of 6.80 N*s.

Two of the four strain gauges (the proximal radius and distal ulna gauges) were damaged on impact, so the data were not considered useable. The centre of the stacked strain gauge rosettes was located approximately 112 mm from the ulnar styloid process on the ulna and 90 mm from the radial styloid process on the radius (Figure 5.3). The fracture occurred approximately 28 mm proximal to where the radius strain was measured, while the ulnar strain was closer, approximately 23 mm distal to the fracture site. Based on the strain data, the radius fractured before the ulna. However, one of the ulna strain gauges broke before reaching the maximum strain (as determined by the other two strain gauges in the rosette) and as such, the data was not usable. The maximum principal strain on the radius measured 12,580 με (1.26%, Figure 5.4). The maximum principal strain on the ulna was 6,661 με (0.67%) at the time of radius fracture. As such, both the ulnar and radius failure strain were set to 1.26% for the THUMS simulations.

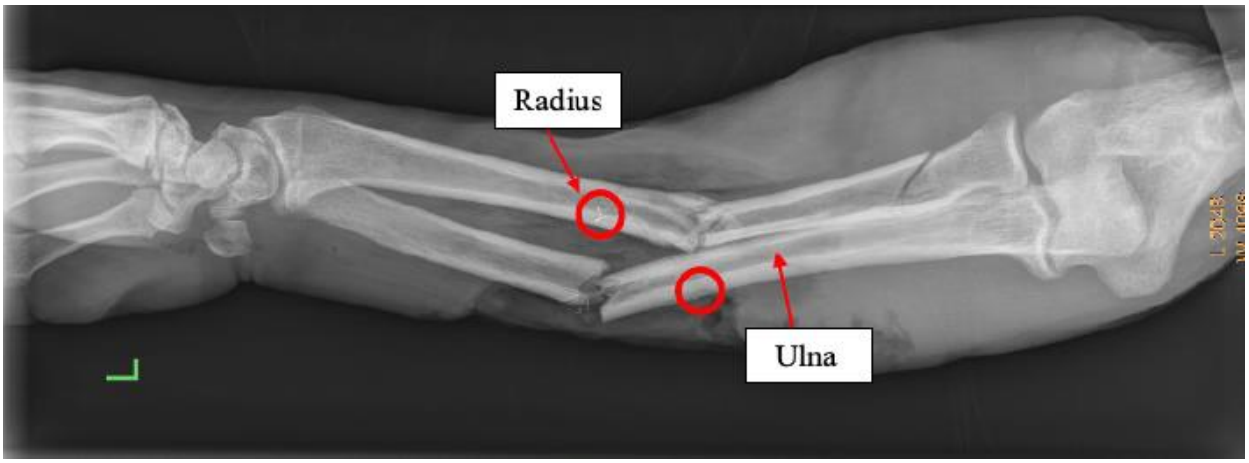

Figure 5.3: X-ray image of specimen after it was fractured. The locations of the two strain gauges have been indicated (red).

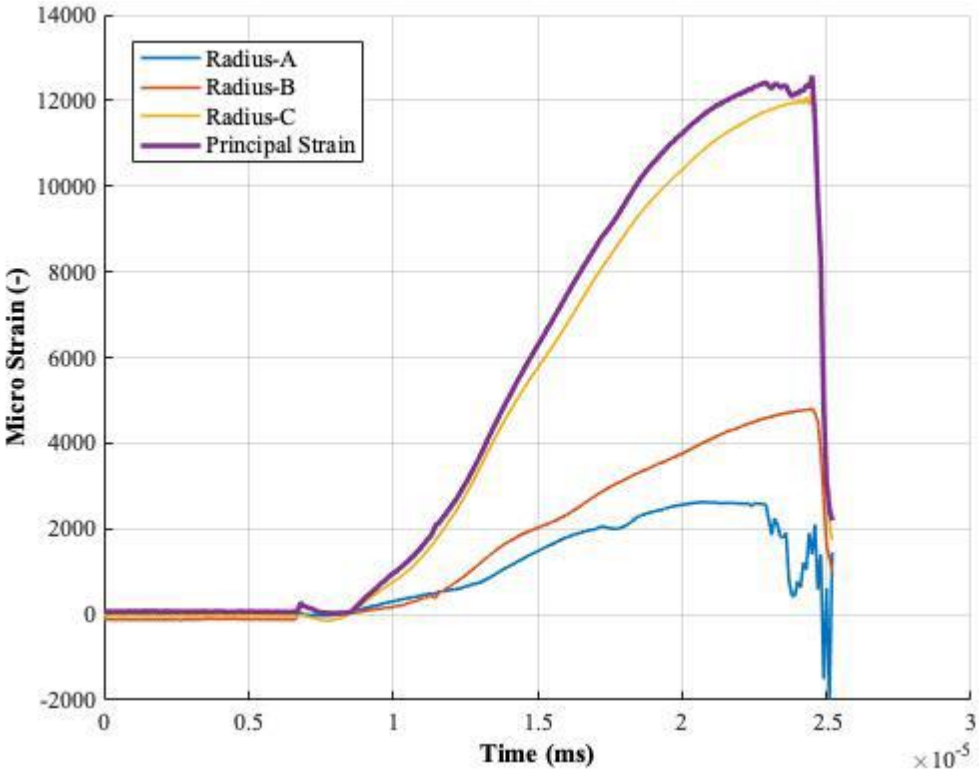

Figure 5.4: Radial strain with respect to time.

The peak force measured in the 14.7 m/s subject-specific test condition in the THUMS test was 2,815 N (0.8 % lower than the experimental work obtained from this specific impact). Both bones fractured in the simulation, in agreement with the experimental impact; however, the radius only fractured at one point in contrast to the experimental impact. The ulna fracture was located proximal to the ulnar styloid process by approximately 139 mm (in comparison to 89 mm on the experimental impact, Figure 5.5). The radius fracture was located approximately 136 mm from the distal radius (compared to 118 mm in the experimental impact). The radius also fractured before the ulna in the simulation results.

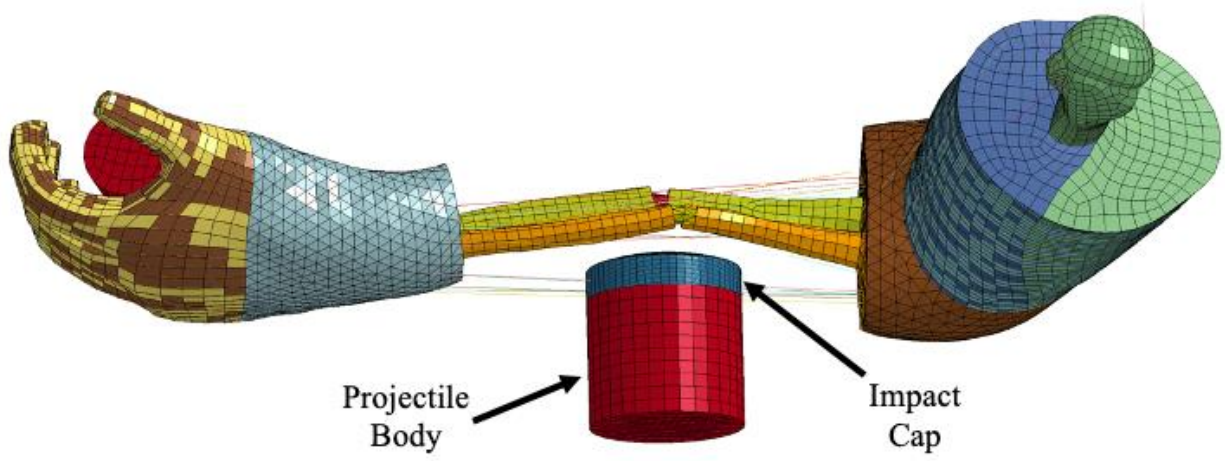

Figure 5.5: Ulna and radius fractures resulting from the THUMS simulation.
Note the soft tissue surrounding the forearm was hidden for visualization of the fractures.

The experimental results had a large initial peak, followed by a drop and then an increase in applied force again (Figure 5.6). The simulation did not display this, as the peak was reached after the experimental peak. The mean failure loads of the forearm in this experimental study were 3,011 ± 656 N. The peak force measured during the simulation representing the average impacts

was 3,332 N. The subject-specific test condition simulation duration was 4.30 ms, and the impulse was 5.54 N*s, which aligned well with the experimental impulse, 6.80 N*s (Table 5.1).

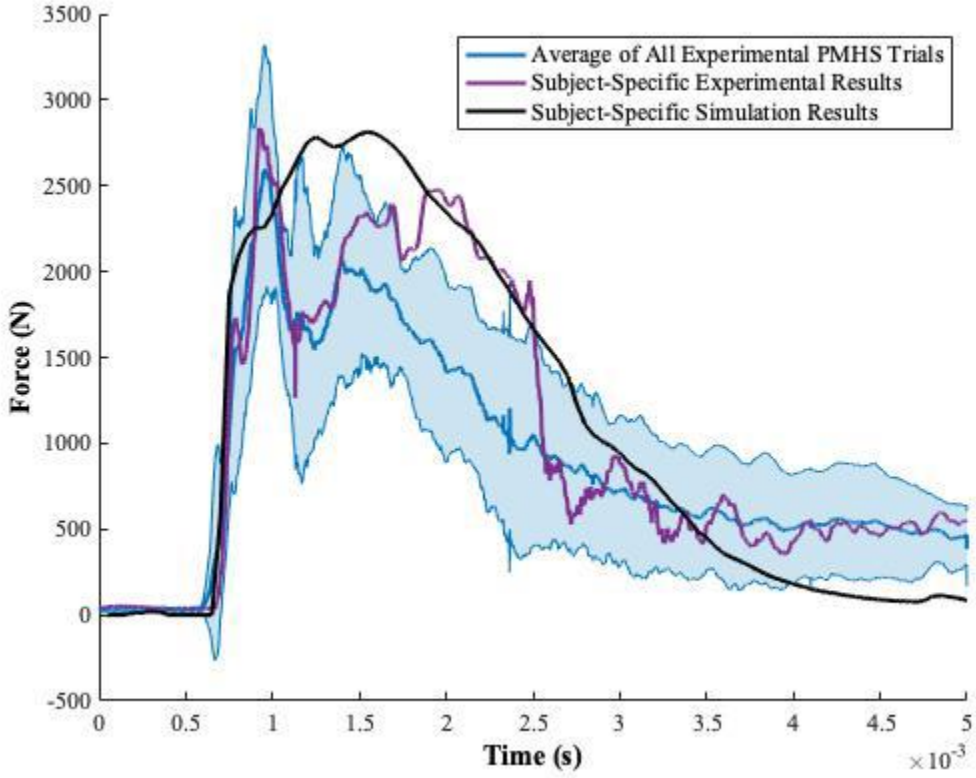

Figure 5.6: Force-time traces for experimental and simulation data.
The force-time experimental curve, all experimental PMHS trials (line represents the mean while the shaded regions represent the standard deviation of the repeated trials) [92] and the subject-specific simulation results is displayed here. All PMHS data followed the same general shape, with an initial peak followed by a substantial drop and then an increase in force again. The THUMS reached the peak after the experimental data but had a smaller duration than the experimental data, and the shape of the curve did not match that of the PMHS data.

Table 5.1: Summary of Experimental and Simulation Results
The simulation impacts were substantially shorter than the PMHS impacts, while the peak forces and resulting impulses were similar.

	Peak Force (N)	Duration (ms)	Impulse (N*s)
All Experimental PMHS Trials	3,011	8.09	6.41
Simulation Representing the Average	3,332	4.40	6.17
% Difference	10.1%	59.1%	3.8%
Subject-Specific Experimental Impact	2,837	7.39	6.80
Simulation Subject-Specific Test Conditions	2,815	4.3	5.54
% Difference	0.8%	52.9%	20.4%

5.4 Discussion

This was the first study of its kind to evaluate the response of the THUMS upper extremity to high-rate loading and compare with experimental data under the same conditions. It used bone strain from experimental impacts to inform the failure threshold of the model, and accurately predicted fracture at the given loading rate. The shape of the force-time curve did not match that of the PMHS data, indicating future work on this model to better represent the upper extremity response (particularly post-failure) would be valuable.

The failure strains in this study were within a similar range of those reported in a previous study, where they reported the ulna strain as 1.02 ± 0.42% and the radius at 1.17 ± 0.36 (this study 1.26%) [54]. However, the higher strains in the present work may be attributed to a slightly different impact and instrumentation location, where Duma *et al.* instrumented and struck the 1/3 distal forearm, whereas this work aimed at the midpoint. However, the strain generated from this

work did fall within their standard deviations. The peak ulna strain did not occur at the same time as the peak radius strain, with a delay in approximately 34 ms, indicating the radius fractured first, in agreement with previous studies [54, 62].

The THUMS AM50 demonstrated an ability to predict radius and ulna fracture for shield BABT events in agreement with experimental data. The time duration was 53% longer in the experimental impact in comparison to the simulation for the subject-specific impact parameters. The impulse was 20% higher in the subject-specific experimental data as compared to the subject-specific simulation. The initial drop in force observed in the simulation was likely due to the radius fracturing, followed by an increase in force as the ulna was loaded, which has been seen experimentally in previous studies [84]. However, the drop in force appears much steeper experimentally as compared to the simulated results. Element deletion in the models remove material that in reality is there, so this may have contributed to the delayed increase in applied force in comparison to the experimental data. Relying simply on peak force as the output from finite element studies may not provide an accurate depiction of the event.

Although the peak force measured during the subject-specific simulation aligned well with the experimental peak force averaged across all subjects, the shape of the curve did not align with the overall mean response of the PMHS (*i.e.*, did not fall within one standard deviation). The shape of the curve falling within one standard deviation provides an objective evaluation of time-history signals derived from both the experiments and simulations. This could be due to a variety of factors that differed between the PMHS and simulation study. In the PMHS study, a pneumatic impacting apparatus was used to apply load, which accelerated a projectile down a tube via a burst of compressed air. There is no pressure relief behind the projectile once the pressurized air is released. This may mean that in the experimental study there may have been a greater application of force

due to the compressed air continually pressing against the projectile. This was not represented in the simulation, where an initial velocity was specified for the projectile only.

The THUMS AM50 was not developed for behind-shield blunt trauma applications, as it was designed for automotive conditions. The purpose of this work was to investigate the potential of the existing THUMS AM50 for high-rate loading applications, given the known rate effects for biological tissues. The use of a finite element upper extremity model that is capable of predicting fracture as a result of behind shield blunt trauma would be valuable for future shield designs.

5.4.1 Limitations

This study had a few limitations. First, the peak strain as determined by the strain gauge rosettes from the experimental portion of this work was collected some distance away from the location of fracture. As strain gauges are very fragile and in experimental impact testing are prone to damage, the aim was to place them close to the expected fracture site while ensuring data were collected during impact. Strain gauge locations along the ulna and radius were selected and intended to be on either side of the fracture site; however, the exact location of fracture is challenging to predict and only two strain gauges survived the experimental impact. Thus, the viable strain data ended up being 28 cm away from the radius fracture on the radius, and the peak strain measured 23 cm away from the ulna fracture site on the ulna unfortunately could not be used to inform the model. As such, the radius strain had to be used for both the ulna and radius, which may not be an accurate depiction of the peak fracture strain associated with the radius and ulna. However, most bone failure finite element erosion technique studies use a 2% strain (*e.g.*, [99]), which has limited biomechanics basis for the upper extremity where the strain rates have been reported much lower, at 1.02% for the ulna and 1.17% for the radius [54]. Using strain data

obtained experimentally as threshold values to inform the simulation for the given impact parameters was advantageous as it allowed for a direct comparison between the simulation and experimental results. In this BSBT experimental work, the radius reached peak strain at 1.26%, which is does vary as peak strain up to 3.7% has been reported in previous studies [55]. Lastly, there were differences in boundary conditions – it was challenging to 'grip' the handle with the hand, so a simplified boundary condition of fixing the elements on the palm of the hand with the handle was used. The wrapping of the hand with a tensor bandage was considered an acceptable exclusion for this portion of the work, as the forearm fracture was the focus. This may not have accurately depicted the experimental boundary conditions in which a gripping posture was replicated.

Overall limitations associated with Finite Element Modelling also need to be addressed. A limitation to using the deletion of elements at a critical value of strain to represent fracture is this means there is removal of material from the calculation at these points. Element deletion is simplified, but a computationally necessary process in modelling fracture. The THUMS AM50 upper extremity model did perform well up until failure initiated, so if researchers use this as a threshold carefully, the model may be a valuable tool, but not at this stage for post-failure representation. They also must be validated in a hierarchical manner (*i.e.*, from each system up) to ensure confidence in the model and risk the development of models for a very specific dataset. Human body model material properties and their implementation are often associated with large uncertainty because of general biological variability and limitations associated with experimental methods chosen for the constitutive tests [32]. Higher variability in experimental data can also provide a good apparent correspondence with model response due to wide response corridors produced from experimental work. However, given the low coefficient of variation in our

experimental study (21.8%) as compared to previous forearm experimental studies (*e.g.*, 34.3%, [65]), this was likely an improvement upon other verification corridors when evaluating model response in comparison to experimental data.

5.4.2 Future Work

It would be helpful to evaluate the response of the THUMS in comparison to the GHBMC to assess which had a more realistic response (*i.e.*, which model is closely aligned with PMHS data). Further, since the THUMS has the ability to predict fracture at these levels, it would be interesting to investigate how the injury limit may change with muscle activation, something that is typically not possible with PMHS studies. This may help to quantify the inherent limitations of using PMHS material to develop injury risk corridors for the living population. Lastly, it would be useful to explore the differences in response of the THUMS at a higher velocity (*e.g.*, 215 m/s from ballistic testing [82]) to quantify the effects of the impact velocity. A stroke-limiting impact and a free-flying (projectile) impact would also be useful to assess equivalencies with the laboratory-based replications of the ballistic testing conducted herein.

Once modified, a correlation and analysis objective rating tool (CORA Software) analysis would also be helpful to assess how effective the segmented THUMS upper extremity is at replicating the experimental conditions. The use of CORA provides an objective evaluation of time-history signals derived from both the experiments and simulations and quantifies this correlation. Due to substantial differences in injury outcome even within population groups, responses within one standard deviation of the injury curve are generally considered a good predictor of injury. As such, the THUMS AM50 needs to be modified in order to be considered a good predictor of injury at BSBT injury levels.

There are several modifications that may be made to the THUMS AM50 to better represent the high-rate material response that is required for behind-shield blunt trauma applications. A more advanced failure representation to predict bone failure is one step forward. Updating other material models (*i.e.*, soft tissue) to better reflect their properties under high-rate loading may also be beneficial, as this was not investigated in the present study. Assessing the THUMS AM50 at other impact locations that also have a fracture threshold identified (*i.e.*, hand, wrist and forearm) for high-rate loading typical of BSBT may also be useful. A working model that accurately predicts fracture along the upper extremity when subjected to these types of loads would be a useful tool for the design and development of new light-weight ballistic shields. Further modifications are required before shield manufacturers could use this model for injury risk resulting from BSBT. Further, extensive validation and verification would be needed of complex shield material properties (which have historically been challenging to model) in order to accurately depict injury risk resulting from rapidly deforming ballistic shields.

5.4.3 Conclusion

This chapter presented a preliminary assessment of the response of the THUMS AM50 to shield BABT for its ability to predict bone fracture. The model effectively predicted a fracture of the radius and ulna, consistent with experimental data obtained under the same loading conditions. Although the peak force in the model experienced closely aligned with that obtained in the experimental conditions, the shape of the curve did not, indicating that further modifications are required (aside from informing a bone strain limit) to use the THUMS AM50 for BSBT purposes.

Chapter 6 – General Discussion and Conclusions

Overview: *In this chapter, the objectives and hypotheses set out in Chapter 1 are reviewed, and a summary of the main outcomes from this work are provided. The overall strengths and limitations of this thesis are discussed, and future directions for further investigations are presented alongside the impact of this work on the biomechanics research community.*

6.1 Summary

Short-duration high-force loading typical of ballistic shield back-face deformation (BFD) has potential to lead to debilitating injuries, and the potential to place users at a higher risk of severe injury. The current standards for evaluating shield efficacy specify requirements pertaining to projectile penetration, but do not address limiting blunt loading resulting from behind armour blunt trauma (BABT) such as has been specified in other protective equipment standards (*e.g.*, helmets, armour). In order to properly address the risk of upper extremity injury resulting from shield BABT, appropriate injury criteria and a mechanical surrogate were required. The overall purpose of the studies presented in this thesis was to inform a protective standard for evaluating ballistic shields to ensure they are effective at limiting upper extremity injury risk resulting from shield BFD when bullets are absorbed or deflected.

The disconnect between tissue testing (conducted in laboratory settings) *vs.* ballistic testing (conducted in a ballistic ranges) has limited the research conducted in this area. Applied loading behind ballistic shields needed to first be characterized in a ballistic testing facility (at Defence

Research and Development Canada – the Valcartier Research Centre, DRDC – VRC) and then applied to tissues. The first component of this research involved modifying an Anthropomorphic Test Device (ATD) upper extremity to facilitate measuring loading resulting from shield BABT (detailed in Chapter 2). The WorldSID ATD was augmented with additional instrumentation to be capable of measuring forces, speeds and time durations representing shield BFD (*i.e.*, 1 – 20 kN, 0.1 – 1 ms, 0 – 250 m/s). This surrogate was used to measure ballistic loading behind a shield at four discrete locations – the hand, wrist, forearm and elbow – and was shown to be repeatable and reproducible. It was also transferable to the McMaster University Injury Biomechanics Lab to facilitate recreation of these impacts for tissue testing, an essential process for ensuring realistic load curves would be applied. A transferrable testing jig was also generated between the ballistic testing facility and the Injury Biomechanics Lab to support both the ATD and post-mortem human surrogates (PMHS), which was also important to keep boundary conditions consistent among surrogates. Loads ranging from 2,026 N to 18,979 N were recorded on the augmented ATD, with stand-off distances of 10 mm, 15 mm and 20 mm tested (*i.e.*, Objective 1 complete). Impact location had a significant effect on the impact force, indicating that boundary conditions are an important factor in quantifying applied load for the development of injury criteria. Digital image correlation was also conducted to characterize the impact profile of the shield over time on three shots without the ATD positioned behind it, to inform the loading shape for creation of a laboratory-based impact projectile. X-ray images were also conducted post-test to assess the shrapnel dispersal and confirm independent shots were conducted.

The augmented WorldSID ATD was then used to reproduce high-force, short-duration impacts in the pneumatic impacting apparatus at the Injury Biomechanics Lab to investigate the injury tolerance of PMHS upper extremities. A lightweight projectile was developed to apply the

short-duration, high-velocity impacts, where the impact cap matched the shape and stiffness of the deforming ballistic shields collected during ballistic testing [100]. The instrumented projectile and updated pneumatic impacting apparatus system enabled the system to deliver impacts as fast as they had ever run while also allowing measurement of applied force. The system was calibrated by delivering impacts to the WorldSID ATD upper extremity and the peak forces were within 5% of those tested at DRDC – VRC. A relationship was developed relating 50th percentile male PMHS upper extremities to the WorldSID ATD. Paired mid-sized male specimens were impacted until failure; one from each pair being impacted at the hand and forearm, while the contralateral at the wrist and elbow. The use of pairs allowed for isolating effects of anatomical location on injury threshold, while selecting PMHS that fell between the 30th to 70th percentile meant the Coefficient of Variation of our work was over 10% less than previous (*e.g.*, [66]). A pilot specimen pair was used to establish approximate fracture threshold, by increasing the impact energy (velocity) of the projectile in a stepwise fashion until fracture was identified via x-ray imaging. This allowed for studying the effect of boundary conditions on fracture tolerance. The average fracture force for the hand was 3.8 kN, the wrist 5.6 kN, the forearm 3.0 kN, and the elbow 4.7 kN, corresponding to a 10% risk of fracture measured on the modified WorldSID ATD of 11.0 kN, 10.8 kN, 8.1 kN and 12.5 kN, respectively, based on the survivability curves generated (*i.e.*, Objective 2 complete). Other factors were examined for their influence on failure, like bone mineral density, height, radial length, *etc.* The injury criteria established were higher than previously reported criteria developed for automotive levels, highlighting why it is critical to develop injury metrics specific to high-rate conditions (*i.e.*, Hypothesis 1 accepted).

After investigating the response of ATD and PMHS upper extremities to loading representative of shield BABT, an existing human body finite element model upper extremity was

sectioned from the rest of the body to evaluate its ability to predict forearm fractures from these high-rate impacts. One specimen was strain gauged during the experimental impacts, and the results informed the critical strain used in the model. Finite element modelling is the basis of many safety assessments in industry, and as such, would be a useful tool for evaluating future ballistic shield designs to minimize weight while ensuring adequate protection. The upper extremity model was impacted under the same conditions that were conducted experimentally and evaluated for its potential to predict injury by including an element erosion technique that deleted elements when they reached a critical strain, determined from the experimental portion of this work (*i.e.*, Objective 3 completed). The results were compared to the strain gauged specimen as well as the group of 8 PMHS tested and assessed for its performance. The model performed well in terms of peak force measured and predicting fracture; however, the shape of the force-time curve did not fully represent PMHS testing results (*i.e.*, Hypothesis 2 accepted). Recommendations were thus made to improve this response.

6.2 Strengths and Limitations

Specific strengths and limitations of each study are addressed directly in their chapters. However, there are some that are generally applicable to the thesis as a whole. This study was the first of its kind to investigate high-rate loading resulting from ballistic shield deformation on injury outcome, a novel contribution to the injury biomechanics field. Using a step-wise approach of first characterizing the loading profile in a ballistic testing facility provided a controlled, reproducible and accurate depiction of the applied load in order to replicate these impacts on PMHS. A strength of this work is the large number of PMHS tested, and the use of paired specimens. Maximizing

the value from a specimen also ensured the donor factors wouldn't affect relative comparisons. This allowed for isolation of the effect of boundary conditions (*i.e.,* anatomical locations) under the same impact conditions on fracture tolerance. To the author's knowledge, this has not been conducted before. Further, the strict height and weight limits for selecting the test group was also advantageous as it allowed for reducing variability across specimens. The injury risk curves that were generated from these studies indicate that impact velocity and loading rate have an effect on injury outcome and therefore injury criteria developed for other loading events (*e.g.*, airbags deploying in automotive collisions) are not directly applicable to shield standards. Keeping the upper extremity soft tissue intact was also advantageous as many previously-conducted three-point bending tests on the isolated radius and ulna provide overly simplified boundary and loading conditions. Further, steps to validate an existing human body model for high-rate loading scenarios is a valuable contribution that could be used to evaluate future shield iterations beyond the scope of this project.

There are also several limitations that need to be noted in order to understand and apply the data produced accurately. In the ballistic loading assessment, only one type of shield was evaluated, and thus different shields may have different back-face deformation (BFD) under these conditions. The ATD used for this study was also modified to allow for additional instrumentation, affecting the surrogate's biofidelity. The loading scenario applied to the PMHS was a simplification of what may occur in real-life behind shield blunt trauma events. The use of ex-vivo testing to approximate the in-vivo response is an approximation but is a necessary concession for the testing of fracture tolerance. There is no ethical way to conduct human ballistic testing in-vivo and the challenges associated with muscular contraction of ex-vivo surrogates is vast and uncertain. This work also focusses only on fracture and does not address the soft tissue injuries

that may occur as a result of shield BFD. Sprains or contusions may cause an individual to drop a shield, which would put users at greater risk of injury, but is challenging to quantify and assess. As shield BABT occurs very quickly (less than 0.5 ms), muscle response is not a limiting factor; however, the initial tension of muscle (static muscle forces to support the shield) would have been present. Tensed muscles may have allowed the PMHS upper extremities to sustain higher loads prior to failure. Pre-tensing musculature is not commonly conducted in injury limit testing, so there is no standardized procedure. It is also invasive, and the amount of pretension required is unknown. Further, the downwards force associated with holding the shield is approximately 2% the fracture tolerance of the forearm (*i.e.*, the most vulnerable location) and as such, is not expected to have a substantial effect on injury threshold. The upper extremities were also segmented at the mid-humerus, to reduce the complexity and cost associated with full-body tests and provide a direct comparison with the WorldSID ATD and sectioned THUMS AM50 upper extremity. As a result, potting the humerus and fixing the hand to an aluminum handle were required, which likely represented overly rigid boundary conditions than would be expected in use. The same was true for the wrist and elbow impacts, in which a rigid support was required behind these locations and may have reduced the failure threshold. The use of intact specimens also made aligning the hand and carpal bones challenging, which may have led to some variation in the fractures generated.

Further, both the experimental and simulation testing examined loading in the transverse direction only. In most loading scenarios, the impacts applied to the upper extremity are combined with bending moments, off-plane impacts, and would potentially have a torso/individual behind the arm which would dramatically affect the injury risk. However, loading due to BSBT is highly focal, so the loading scenario that was conducted in this work was considered an acceptable simplification.

This research investigated the injury tolerance of the hand, wrist, forearm and elbow using eight 50th percentile male PMHS upper extremities. These locations were selected due to their complex geometry and close proximity to the back of the shield; however, there is no guarantee these are the most vulnerable locations of the upper extremity. During testing, only 14 of the 62 tests generated a fracture on the first impact for that anatomical location, while all other impact locations required additional impacts at higher severities. These repeated impacts may have caused residual damage that was not detected by x-ray imaging, resulting in lower fracture thresholds. To control for this, the peak force during all impacts was used as the fracture force. Further, the failure forces did not differ between the first shot generating injury and forces collected after repeated impacts, meaning this likely did not have a substantial effect on the proposed threshold. However, if anything this represents a slightly more conservative injury limit, providing enhanced protection for the ballistic shield user.

A final limitation of this work was the higher than desirable mass of the projectile. Although efforts were made to maximize the projectile strength to weight ratio while also instrumenting to measure applied force, a mass of 434 g was the lightest projectile possible within the parameters of this project. As a result, it was not possible to replicate the energy associated with behind shield blunt trauma nor the impulse, but instead the peak force was targeted, and duration was kept as short as possible. This may have underestimated the bone fracture tolerance to shield BABT as bone is a viscoelastic material with strain rate dependencies. Additionally, when developing a relationship between the ATD and PMHS, due to instrumentation capability limits with the ATD, extrapolation outside of the known impacts was conducted on the PMHS. This likely introduced uncertainty into the magnitude of the applied impacts. The 10% injury threshold

was calculated via the relationship developed between the ATD and PMHS due to these instrumentation capabilities, so caution must be used when applying this threshold.

6.3 Future Directions

This research focused on determining the fracture threshold of 50th percentile male specimens. This was selected as a starting point for developing injury thresholds as the Canadian Armed Forces remains predominantly male. However, in order to account for all population sizes and the female sex, a wider range of specimen groups is required. It is crucial to adequately protect all demographics of the population from injury when developing a safety standard, so a broader donor group would be beneficial.

The results produced in this study need to be put into use to develop a protective test standard to limit shield back-face deformation. As the estimated 10% injury threshold limit exceeded measurements obtained on the WorldSID ATD in the ballistic testing facility at the DRDC – VRC, current Level III ballistic shields likely do not adhere to the safety limits required to limit fracture from shield BABT. The results used from this study could also provide insight into where the use of a trauma-attenuated backing would be effective, and whether localized protection is worthwhile to limit shield mass.

Assessing the THUMS finite element model for its ability to predict the fracture of the forearm is a useful contribution for evaluating future shield iterations. Fine-tuning the material properties of other elements of the THUMS AM50 upper extremity model to more accurately represent the force-time response generated during experimental conditions would further improve the confidence of the model. The addition of element erosion in the metacarpals, carpal bones, and

humerus would also allow for identification of injury in the other anatomical areas tested in this study and could be validated using the experimental data produced herein. A CORA Analysis would also be beneficial to provide a metric for its predictive abilities. Employing an updated THUMS finite element model would be beneficial to assess varying design properties (*i.e.*, shield thickness) in future shield developments.

6.4 Significance

In conclusion, this work represents the first critical step in understanding the response and tolerance of the upper extremity to shield BABT. New injury criteria have been proposed for the hand, wrist, forearm and elbow that are specific to these types of short-duration, localized, and high-force impacts typical of the back-face deformation of ballistic shields absorbing or deflecting projectiles. The augmented WorldSID ATD was used as a repeatable mechanical tool in which a binary limit can be applied to investigate whether ballistic shields are effective at limiting injury or not. The THUMS AM50 upper extremity was evaluated to assess for its effectiveness at predicting radial and ulnar fractures and performed well in conditions replicating those conducted experimentally in this work. The results from this work will aid in the development of a protective standard for ballistic shields in order to protect the Canadian Armed Forces and reduce the incidence of harmful upper extremity fractures.

References

[1] L. Cannon, "Behind Armour Blunt Trauma - An Emerging Problem," J. R. Army Med. Corps, vol. 147, no. 1, pp. 87-96, 2001.

[2] National Institute of Justice, "Ballistic Resistant Protective Materials," NIJ Standard 0108.01, Washington, D.C., 1985.

[3] K. Schmitt, P. Niederer, M. Muser and F. Walz, "Injuries of the Upper Extremities," in Trauma Biomechanics, Berlin, Springer, 2010.

[4] M. Wang, R. Rao, N. Yoganandan and F. Pintar, "Upper Extremity Injury Biomechanics," in Accidental Injury: Biomechanics and Prevention (Third Edition), New York, Springer Science & Business Media, 2015.

[5] E. F. Morgan, G. U. Unnikrisnan and A. I. Hussein, "Bone mechanical properties in healthy and diseased states," Annual review of biomedical engineering, no. 20, pp. 119-143, 2018.

[6] M. Gomez and A. Nahum, "Biomechanics of bone." in Accidental Injury, New York, Springer, 2002, pp. 206-227.

[7] U. Hansen, P. Zioupos, R. Simpson, J. Currey and D. Hynd, "The effect of strain rate on the mechanical properties of human cortical bone," Journal of Biomechanical Engineering, vol. 130, no. 1, pp. 1-8, 2008.

[8] H. Yamada, Strength of biological materials, Baltimore: Williams & Wilkins, 1970.

[9] Z. A. Haverfield, R. L. Hunter, K. L. Loftis and A. M. Agnew, "Skeletal Site and Method-dependent Variability of Bone Mineral Density in Injury Biomechanics Research," in Proceedings of the IRCOBI Conference, Porto, 2022.

[10] World Health Organization. (1994). Assessment of fracture risk and its application to screening for postmenopausal osteoporosis: report of a WHO study group [meeting held in Rome from 22 to 25 June 1992]. World Health Organization.

[11] D. Albano, P. M. Agnollitto, M. Petrini, A. Biacca, F. M. Ulivieri, L. M. Sconfienza and C. Messina, "Operator-related errors and pitfalls in dual energy X-ray absorptiometry: how to recognize and avoid them," Academic Radiology, vol. 9, no. 28, pp. 1272-1286, 2021.

[12] C. M. de Bakker, W. J. Tseng, Y. Li, H. Zhao and X. S. Liu, "Clinical evaluation of bone strength and fracture risk," Current osteoporosis reports, pp. 35-42, 2017.

[13] American College of Radiology (ACR), the Society for Pediatric Radiology (SPR) and the Society of Skeletal Radiology (SSR), "ACR-SPR-SSR Practice Parameter for the Performance of Quantitative Computed Tomography (QCT) Bone Mineral Density," Practice Parameter, Resolution 15 (Revised 2023), 2023.

[14] D. J. Carr, I. Horsfall and C. Malbon, "Is behind armour blunt trauma a real threat to users of body armour? A systematic review.," BMJ Military Health, vol. 162, no. 1, pp. 8-11, 2016.

[15] W. Błaszczyk, M. Fejdys and M. Landwijt, "Composite ballistic shields," Techniczne Wyroby Włókiennicze, vol. 17, no. 2, pp. 28-32, 2009.

[16] G. Cooper and P. Gotts, "Ballistic Protection," in Ballistic Trauma, London, Springer, 2005, pp. 67-90.

[17] J. Pach, D. Pyka, K. Jamroziak and P. Mayer, "The experimental and numerical analysis of the ballistic resistance of polymer composites," Composites Part B: Engineering, no. 113, pp. 24-30, 2017.

[18] M. Rojek, M. Szymiczek, J. Stabik, A. Mężyk, K. Jamroziak, E. Krzystala and J. Kurowski, "Composite materials with the polymeric matrix applied to ballistic shields," Archives of Materials Science and Engineering, vol. 1, no. 63, pp. 26-35, 2013.

[19] A. Sondén, D. Rocksén, L. Riddez, J. Davidsson, J. Persson, D. Gryth, J. Bursell and U. Arborelius, "Trauma attenuating backing improves protection against behind armor blunt trauma," Journal of Trauma and Acute Care Surgery, vol. 67, no. 6, pp. 1191-9, 2009.

[20] National Institute of Justice, "Ballistic Resistance of Body Armor," NIJ Standard 0101.06, Washington, D.C., 2008.

[21] J. Croft and D. Longhurst, "HOSDB body armour standards for UK police (2007) Part 2: ballistic resistance," Crown Copyright, 2007.

[22] E. Hanlon and P. Gillich, "Origin of the 44-mm behind-armor blunt trauma standard," Military Medicine, vol. 3, no. 177, pp. 333-339, 2012.

[23] K. U. Schmitt, P. F. Niederer, D. S. Cronin, B. Morrison III, M. H. Muser and F. Walz, "Ballistic and blast trauma," in Trauma Biomechanics, Cham, Springer, 2019, pp. 247-280.

[24] J. Roberts, E. Ward, A. Merkle and J. O'Connor, "Assessing behind armour blunt trauma in accordance with the National Institute of Justice Standard for Personal Body Armour Protection using finite element modelling," J Trauma Acute Care Surg, vol. 62 , no. 5, pp. 1127-1133, 2007.

[25] K. Schmitt, P. Niederer, D. Cronin, M. Muser and F. Walz, "Ballistic and blast trauma," in Trauma Biomechanics: An Introduction to Injury Biomechanics, Berlin, Springer-Verlag, 2014, pp. 202-235.

[26] C. Bass, R. Salzar, S. Lucas, M. Davis, L. Donnellan, B. Folk, E. Sanderson and S. Waclawik, "Injury risk in behind armor blunt thoracic trauma," International journal of occupational safety and ergonomics, vol. 12, no. 4, pp. 429-422, 2006.

[27] C. Bir, R. Lance, S. Stojsih-Sherman and J. Cavanaugh, "Behind armour blunt trauma: recreation of field cases for the assessment of backface signature testing," in 30th International Symposium on Ballistics, 2017.

[28] N. Prat, F. Rongiras, J. Sarron, A. Miras and E. Voiglio, "Contemporary body armor: technical data, injuries and limits," European Journal of Trauma and Emergency Surgery, vol. 38, no. 2, pp. 95-105, 2012.

[29] H. J. Mertz and A. L. Irwin, "Anthropomorphic Test Devices and Injury Risk Assessments," in Accidental Injury: Biomechanics and Prevention, New York, Springer, 2014, pp. 83-112.

[30] North Atlantic Treaty Organization (NATO), "Test Methodology for Protection of Vehicle Occupants Against Anti-Vehicular Landmine Effects," RTO Technical Report, 2007.

[31] Association for the Advancement of Automotive Medicine, "The Abbreviated Injury Scale: 2015 Revision (6 ed.)," Chicago, 2018.

[32] "Methods in Trauma Biomechanics," in Trauma Biomechanics, Cham, Springer, 2019, pp. 15-61.

[33] J.-S. Wang, "MAIS(05/08) Injury Probability Curves as Functions of Delta V," National Highway Traffic Safety Administration, 2022.

[34] H. J. Mertz, "Anthropomorphic Test Devices," in Accidental Injury, New York, Springer, 1993, pp. 66-84.

[35] Insurance Institute for Highway Safety, "Side Impact Crashworthiness Evaluation 2.0 Rating Guidelines - Version I," Ruckersville, September 2021.

[36] J. Crandall, D. Bose, J. Forman, C. Untaroiu, C. Arregui-Dalmases, C. Shaw and J. Kerrigan, "Human surrogates for injury biomechanics research," Clinical Anatomy, vol. 24, no. 3, pp. 362-371, 2011.

[37] J. Funk, "Ankle injury mechanisms: lessons learned from cadaveric studies," Clinical Anatomy, vol. 3, no. 24, pp. 350-361, 2011.

[38] A. King, The biomechanics of impact injury, Cham: Springer, 2018.

[39] J. Melvin, "The Engineering Design, Development, Testing, and Evaluation of an Advanced Anthropomorphic Test Device," National Highway Traffic Safety Administration, Washington, 1985.

[40] A. Kemper, J. Stitzel, S. Duma, F. Matsuoka and M. Masuda, "Biofidelity of the SID-IIs and a modified SID-IIs upper extremity: biomechanical properties of the human humerus," in Proc. of the 19th Int. Tec. Conf. on the Enhanced Safety of Vehicles, Washington, 2005.

[41] A. R. Kemper, "Response corridors for the medial-lateral compressive stiffness of the human arm: Implications for side impact protection," Accident Analysis & Prevention, vol. 1, no. 50, pp. 204-222, 2013.

[42] D. Parent, M. Craig and K. Moorhouse, "Biofidelity evaluation of the THOR and Hybrid III 50th percentile male frontal impact anthropomorphic test devices," Stapp car crash journal, no. 61, pp. 227-276, 2017.

[43] R. Scherer, K. Bortenschlager, A. Akiyama, S. Tylko, M. Hartlieb and T. Harigae, "WorldSID production dummy biomechanical responses," Experimental Safety of Vehicles, pp. 18-22, 2009.

[44] D. Hynd, M. Page, K. Bortenschlager, B. Been and M. van Ratingen, "Status of Side Impact Dummy Developments: WorldSID Development," European Enhanced Vehicle-Safety Committee, January 2004.

[45] M. Iwamoto, Y. Kisanuki, I. Watanabe, K. Furusu, K. Miki and J. Hasegawa, "Development of a finite element model of the total human model for safety (THUMS) and application to injury reconstruction.," in Proceedings of the international IRCOBI Conference, Munich, 2002.

[46] H. Haug, "H-model overview description," in Proceedings of the Twenty-Ninth International Workshop on Human Subjects for Injury Biomechanics Research, 2001.

[47] Toyota Motor Corporation, "Total Juman Model for Safety (THUMS) AM50 Occupant Model Version 6.1," Toyota Central R&D Labs., Inc., 2021.

[48] M. Iwamoto, Y. Nakahira and H. Kimpara, "Development and validation of the total human model for safety (THUMS) toward further understanding of occupant injury mechanisms in precrash and during crash," Traffic Injury Prevention, no. sup1, pp. S36-S48, 2015.

[49] K. Sverrisdóttir, Improvements and Validation of THUMS Upper Extremity: Refinements of the Elbow Joint for Improved Biofidelity, Master's Thesis: KTH Royal Institute of Technology, 2019.

[50] G. Park, T. Kim, M. Panzer and J. Crandall, "Validation of shoulder response of human body finite-element model (GHBMC) under whole body lateral impact condition," Annals of Biomedical Engineering, pp. 2558-2576, 2016.

[51] S. Robin, "HUMOS: Human model for safety - A joint effort towards the development of refined human-like car occupant models," SAE Technical Paper, pp. No. 2001-06-0129, 2001.

[52] W. Hardy and L. Schneider, "Investigation of inertial factors involved in airbag-induced forearm fractures," in International Technical Conference on Enhanced Safety of Vehicles, Windsor, 1998.

[53] A. Amis and J. Miller, "The mechanisms of elbow fractures: an investigation using impact tests in vitro," Injury, vol. 3, no. 26, pp. 163-168, 1995.

[54] S. Duma, P. Schreiber, J. McMaster, J. Crandall and C. Bass, "Fracture tolerance of the male forearm: the effect of pronation versus supination," Proceedings of the Institution of Mechanical Engineers, Part D: Journal of Automobile Engineering, vol. 8, no. 216, pp. 649-654, 2002.

[55] S. Duma, P. Schreiber, J. McMaster, J. Crandall, C. Bass and W. Pilkey, "Dynamic injury tolerances for long bones of the female upper extremity," The Journal of Anatomy, vol. 3, no. 194, pp. 463-471, 1999.

[56] D. Carter and W. Caler, "Cycle-dependent and time-dependent bone fracture with repeated loading," pp. 166-170, 1983.

[57] J. McElhaney, "Dynamic response of bone and muscle tissue," Journal of Applied Physiology, vol. 21, no. 4, pp. 1231-1236, 1966.

[58] A. Martinez, A. Chakravarty and C. Quenneville, "The effect of impact duration on the axial fracture tolerance of the isolated tibia during automotive and military impacts," Journal of the Mechanical Behaviour of Biomedical Materials, vol. 78, pp. 315-320, 2018.

[59] D. Carpanen, A. E. Kedgley, D. S. Shah, D. S. Edwards, D. J. Plant and S. D. Masouros, "Injury Risk of Interphalangeal and Metacarpophalangeal Joints Under Impact Loading," Journal of the Mechanical Behaviour of Biomedical Materials, vol. 97, pp. 306-311, 2019.

[60] E. Sosa and F. Alessa, "Experimental evaluation of protected and unprotected hands under impact loading," Journal of Biomechanics, no. 118, p. 110326, 2021.

[61] J. Spadaro, F. Werner, R. Brenner, M. Fortino, L. Fay and W. Edwards, "Cortical and trabecular bone contribute strength to the osteopenic distal radius," Journal of Orthopaedic Research, vol. 12, no. 2, pp. 211-218, 1994.

[62] J. Reeves, T. Burkhart and C. Dunning, "The effect of static muscle forces on the fracture strength of the intact distal radius in vitro in response to simulated forward fall impacts," Journal of Biomechanics, vol. 47, no. 11, pp. 2672-2678, 2014.

[63] S. Duma, B. Boggess, J. Crandall, S. Hurwitz, K. Seki and T. Aoki, "Analysis of upper extremity response under side air bag loading," SAE Technical Paper, no. No. 2001-06-0016, 2001.

[64] R. Saul, S. Backaitis, M. Beebe and L. Ore, "Hybrid III Dummy Instrumentation and Assessment of Arm Injuries During Air Bag Deployment," Society of Automotive Engineers, pp. 1776-1785, 1996.

[65] F. Pintar, N. Yoganandan and R. Eppinger, "Response and tolerance of the human forearm to impact loading," SAE Transactions, pp. 2712-2719, 1998.

[66] F. Pintar and N. Yoganandan, "Dynamic Bending Tolerance of the Human Forearm," Traffic Injury Prevention, vol. 3, no. 1, pp. 43-48, 2002.

[67] W. Hardy, L. Schneider and M. Reed, "Comparison of airbag-aggressivity predictors in relation to forearm fractures," SAE transactions, pp. 1366-1379, 1998.

[68] S. Duma, G. Hansen, E. Kennedy, A. Rath, C. McNally, A. Kemper, E. Smith, P. Brolison, J. Stitzel, M. Davis and C. Bass, "Upper extremity interaction with a helicopter side airbag:

injury criteria for dynamic hyperextension of the female elbow joint," SAE Technical Paper, pp. No. 2004-22-0007, 2004.

[69] M. Bolduc, J.-S. Binette, D. Fisher and D. Hammond, "Tactical ballistic shields operational testing protocol definition," in Personal Armour Systems Symposium, 2018.

[70] N. Steinmann, J. de Lange, J.-S. Binette and C. Quenneville, "Quantification of Behind Shield Blunt Trauma Impacts Using a Modified Upper Extremity Anthropomorphic Test Device," Journal of Biomechanical Engineering, vol. 144, no. 9, pp. 0910101-8, 2021.

[71] N. Steinmann, "Development of a Modified Anthropomorphic Test Device for the Quantification of Behind Shield Blunt Impacts," M.A.Sc. Thesis, McMaster University, 2020.

[72] Statistics Canada, "Statistics of women in the Canadian Armed Forces," Government of Canada, Ottawa, 2022.

[73] J. Mölsä, U. Kujala, P. Myllynen, I. Torstila and O. Airaksinen, "Injuries to the upper extremity in ice hockey: analysis of a series of 760 injuries," The American Journal of Sports Medicine, vol. 5, no. 31, pp. 751-757, 2013.

[74] C. Freitas, J. Mathis, N. Scott, R. Bigger and J. MacKiewicz, "Dynamic response due to behind helmet blunt trauma measured with a human head surrogate," International Journal of Medical Sciences, vol. 11, no. 5, p. 409, 2014.

[75] K. Rafaels, H. Cutcliffe, R. Salzar, M. Davis, B. Boggess, B. Bush and C. Bass, "Injuries of the head from backface deformation of ballistic protective helmets under ballistic impact," Journal of Forensic Sciences , vol. 60, no. 1, pp. 219-225, 2015.

[76] L. Allanson-Bailey, Improved Cranial Fracture Metrics For Assessing The Protective Benefits Of Helmet Systems [doctoral dissertation], Platform Sciences Division, Dstl Porton Down: The Open University, 2016.

[77] C. Bir, The evaluation of blunt ballistic impacts of the thorax [doctoral dissertation], Detroit, MI, USA: Wayne State University, 2000.

[78] D. Hisley, J. Gurganus and A. Drysdale, "Experimental methodology using digital image correlation to assess ballistic helmet blunt trauma," Journal of Applied Mechanics, vol. 78, no. 051022, pp. 1-7, 2011.

[79] C. Weisenbach, K. Logsdon, R. Salzar, V. Chancey and F. Brozoski, "Preliminary investigation of skull fracture patterns using an impactor representative of helmet back-face deformation," Military Medicine , vol. suppl_1, no. 183, pp. 297-293, 2018.

[80] L. Griffin, R. Harris, R. Hayda and M. Rountree, "Loading Rate and Torsional Moments Predict Pilon Fractures for Antipersonnel Blast Mine Loading," in IRCOBI Conference Proceedings, 2001.

[81] C. Quenneville and C. Dunning, "Evaluation of the biofidelity of the HIII and MIL-Lx lower leg surrogates under axial impact loading," Traffic injury prevention, vol. 13, no. 1, pp. 81-85, 2012.

[82] J. de Lange, L. Burrows, J.-S. Binette and C. Quenneville, "Behind Shield Blunt Trauma: Characterizing the Back-Face Deformation of Shields with a Focus on Upper Limb Loading," Annals of Biomedical Engineering, pp. 1-12, 2023.

[83] S. Duma, B. Boggess, J. Crandall and C. MacMahon, "Injury risk function for the small female wrist in axial loading," Accident Analysis & Prevention, vol. 6, no. 35, pp. 869-875, 2003.

[84] P. C. Begeman and K. Pratima, "Bending Strength of the Human Cadaveric Forearm Due to Lateral Loads," SAE Technical Paper, p. No. 99SC24, 1999.

[85] J. de Lange and C. Quenneville, "The axial impact response and plantar load distribution of the Hybrid III and MIL-Lx under altered ankle postures," Journal of Biomechanical Engineering, vol. 144, no. 1, pp. 1-7, 2022.

[86] A. B. Chakravarty, A. A. Martinez and C. E. Quenneville, "The injury tolerance of the tibia under off-axis impact loading," Biomedical Engineering Society, vol. 45, no. 6, pp. 1534-1542, 2017.

[87] A. A. Keefe, H. Angel and B. Mangan, "2012 Canadian Forces Anthropometric Survey (CFAS)," Defence Research and Development Canada, 2015.

[88] C. Quenneville, S. McLachlin, G. Greeley and C. Dunning, "Injury tolerance criteria for short-duration axial impulse loading of the isolated tibia," Journal of Trauma, vol. 70, pp. 13-18, 2011.

[89] 1. ISO/TS, "Procedure to construct injury risk curves for the evaluation of road user protection in crash tests," ISO, Geneva, 2014.

[90] H. E. Meema and S. Meema, "Compact bone mineral density of the normal human radius," Acta Radiologica: Oncology, Radiation, Physics, Biology, vol. 17, no. 4, pp. 342-352, 1978.

[91] A. King, D. Viano, N. Mizeres and J. States, "Humanitarian benefits of cadaver research on injury prevention," The Journal of Trauma-Injury Infection & Critical Care, vol. 4, no. 38, pp. 564-569, 1995.

[92] J. de Lange, L. Burrows, A. Wadera and C. Quenneville, "Injury risk for the hand and forearm under shield behind armour blunt trauma loading," Submitted to Annals of Biomedical Engineering, 2023.

[93] I. Acharya, J. T. Van Tuyl, J. de Lange and C. E. Quenneville, "A force-sensing insole to quantify impact loading to the foot," Journal of Biomechanical Engineering, vol. 2, no. 141, pp. 024501-024507, 2018.

[94] J. Lubahn, R. Englund, G. Trinidad, J. Lyons, D. Ivance and F. Buczek, "Adequacy of laboratory simulation of in-line skater falls," The journal of hand surgery, vol. 30, no. 2, pp. 283-288, 2005.

[95] D. Fressmann, T. Münz, O. Graf and K. Schweizerhof, "FE Human Modelling in Crash–Aspects of the numerical Modelling and current Applications in the Automotive Industry," LS-Dyna Anwenderforum, Frankenthal, 2007.

[96] C. Brewer, A. Shakib, J. de Lange and C. Quenneville, "Estimation of Injury Limits at Vulnerable Impact Locations Along the Forearm via the THUMS AM50 Finite Element Model," Under Revision, 2023.

[97] D. S. Cronin, M. C. Bustamante, J. Barker, D. Singh, K. A. Rafaels and C. Bir, "Assessment of thorax finite element model response for behind armor blunt trauma impact loading using an epidemiological database.," Journal of Biomechanical Engineering, vol. 143, no. 3, pp. 0310071-12, 2021.

[98] M. Panjabi, A. White III and W. Southwick, "Mechanical properties of bone as a function of rate of deformation," JBJS, vol. 55, no. 2, pp. 322-330, 1973.

[99] D. Cronin, "Application of a detailed thorax model to investigate behind armour blunt trauma," in IRCOBI Conference Proceedings (No. IRC-12-92)., Dublin, 2012.

[100] L. Burrows, QUANTIFYING THE EFFECT OF USER SIZE ON INJURY TOLERANCE OF THE UPPER EXTREMITY SUBJECTED TO BEHIND-SHIELD BLUNT TRAUMA, Hamilton, Ontario: M.A.Sc. Thesis, McMaster University, 2023.

[101] N. Yoganandan, F. Pintar, M. Boynton, P. Begeman, P. Prasad, S. Kuppa, R. Morgan and R. Eppinger, "Dynamic axial tolerance of the human foot-ankle complex," SAE Transactions, pp. 1887-1898, 1996.

[102] M. Iwamoto and Y. Nakahira, "Development and validation of the Total HUman Model for Safety (THUMS) version 5 containing multiple 1D muscles for estimating occupant motions with muscle activation during side impacts," SAE Technical Paper, 2015.

[103] J. Funk, J. Crandall, L. Tourret, C. MacMahon, C. Bass, J. Patrie, N. Khaewpong and R. Eppinger, "The axial injury tolerance of the human foot/ankle complex and the effect of Achilles tension," Journal of Biomechanical Engineering, pp. 750-757, 2002.

[104] Association for the Advancement of Automotive Medicine, "Abbreviated Injury Scale (c) 2005 Update 2008.," Chicago, 2016.

Appendix A – Glossary of Anatomical Terms

This appendix contains a list of anatomical terms used frequently throughout this thesis, to aid the reader who may be unfamiliar with this terminology.

Anatomical Position	When the body is upright, with the face and palms forward and the upper limbs placed at the sides.
Anterior	Situated towards the front of the body from the midline.
Anthropomorphic	Made to resemble human form.
Articulation	The contact junction between two bones for the purposes of facilitating motion.
Biofidelity	Ability to accurately represent biological responses.
Cadaveric	Of, or pertaining to, a human body.
Cancellous Bone	Also referred to as trabecular bone, is characterized by its spongy, lattice-like structure and is typically found at the ends of long bones.
Capitellum	The lateral humeral condyle that articulates with the radial head.
Carpal bones	The bones of the wrist connecting the hand to the forearm.
Cartilage	Connective tissue covering surfaces in joints, allows for motion not disrupted by friction and absorbs shocks.
Collagen	The main protein in connective tissue that provides structural support to the tissues of the body.
Contralateral	Denoting the side of the body opposite to that affected.
Cortical Bone	Dense bone that provides the majority of the body's structural support.
Diaphysis	The shaft/central part of a long bone.

Distal	Further away from the center of the body or the point of attachment.
Epicondyle	The medial and lateral prominences of the distal end of the humerus.
Epiphysis	The end of a long bone.
Extension	Movement increasing the angle between two body segments.
Ex-Vivo	Out of the living.
Flexion	Movement decreasing the angle between two body segments.
Frontal	A vertical plane that divides the body into its anterior and posterior portions.
Humerus	Long bone between the elbow and shoulder.
In Vivo	In a living organism.
Interphalangeal Joint	The joints within the fingers of the hand, in the middle (proximal) and closest to the tip (distal) of the finger.
Intramedullary Canal	The marrow cavity of long bones.
Joint	Location of contact between two bones that permits bone movement.
Lateral	Further away from the vertical midline of the body.
Ligament	Connective tissue attaching bone to another bone.
Marrow	Spongey substance found in the center of bones.
Medial	Closer to the vertical midline of the body.
Metacarpal	The five bones of the palm.
Metacarpophalangeal Joint	The joint at the base of each of the fingers connecting them to the palm.
Olecranon Fossa	Deep depression on the posterior side of the distal humerus.

Olecranon Process	The tip of the elbow; posterior side of the proximal ulna.
Osteon	Functional unit of cortical bone.
Posterior	Situated toward the back of the body from the midline, synonymous with dorsal.
Prone	Facing downward, palms situated downward.
Proximal	Closer to the center of the body or the point of attachment.
Radius	The shorter of the two long bones of the forearm, that is proximal to the thumb.
Sagittal	Anatomical plane dividing the body into right and left sections.
Stature	An individual's height.
Styloid Process	Bony protrusion on the distal end of the radius and ulna.
Supine	Facing upward, palms situated upward.
Tendon	Connective tissue attaching muscle to bone.
Transverse	Anatomical plane that divides the body into superior and inferior sections.
Ulna	The longer of the two long bones of the forearm, that is proximal to the fifth digit.
Upper Extremity	Portion of the body extending from the shoulder joint to the fingers, containing three sections: the upper arm, the forearm, and the hand.

Appendix B – Determining Projectile Impact Velocity

This appendix details how the impact velocity was determined for the laboratory-based replication of the ballistic experiments in which the back-face deformation deformed rapidly.

Impulse: The smallest impulse obtained experimentally was 1.44N*s (only 9.7% higher than 20 mm standoff) but the force was too low to generate fracture (4.1kN). If we were to increase the force (to about 15 kN), the impulse becomes about 236% higher. Impulse became substantially higher with increasing impact force.

Energy of BFD: In consideration of the affected area of the shield, the energy is way too high to replicate. It would have to range between 0.4 kg at 120 m/s (unable to generate a projectile velocity that high) up to 10.2 kg at 23 m/s (which would generate a substantial amount of force, and unable to get a projectile that heavy to accelerate that quickly given the pneumatic impacting apparatus device constraints).

Velocity of BFD: Averaged about 215 m/s across impacts in Chapter 2 of this work, but was much lower in Steinmann and colleagues [71], ranging from 6.5 – 163.6 m/s. The lower impact velocity represents a conservative injury limit.

Momentum: Considering the mass of the bullet (9.6 g) and velocity of the back-face deformation (215 m/s), an impact velocity of 20 m/s would correspond to a projectile mass of roughly 408 g.

Duration of Impact: This ranges from 2.4% higher (4.1 kN impact) to 5.4% higher (15 kN).

In consideration of the above, the low-end of the velocity was selected (representing a conservative limit), while keeping the duration of the impact low and conserving momentum between the ballistic testing facility and the laboratory facility.

Appendix C – Anatomical Data Collected

This appendix presents all of the anatomical data that were collected for each of the specimens prior to impacting. The measurements were collected three times, and the mean result is presented here.

			Forearm Circumference			
Specimen ID	**Hand Length[9] (cm)**	**Elbow-Wrist Length (cm)**	**Minimum (cm)**	**Maximum (cm)**	**Midpoint (Impact Location, cm)**	**Weight (kg)**
211357-L	21.3	27.7	18.4	25.5	22.9	2.5
211357-R	21.5	28.4	17.7	26.3	23.5	2.4
210891-L	20.3	26.3	18.2	28.7	24.3	2.2
210891-R	20.4	26.5	18.0	27.9	24.5	2.1
210897-L	21.3	26.4	18.1	26.9	23.3	2.0
210897-R	20.9	26.9	17.9	29.9	24.0	2.3
211127-L	21.0	25.8	17.2	24.6	19.2	1.6
211127-R	21.0	27.0	17.8	21.8	19.1	1.7
221296-L	21.4	27.2	18.2	27.2	22.8	1.9
221296-R	19.6	28.2	18.4	28.5	19.6	2.1
220316-L	21.4	25.6	19.7	29.3	26.5	2.5
220316-R	21.7	27.7	19.8	30.2	23.6	2.5
230246-L	18.5	24.1	17.5	25.5	23.4	1.6
230246-R	19.4	25.2	17.4	27.4	22.3	1.8
230522-L	20.8	27.5	17.0	27.7	21.3	1.9
230522-R	21.5	28.8	17.5	28.1	20.9	2.0
Mean ± Standard Deviation	20.8 ± 0.4	26.8 ± 0.8	18.1 ± 0.3	27.2 ± 2.5	22.6 ± 2.2	2.1 ± 0.3

[9] As measured from the tip of the 3rd distal phalanx to the line connecting the ulnar and radial distal styloid processes.

Appendix D – Impact Locations

This appendix details the approximate location of impact for the experimental portions of this work.

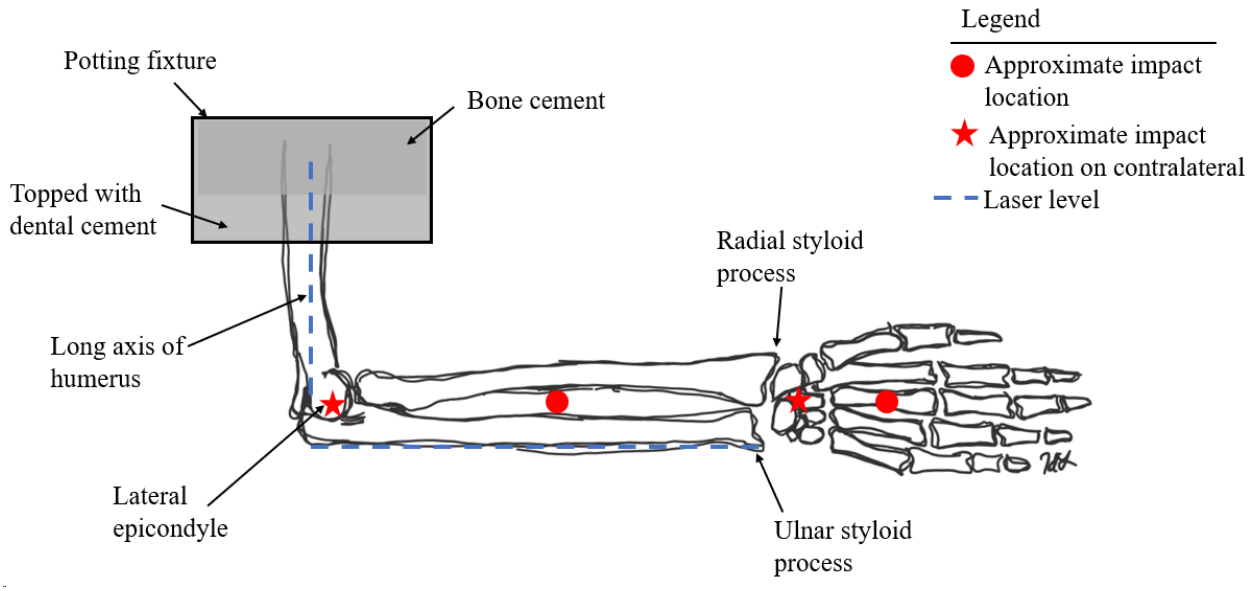

Appendix E – Matlab® Code for Determining Weibull Fit

This appendix details how the log-normal, log-logistic and Weibull distributions were assessed for their fit according to the lowest Akaike Information Criterion (AIC).

```
clc
clear all
close all

%% Read in Data for IRC
% 50th percentile data - HAND
force_h = xlsread('PMHS PLS Practice.xlsx','Force Data','G20:G35');
censor_h = xlsread('PMHS PLS Practice.xlsx','Force Data','H20:H35');
h50f = force_h(:)';
h50c = censor_h(:)';

% 50th percentile data - FOREARM
force_f = xlsread('PMHS PLS Practice.xlsx','Force Data','P23:P41');
censor_f = xlsread('PMHS PLS Practice.xlsx','Force Data','Q23:Q41');
f50f = force_f(:)';
f50c = censor_f(:)';

% Load data
data = [f50f]';
% Define candidate distributions
distributions = {'wbl', 'lognormal', 'loglogistic'};
% Initialize variables
best_aic = Inf;
best_dist = [];
% Loop over candidate distributions
for i = 1:length(distributions)
    % Fit distribution to data
    pd = fitdist(data, distributions{i},'censoring',f50c');
    % Compute AIC
    aic = 2 * pd.NumParameters - 2 * sum(log(pdf(pd, data)));
    % Update best distribution if AIC is lower
    if aic < best_aic
        best_aic = aic;
        best_dist = pd;
    end
end

% Print best distribution and AIC
disp(['Best distribution: ' best_dist.DistributionName]);
disp(['AIC: ' num2str(best_aic)]);
```

Appendix F – Post-Fracture X-ray Images

X-ray imaging was conducted on each of the post-mortem human subjects after they sustained fracture (Chapters 3 and 4). This appendix presents images of the hand, wrist, forearm and elbow after fracture occurred. The fractures are indicated in red. If no x-ray image was available, a CT scan was used.


R
210891
R
210891

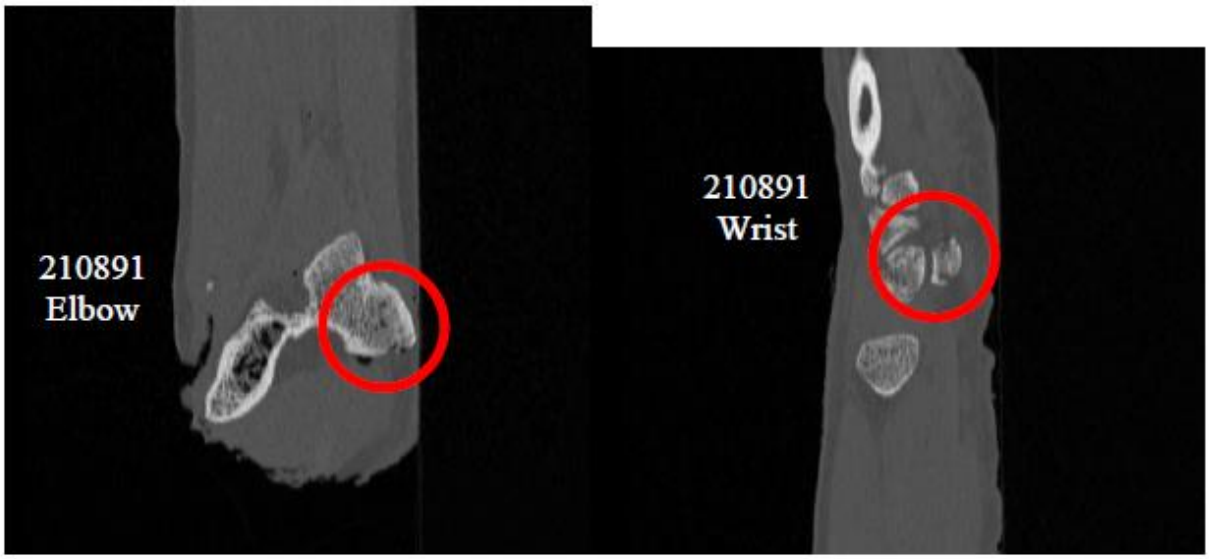
210891
Elbow
210891
Wrist


L 211127


211127
L


211127
R


211357
211357
L
211357
211357


220316
220316
R
220316
220316


L
221296
14


221296
L


221296


221296


230522


230522


230522


230246


230246
L


230246


230246
L 2048

Appendix G – Principal Strain Calculations

This appendix details the determination of the maximum principal radial strains that were used in Chapter 5.

$$\varepsilon_{maximum}, \varepsilon_{minimum} = \frac{1}{2}(\varepsilon_a + \varepsilon_c \pm \sqrt{2(\varepsilon_a - \varepsilon_b)^2 + 2(\varepsilon_b - \varepsilon_c)^2})$$

$$tan2\theta = \frac{2\varepsilon_b - \varepsilon_a - \varepsilon_c}{\varepsilon_a - \varepsilon_c}$$

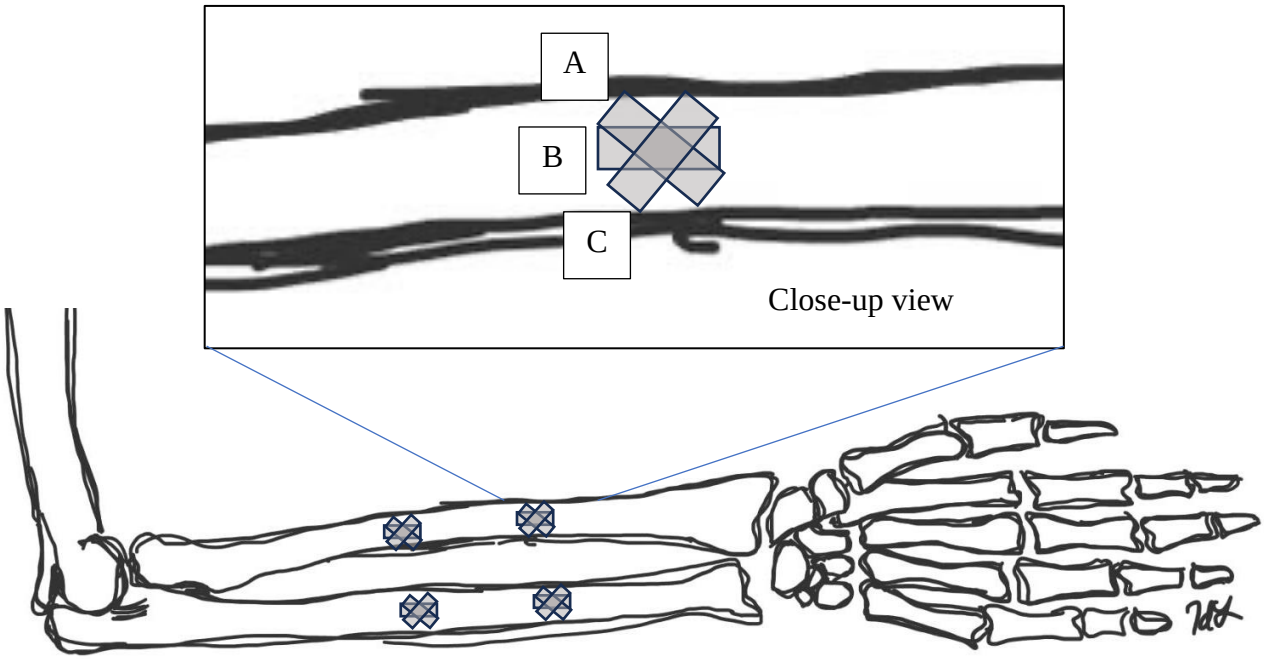

Medial view of the right upper extremity (opposite the impact point)